Monitoring Individual Cells within Cell Cultures using Image Processing and Pattern Recognition Techniques

Keele University

Katherine Dempsey

October 2017

A thesis submitted to Keele University for the degree of doctor of philosophy in the Faculty of Natural Sciences

Abstract

Cells are the building blocks of the human body which are normally specialised by type in accordance with their function. Human cells interact with each other to form the tissues that make up the body. Consequently, it is important to study the behaviour and interactions of these cells at the microscale level, so that the causes of cellular irregularities can be identified; and, possible treatments can be devised. This project aimed to create algorithms that were capable of tracking a variety of cells types within both single cultures and mixed cultures, and from this generate data that was relevant to current clinical trials. There have been successes in tracking some cells types, most notably articular chondrocytes and spinal disk cells. In terms of data generated there has been successes in a whole variety of different types of clinical trials. The algorithms used here have been able to identify the point of mitosis. They have created a better method of determining neural growth and from this have shown that neurons co-cultured with MCSs can grow in places with neural inhibitors. Through the use of algorithms that can analyse culture in three dimensional structures it has been shown that neurons are more affected by topographical cues than chemical cues in their direction of growth. It has also been shown that vesicles are more likely to appear on smaller back disk cells. In the study of gels, it has been found that the more transparent gels are better for imaging. Finally, it has been shown that MSCs and chondrocytes behave differently when in single and co-cultures. These discoveries would not have been possible without the use of the algorithms that allowed for the study of individual cells within a larger culture.

Contents

Monitoring Individual Cells within Cell Cultures using Image processing and Pattern Recognition Techniques 0
Keele University 0
..... 0
Katherine Dempsey 0
Abstract 1
Contents 2
List of publications 6
Authors contributions to the research 7
Abbreviations 9
Contributions of this thesis 10
1. Introduction 11
1.1. Fixed cells 12
1.2. Time lapse microscopy 13
1.3. Spatiotemporal Information 13
1.4. Fluorescence 15
1.5. Phase contrast microscopy 17
1.6. Aims 22
1.7. Objectives 22
1.8. Thesis organisation 23
2. Background 24
2.1. Biology 24
2.1.1. Mesenchymal stem cells 24
2.1.2. Vesicles within back disk cells 30
2.1.3. Hippocampal neurons 33
2.2. Cell Tracking 36
2.2.1. Confluence in cell culture monitoring 36
2.2.2. Distinguishing cells from the background 38
2.2.3. Automated cell tracking 41
2.2.4. Current software tracking cells in phase contrast microscopy 41
2.2.5. Cells in three dimensions 47
2.3. Remarks 48
3. Searching for Mitosis in a Flash 49
3.1. Experimental Background 49
3.2. Methods 51
3.2.1. Cell Collection and Preparation 51

3.2.2. Imaging 52
3.3.3. Algorithm development 53
3.3.4. Algorithm 62
3.3. Results 63
3.3.1. Finding mitosis 63
3.3.2. Measuring confluence 65
3.4. Observations and further work 69
4. A Computational Approach to Quantifying Axon Regeneration in the Presence of Mesenchymal Stem Cells 70
4.1. Introduction 70
4.2. Methods 71
4.2.1. Cell preparation 71
4.2.2. Imaging 73
4.2.3. Algorithm development 75
4.2.4. Algorithm 78
4.3. Results 80
4.3.1. Complexity measures 80
4.3.2. Confluence 83
4.4. Observations and further work 82
5. 4-D Hippocampus Measurements of Neurite Growth In Vitro 85
5.1. Introduction 85
5.2. Methods 85
5.2.1. Plate set up 86
5.2.2. Imaging 87
5.2.3. Computational Methods 88
5.2.4. Algorithm 92
5.3. Results 92
5.3.1. Estimating the Focus 93
5.3.2. Neurite Length Measurements 96
5.4. Observations and further work 98
6. On tracking of spinal disk cells 99
6.1. Introduction 99
6.2. Methods 100
6.2.1. Segmentation based on entropy 100
6.2.2. Cell tracking 103
6.2.3. Vesicle quantifying 105
.6.2.4. Algorithm 106
6.4. Results 108

6.4.1. Validations 109
6.4.2. Vesicles 112
6.5. Observations and Further Work 116
7. Tracking chondrocyte movement in 3D gels 117
7.1. Introduction 117
7.2. Methods 117
7.2.1. Plate set up 118
7.2.2. Imaging 119
7.2.3. Focus measures 119
7.2.4. Tracking methods 120
7.2.5. Algorithm 122
7.3. Results 124
7.4. Observations and Further Work 130
8. Monitoring Stem Cells in Phase Contrast Imaging 131
8.1. Introduction 131
8.2. Methods 132
8.2.1. CMT's Image Analyser (Version MA4.3.0.0) 133
8.2.2. Microscopy 137
8.2.3. Algorithm 141
8.3. Results 141
8.3.1 Preliminary exploratory analysis 141
8.3.2. Singular spectrum analysis 145
8.3.3. Biological results 147
8.4. Observations and further work 150
9. Discussion and Summary 152
9.1. Tracking the movement of non-neural type cells 153
9.2. Tracking of neural tips as they grow in vitro 156
9.3. The extraction of a suitable set of cell biometrics that can be used in the context of cell cycle to determine the points of mitosis, differentiation and apoptosis. 159
9.4. The behaviour of cells in gels and to determine the limits of microscopy on the gels. 161
9.5. The extraction of a suitable set of cell biometrics that can be used in the context of a co-culture to distinguish the cell types without labelling 163
9.6. Getting the science into practice 165
9.7. Conclusion 166
10. References 168

List of publications

The work of this thesis is based on the following publications:

1. Dempsey, K. P., Lam, K. P., Wright, K. T., & Richardson, J. B. (2013.). Searching for Mitosis in a Flash.
2. Lam, K. P., Dempsey, K. P., Smith, W. A., Wright, K. T., Masri, W. E., & Richardson, J. B. (2013a). A Computational Approach to Quantifying Axon Regeneration in the Presence of Mesenchymal Stem Cells (MSCs) *. IEEE Neural Engineering Conference.
3. Dempsey, K. P., Richardson, J. B., & Lam, K. P. (2014). On measuring cell confluence in phase contrast microscopy. In D. L. Farkas, D. V. Nicolau, & R. C. Leif (Eds.), SPIE BiOS. International Society for Optics and Photonics.
4. Dempsey, K. P., Lam, K. P., Smith, W. A., Collins, D. J., Jones, D. J. M., Yang, Y., & Richardson, J. B. (2014). 4-D Hippocampus Measurements of Neurite Growth in vitro. In 2014 IEEE International Conference on Computer and Information Technology
5. Dempsey, K., Brown, S., Richardson, J., & Lam, K. (2015). On Tracking Spinal Disc Cells. Proc. SPIE.
6. Lam, K. P., Dempsey, K. P., Collins, D. J., & Richardson, J. B. (2016). Monitoring stem cells in phase contrast imaging. In D. L. Farkas, D. V. Nicolau, & R. C. Leif (Eds.) (p. 97110E). International Society for Optics and Photonics.
7. Smith, W. A., Lam, K.-P., Dempsey, K. P., Mazzocchi-Jones, D., Richardson, J. B., & Yang, Y. (2014). Label free cell tracking in 3D tissue engineering constructs with high resolution imaging. *SPIE BiOS* (p. 894209). International Society for Optics and Photonics.

Authors contributions to the research

This research has come about with a great deal of input from many people both from the computer science department at Keele and from the Robert Jones and Agnes Hunt Orthopaedic hospital in Oswestry. The specific contributions of the author are detailed below as they relate to each of the methods and results chapters.

Chapter 3: Writing the algorithms for both the mitosis finding and the confluence calculating algorithm in addition to the Canny based algorithm. Running the PHANTAST algorithm for comparison, creating the manual comparison.

Chapter 4: Culturing the MSCs, writing the confluence algorithm, developing the complexity model of neural growth, writing the complexity algorithm of neural growth.

Chapter 5: Setting up and maintaining the microscope during the experiment. Manually tracking the cells, combining the manual tracking with the depth based algorithm to generate biologically meaningful results.

Chapter 6: Maintaining and culturing the cells, setting up cells for imaging and maintaining the microscope during the experiment. Developing entropy based segmentation model, developing weighted index and combining this with normalised cross correlation for the purpose of cell tracking. Creating algorithm that tracked the cells and recorded morphological information about the cells and the vesicles within.

Chapter 7: Maintaining and culturing the cells, making up the gels, setting up cells for imaging and maintaining the microscope during the experiment. Developing entropy based segmentation model, developing weighted index and combining this with normalised cross correlation for the purpose of cell tracking. Combined these with 2.5D tracking algorithms.

Creating algorithm that tracked the cells and recorded morphological information about the cells and the vesicles within.

Chapter 8: Culturing the cells, labelling the cells setting up cells for imaging and maintaining the microscope during the experiment. Tracking the cells manually and developing the algorithm to track the cells and recorded morphological information about the cells. Combining in the SSA algorithm with the data generated so that complex statistics could be drawn from the data

Abbreviations

bFGF: Basic fibroblast growth factor

D_f: Fractal dimension

DMEM: Dulbecco's modified eagle medium

ECM: Extra cellular matrix

FFT: Fast Fourier Transform

FOV: Field of view

MSC: Mesenchymal Stem Cells

NCC: Normalised cross correlation

NCM: Neural culture medium

NV: Normalised variance

PBS: Phosphate-buffered saline

SAD: Sum of absolute difference

SML: Sum Modified Laplacian

SSA: Singular spectrum analysis

STD: Standard deviation

Contributions of this thesis

Chapter 3: The main contribution of this section is the creation of a mitosis finding algorithm that is linked to a tracking algorithm and an improvement on current confluence finding algorithms.

Chapter 4: The main contributions of this section are the creation of an algorithm that uses an automated method to determine whether the cells had adhered and an algorithm was created that could quantify the neural complexity.

Chapter 5: The main contributions of this section are the use of an algorithm that finds the depth of the neurons as they grow and from this show that the neurons grow along the scaffolds rather than towards the cell adherent.

Chapter 6: The main contributions of this section are the creation of an algorithm that segmented the cells through their entropy, tracked the cells as they moved through the culture and quantified the vesicles at each time point. With this the biological conclusion that there are more vesicles on smaller cells was found.

Chapter 7: The main contribution of this section is the combining of the two dimensional and three-dimensional tracking to see the behaviour of the individual cells in the culture.

Chapter 8: The main contribution of this section is the feature extraction algorithm from Chapter 3 with singular spectrum analysis to investigate whether chondrocytes and MSCs were distinguishable from each other when cultured together unlabelled.

1. Introduction

Cells are the building blocks of the human body which are normally specialised by type in accordance with their function. Human cells interact with each other to form the tissues that make up the body. A malfunctioning of the cells can lead to a number of diseases, such as arthritis (loss of cartilage cells), Alzheimer's (loss of neurons) and lumbar degenerative disorder (loss of back disk cells). Equally a change in the function of the cells can cause problems such as cancer and lysosomal storage diseases (a group of Alzheimer's like diseases in children). Consequently, it is important to study the behaviour and interactions of these cells at the microscale level, so that the causes of cellular irregularities can be identified; and from this, possible treatments can be devised.

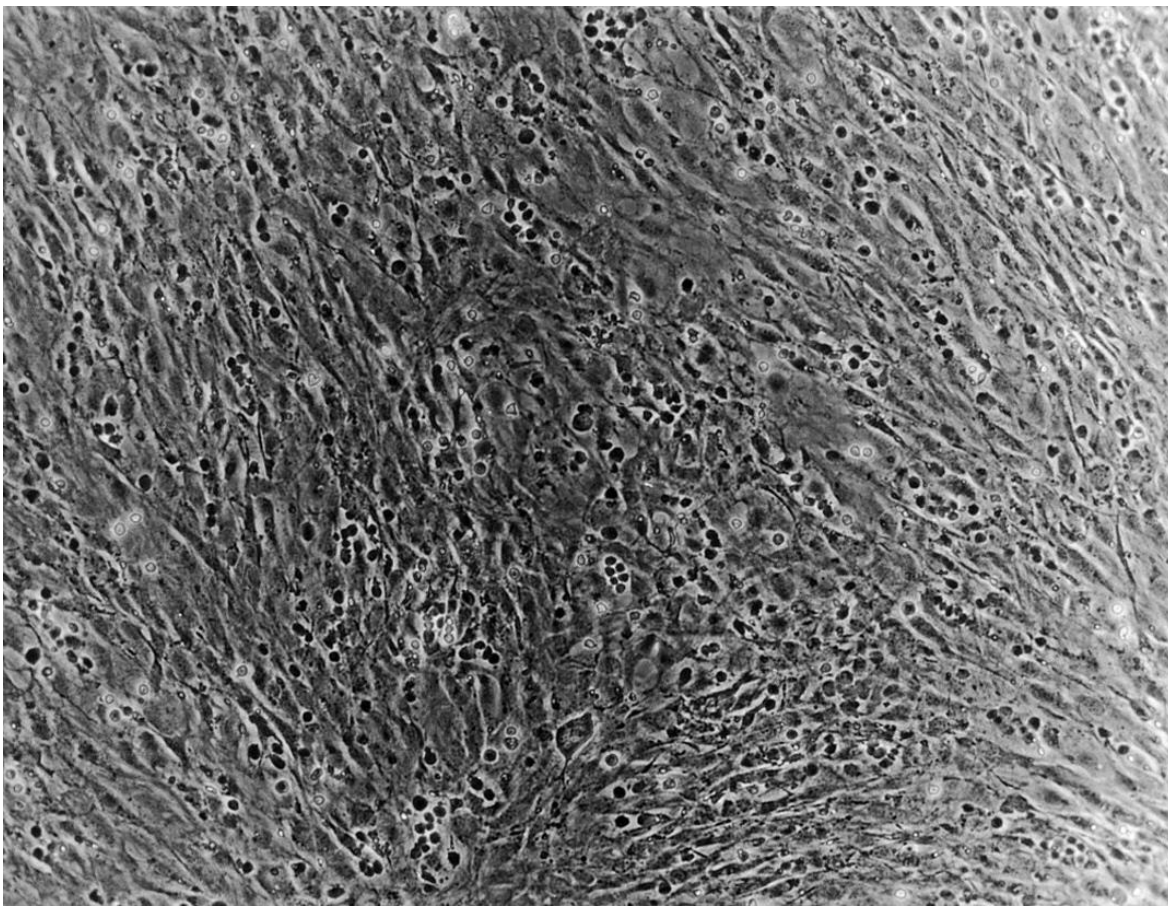

Figure 1: A stromal culture preserved in formaldehyde, these cells have preserved their morphology from the time of fixing, adapted from (Burger et al., 1999)

1.1. Fixed cells

The most common method of studying cells is to *fix* the cell in formaldehyde and so to see a snapshot of the cell in time. Fixation of tissue is done for several reasons. One of these reasons is to kill the tissue so that post-mortem decay is prevented (Carson & Hladik, 2009). Formaldehyde usually acts to disable intrinsic biomolecules which otherwise digest or damage the sample. In addition, formaldehyde is toxic to most common microorganisms (bacteria in particular) that might exist in a tissue sample or which might otherwise attack the fixed tissue. Finally, formaldehyde alters the cells or tissues on a molecular level to increase their mechanical strength or stability. This increased strength and rigidity can help preserve the *morphology*, i.e. shape and structure, of the sample, shown in Figure 1.

The fixation of tissue has provided insight into the workings of the cell and is still a useful technique that continues to be used to this day (Acosta et al., 2012; de Boer et al., 2012; Hesse et al., 2012; Zheng et al., 2009); however, even the most careful fixation does alter the sample and introduce artefacts that can interfere with interpretation of cellular ultrastructure. Issues such as “Swiss cheese holes”, where the cultures have large circular holes and sponge artefacts that wear away at the edge of the cultures, can be problematic in analysis (Chatterjee, 2014a). As the overall knowledge of microscopy grows the understanding of the causes of these artefacts has also grown. As such there are now methods that either reduce the artefacts or allow image analysis to work around these issues (Chatterjee, 2014b; Ryter, 1988; Sanei & Hassani, 2015). Nevertheless, these artefacts do limit the information that can be gathered from cell fixing. Despite this limitation, the ability to preserve the cell by fixing has given a great insight into the cellular composition (Acosta et al., 2012; Patel, McLaren, Hodge, & Bourne, 2001; Pelvig, Pakkenberg, Stark, & Pakkenberg, 2008; Tarvainen, Saarinen, Laitinen, Korpinen, & Viitanen, 2002; Yong, Dong, Chan-Park, Song, & Chen, 2012). However, such studies are inherently static and cannot be

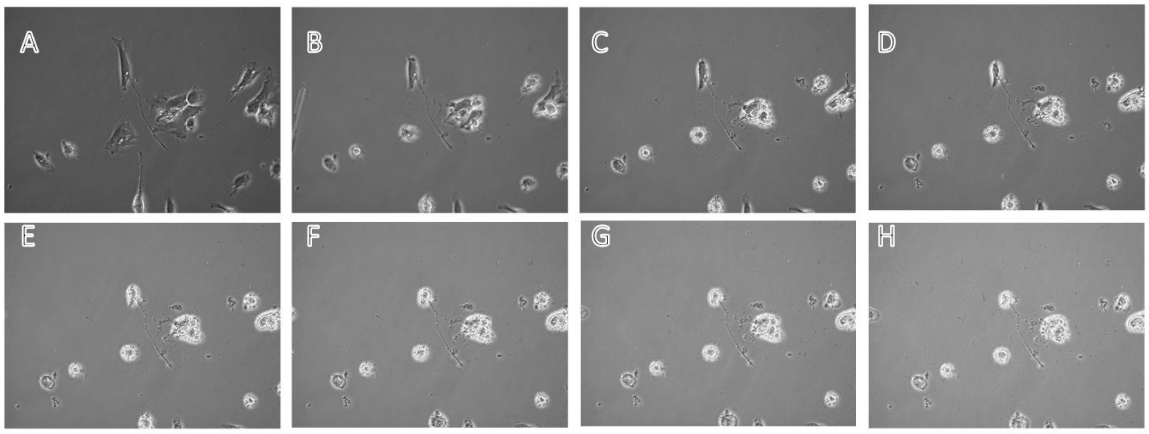

Figure 2: A time lapse of a culture of back disk cells. Each image is taken at the same coordinates on the microscope. In this figure: A is the first image taken under the microscope, each subsequent image (B-H) is taken 20 minutes after the previous one. Using this technique, it is possible to see the morphological changes in each cell.

used to track the lifecycle of a single cell. In order to understand changes in cellular behaviour it is necessary to track the cell over time.

1.2. Time lapse microscopy

Time lapse microscopy is a series of microscope images of a cells in a live culture taken at a certain time frequency. An example with a culture of back disk cells is shown in Figure 1. This technique has been in use since the 1890s, when a series of images of cells was taken on photographic film. More recently the improvement in photographic technology led to this being replaced by video tape and now digital images (Landecker, 2006). In addition to the improvements in imaging technology, there have also been improvements in the techniques used to increase the longevity of cultured cells whilst imaging. The consequence of this has been that a huge amount of data can be generated from a single experiment, resulting in a need for computational algorithms that can produce biologically meaningful results from all of this data.

1.3. Spatiotemporal Information

This thesis looks at a number of cell types that are currently central to many areas of *cell therapy*. Cell therapy is a medical treatment in which cellular material is injected into a

patient; this generally means intact, living cells. For example, *mesenchymal stem cells* (MSCs) can be extracted from a healthy part of a patient and used to regrow cartilage in an arthritic joint (Section 2.1.1.). The outcomes of cell therapy are different for different patients, so whilst 80% of patient that have been treated with cell therapy for osteoarthritis see a 15-year increase in terms of the life of a joint, another 20% will see no improvement (Hanifi, Richardson, Kuiper, Roberts, & Pleshko, 2012).

This is one of a number of studies that aims to investigate this differing outcome. Whilst other projects investigate the genomics and proteomics of the cells, this project aims to create a tool that uses the *spatiotemporal* information of the cells to predict an outcome. The *spatiotemporal* information of the cells is information in the x, y, and z planes as well as in the time dimension (t). From this a set of computationally tractable and biologically meaningful metrics will be developed that capture variations in cellular behaviour, with the aim to link dynamic biological processes of individual cells to the outcomes of a particular experiment. As such, the ensuing research will help identify interventions that improve the culturing of cells for cell therapy by providing the tools needed for these individualised treatments.

Since microscopy is an inherently visual medium, the initial spatiotemporal characteristics to be looked at would be the shape, or *morphology*, of the cell, as well as its path and speed of travel. Some examples of possible static measurements, i.e. those that do not depend on time can be seen in Figure 3. Even within a single cell culture it would be expected that the individual cells would have a different matrix of morphological features. It is necessary here to build up a set that can improve the culturing methods of those working in cell therapy. These measurements act as a basis on which the changing behaviour of the cells can be examined. For example, the area of the cell will change over time. During the course of the experiments presented here it was not known whether these measurements would be useful

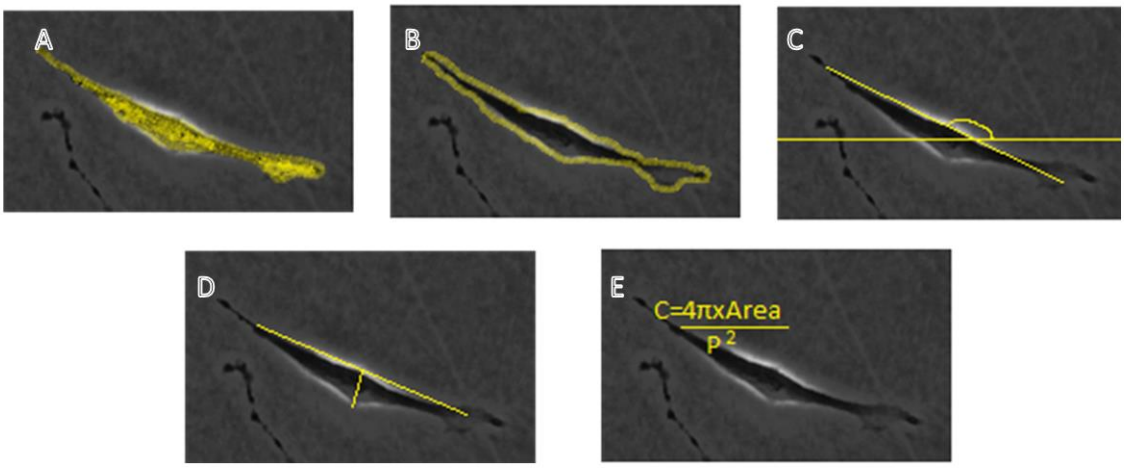

Figure 3: Spatial morphological cell characteristics. left to right, top to bottom: A) Area (total area covered by cell), B) Perimeter (length around the edge of the cell), C) Orientation (angle between the longest length of the cell and a standard outside dimension (x-axis in this case)), D) Major and minor axis length (major length being the longest length of the cell, minor being the length perpendicular to this) and E) circularity (4πxArea/Perimeter)

for the cultures that were being studied, but by having a wide array of measurements it would be possible to determine which were the most useful.

1.4. Fluorescence

Conventionally most of the studies of continuous cell cultures, i.e. those used in time lapse microscopy, have used fluorescent markers to enhance the images obtained with the view to identifying and/or characterising the attributes of interest; e.g. cell types and their chemical fingerprints. This produces a set of images at different wavelengths that can be put together artificially to produce an image such as Figure 4. The cells are made to fluoresce by attaching a fluorescent protein to a protein of interest within the cell. In cell biology, a protein is a large biomolecule that performs a specialist function inside or outside of a cell. There are two main ways by which a fluorescing protein can be attached to a cell: it can either be attached to the whole cell for ease of visibility or it can be attached to specific proteins within the cell to determine their location with respect to the rest of the cell. Looking down a microscope a cell excited by a particular wavelength of light (dependent on the fluorescing protein used) will produce an image in which only the proteins of interest will be fluorescing.

However, the drawback of fluorescent microscopy is that the use of the fluorescent proteins within the cell changes the fundamental biology of the cell. Therefore, the results obtained are not those for the cell in its natural state (Jaccard et al., 2013). In many cases, staining reagents and fluorescence markers are toxic for living cells making them unsuitable for long-term studies due to the limits of the fluorescent lifetime (Olivos-Pérez, Iturbe-Castillo, Sánchez-de-la-Llave, Ramos-García, & Treviño-Palacios, 2006). Importantly, however,

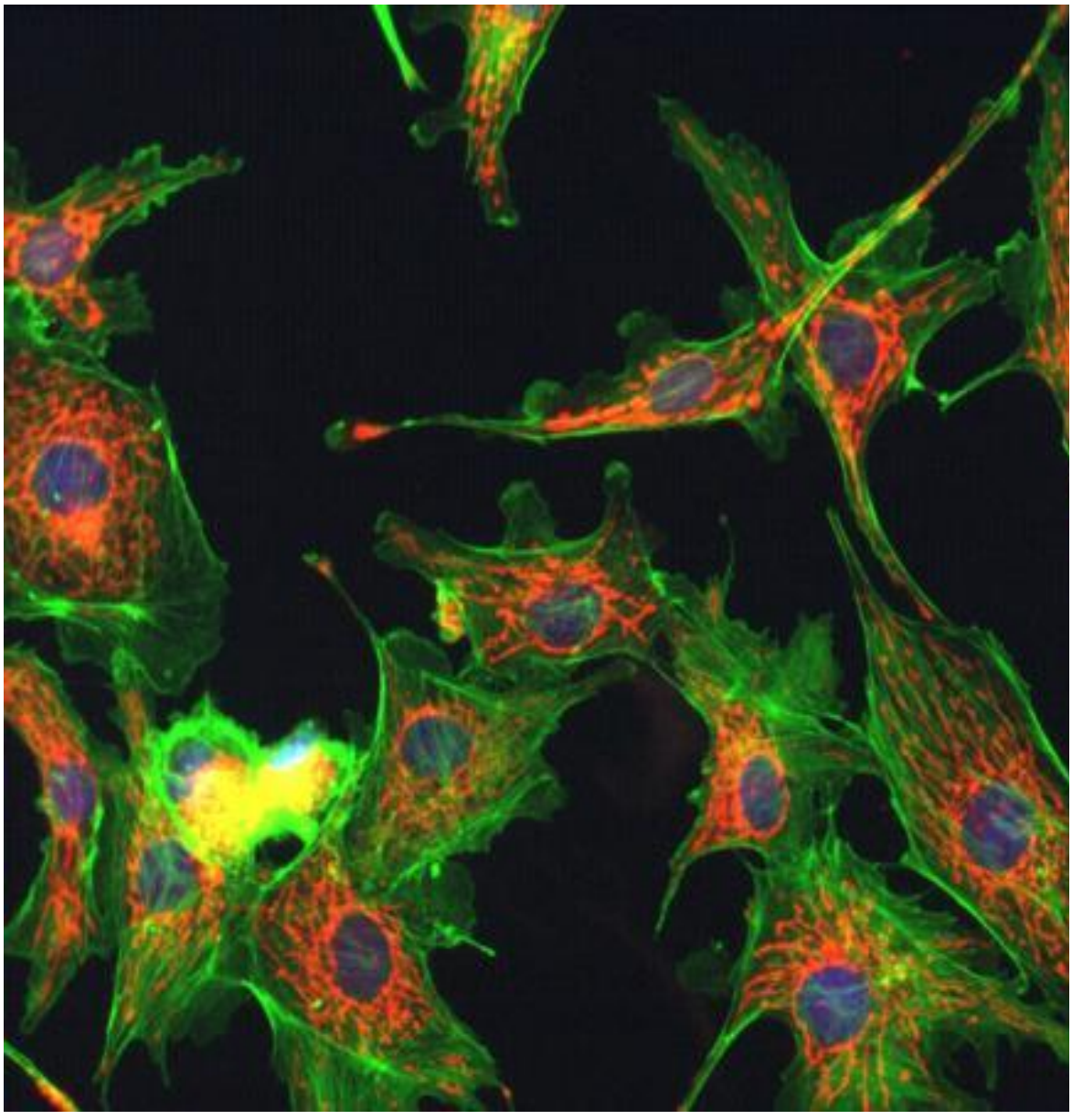

Figure 4:Fluorescence microscopy image of cells, acquired at the Integrated Microscopy Facility, University of California, Santa Barbara, by Dr. Kalju Kahn.

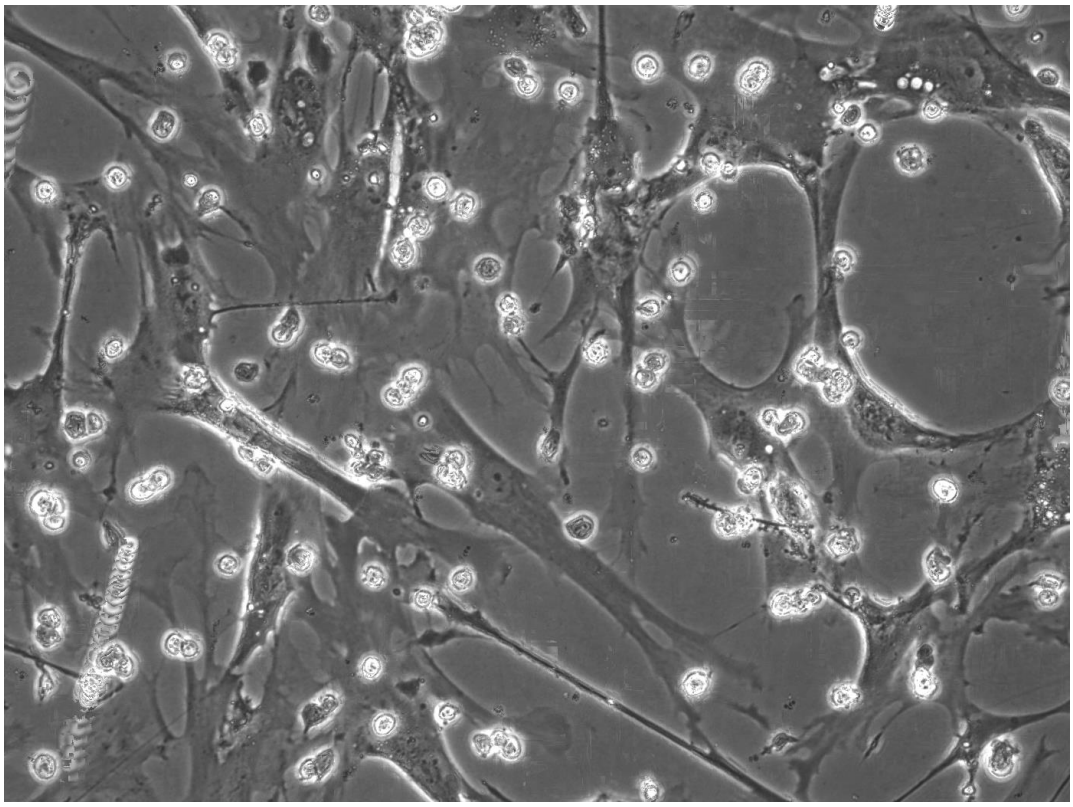

Figure 5: Phase contrast image of a mixed cell culture, MSCs and chondrytes

these cells, altered by fluorescence, cannot be used in humans after they have been studied so an alternative imagining method is needed.

1.5. Phase contrast microscopy

In conjunction with the discovery of different coloured fluorescent proteins, fluorescent technology has become a common choice of microscopy research. Since the primary goal of this project is to investigate cells that can subsequently be used in clinical research it is necessary that the analysis on the cells is non-invasive. A suitable candidate for non-invasive microscopy is phase contrast imaging, as shown in Figure 5; the phase contrast microscope uses the fact that the light passing through a transparent part of the specimen travels slower and, due to this is shifted compared to the uninfluenced light. This difference in phase is not visible to the human eye. However, the change in phase can be increased to half a wavelength by a transparent phase-plate in the microscope and thereby causing a difference in

brightness. This makes the transparent object shine out in contrast to its surroundings since the image produced is that of a phase shift, the final image provides greater contrast than a standard light microscope (Burch & Stock, 1942).The principles behind phase contrast are well established and microscopes that work along these lines are relatively cheap. As a result, phase contrast microscopes can be found in most laboratories. In order to study these cells, algorithms can be created to extract different data. Due to the wide availability of phase contrast microscopes, making algorithms for them will be beneficial to many research groups. Since the cells do not require any enhancement to be seen, when phase contrast microscopy is coupled with an incubator platform it is possible to carry out long term (three days to a week) live cell studies on systems such as the CellIQ2 microscope shown in Figure 6.

Whilst it remains a relatively cheap and useful tool for noninvasively studying cell cultures there are problems in computationally analysing the images that are produced by phase

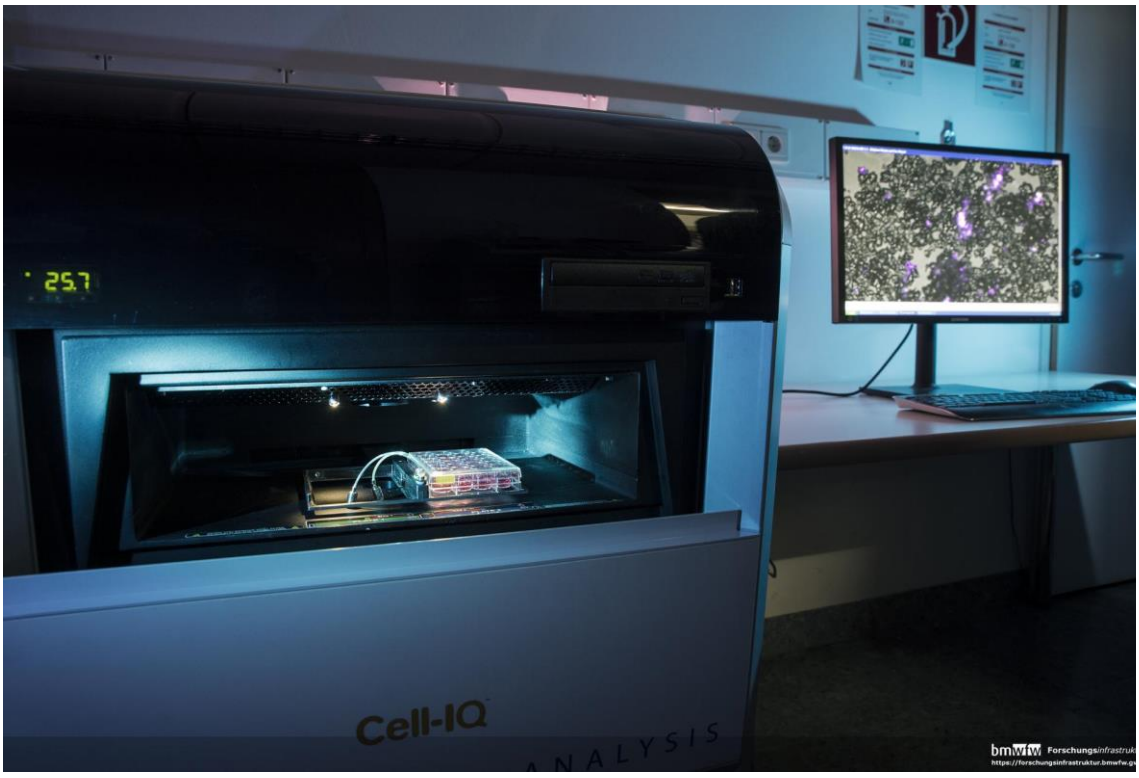

Figure 6: Coupled cell incubator and phase contrast microscope. By imaging the cells in an incubator it is possible to study the behaviour of the culture over a long period of time

contrast imaging. These issues represent the major problems faced in this project. When looking to analyse a cell from a culture the first task is to segment the cell, i.e. distinguish the position of the cell from the background and surrounding cells. Phase contrast microscopy in particular is problematic for this due to the two artefacts that it creates. The major problems associated with automated segmentation of phase contrast images can be attributed to the two artefacts described in Figure 7; namely, (a) the *halo* which is manifested as a bright ring in the image around the cell, and (b) the *shade off*, which is often displayed as a notable reduction of contrast moving from the centre of larger cell objects toward their edges. The halo presents a problem as it makes the cell appear larger than it actually is (by up to 20% (Bradhurst, Boles, & Xiao, 2008)). The shade off is a problem in both distinguishing the cell from the background and in distinguishing it from other cells Attempts have been made to address these artefacts (Bradhurst et al., 2008; Yin, Li, Kanade, & Chen, 2010), however they have either been computationally intensive (Yin et al., 2010), or more importantly they do not work well in high cultures that cover more than 40% of the field of view (Bradhurst et al., 2008).

There are some computer algorithms available for segmenting phase contrast imaging, however a great deal of work is still done with very limited support. For example, to segment the cell in Figure 7, a user would be asked to manually draw the outline of the cell. Since most cultures have over 100 cells this can quickly become a time consuming task. This problem is compounded when we consider live cell microscopy where there would be an image produced every 20 minutes for up to a week. As such, without the use of computational algorithms, it is immensely time consuming to study these living cells in detail, as the cells are constantly changing position and shape so manual tracking would require marking a cell on every frame and following it throughout the whole time sequence.

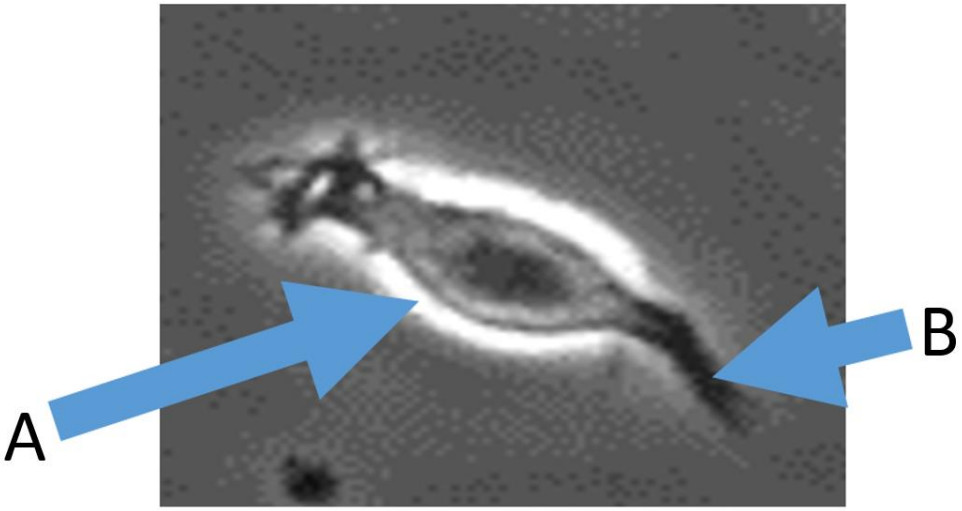

Figure 7: Showing the halo and shade off artefacts. A) Bright halo surrounding parts of the cell making the cell appear larger than it is. B) Shade off where the edge of the cell is indistinguishable from the background

The second part of the image analysis used here is tracking the cells - that is being able to identify a cell on any given image in the time sequence. Figure 8 shows images of the same culture at 1 hour, 2 hours and 24 hours after the start of imaging. Highlighted in red is the same cell at each of these time periods. From this it is clear to see that it is not possible to tell just by looking at the cells which one corresponds to which by the end of the 24-hour period so without an algorithm a researcher would have to manually track the cells once every 20 minutes.

Whilst many laboratories are still monitoring cells by hand (Acosta et al., 2012 for example) in the past decade, cell tracking algorithms and cell linage tracking algorithms have become commercially and freely available, predominantly for fluorescently labelled cells lines (Al-Kofahi, Radke, & Goderie, 2006; Lou & Hamprecht, 2011; Yang, Mackey, Ianzini, Gallardo, & Sonka, 2005) but also for some unlabelled cultures (Debeir, Van Ham, Kiss, & Decaestecker, 2005; Hand, Sun, Barber, Hose, & MacNeil, 2009a; Huh, Ker, Bise, Chen, & Kanade, 2011). Within these are several attempts to overcome the problems presented by phase microscopy. An early approach used an active contour algorithm to detect the position

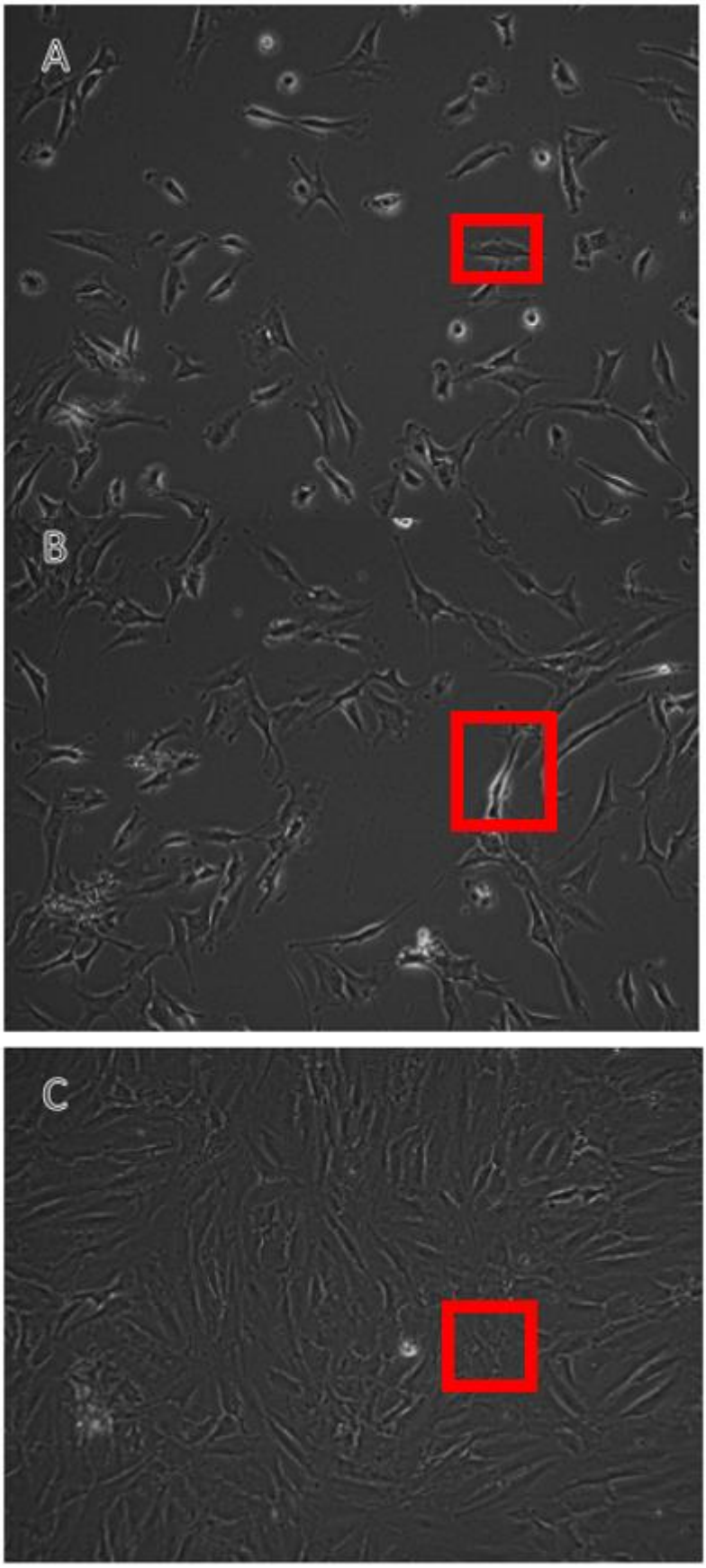

Figure 8: Time lapse image of MSC culture. A) One hour after start of incubation B) two hours after start of incubation C) 24 hours after start of incubation. Highlighted in red is the same cell at each of these

of the cell's leading edge in phase-contrast images (Grimm, Verkhovsky, Mogilner, & Meister, 2003). This approach was subsequently augmented by guiding the active contour (F. Li, Zhou, Zhao, & Wong, 2009). This procedure, however, does not work reliably for the shade off artefact, and would be difficult to extend to the irregular motion of many cell types. In a different approach, a statistical procedure using pattern recognition techniques (Bradhurst et al., 2008) has been used, relying on prior knowledge about the cell shape. Completely automatic algorithms for detecting and tracking large numbers of cells in phase-contrast images have also been presented (Hand, Sun, Barber, Hose, & MacNeil, 2009b; K. Li et al., 2008a) These approaches emphasize tracking performance using concepts from, image registration (Hand et al., 2009b) or multi-model motion filtering (K. Li et al., 2008b). Typically, however, these outline geometries that would be necessary to develop the tools to predict culture outcomes rely heavily on high computational power.

1.6. Aims

The aim of the research described in this thesis is to determine how single cells affect a culture as a whole. With this outcome in mind an algorithm that can track cells and measure some of their morphological features will need to be developed.

This project aims to create an algorithm that is capable of tracking a variety of cells types within both single cultures and mixed cultures, and from this to generate data that is relevant to current clinical trials.

1.7. Objectives

1. To create an algorithm capable of tracking the movement of non-neural type cells.
2. To create an algorithm capable of tracking neural tips as they grow in vitro.

3. To extract from these algorithms a suitable set of cell biometrics that can be used in the context of a co-culture to distinguish the cell types without labelling.
4. To extract from these algorithms a suitable set of cell biometrics that can be used in the context of cell cycle to determine the points of mitosis, differentiation and apoptosis.
5. To determine the behaviour of cells in gels and to determine the limits of microscopy on the gels.

1.8. Thesis organisation

The remainder of this thesis looks at methods that track the movement of individual cells within cultures. In Chapter 2 information is given to the three types of cells that are to be studied in this thesis: mesenchymal stem cells, hippocampal neurons and back disk cells. In Chapter 2 there is also presented the current understanding of the best computational methods to create the algorithms that are needed for this research and the algorithms that are currently available and their strength and limitations. The subsequent chapters look at the methodology used to track the cells within the cultures. Chapter 4 describes a method that was used to identify the events of cellular division. In Chapter 5 a method for quantifying the amount of growth that a neuron has undergone is presented. Chapter 6 expands on this by looking at the growth of hippocampal neurons on a 3D scaffold. In Chapter 7, a method for quantifying the number of vesicles on the back disk cells is proposed. Chapter 8 looks at methods to track chondrocytes as they move through 3D extracellular matrix like gels. Chapter 9 investigates the behaviour of MSCs and chondrocytes in a co-culture. The results of all of these are discussed in Chapter 10.

2. Background

In this chapter, the current literature relating to the cells themselves is presented as well as the methods used to image the cells, and more specifically, how these images can be processed to gain an understanding of the cellular behaviour. This begins now with a basic overview of the cells, before progressing to the algorithms used to track them.

2.1. Biology

This section describes the three different cell types used in this thesis: mesenchymal stem cells, hippocampal neurons and back disk cells. Mesenchymal stem cells (MSCs) are a type of stem cell that are found in the body after birth and can be used in a variety of contexts in regenerative medicine. The context of MSCs in this thesis is repairing the cartilage damage from osteoarthritis in the knee. Hippocampal neurons are the neurons that make up the hippocampus, this plays important roles in the consolidation of information from short-term memory to long-term memory and spatial navigation. The disks of the back support the constituent pieces of the spine; regenerative medicine here, looks to repair certain types of damage to the back. This section looks at these cell types in more detail and how a tracking algorithm could be used within this context. The cells described here are chosen as they are cells that are being studied by clinicians for applications in regenerative medicine.

2.1.1. Mesenchymal stem cells

Regenerative medicine is a branch of research in tissue engineering and molecular biology which deals with the process of replacing, engineering or regenerating human cells, tissues or organs to restore or establish normal function. Mesenchymal stem cells (MSCs) are an example of ‘adult’ stem cells. They are found in the body after birth and not just in the embryo. In 2006, the International Society for Cellular Therapy attempted a universal

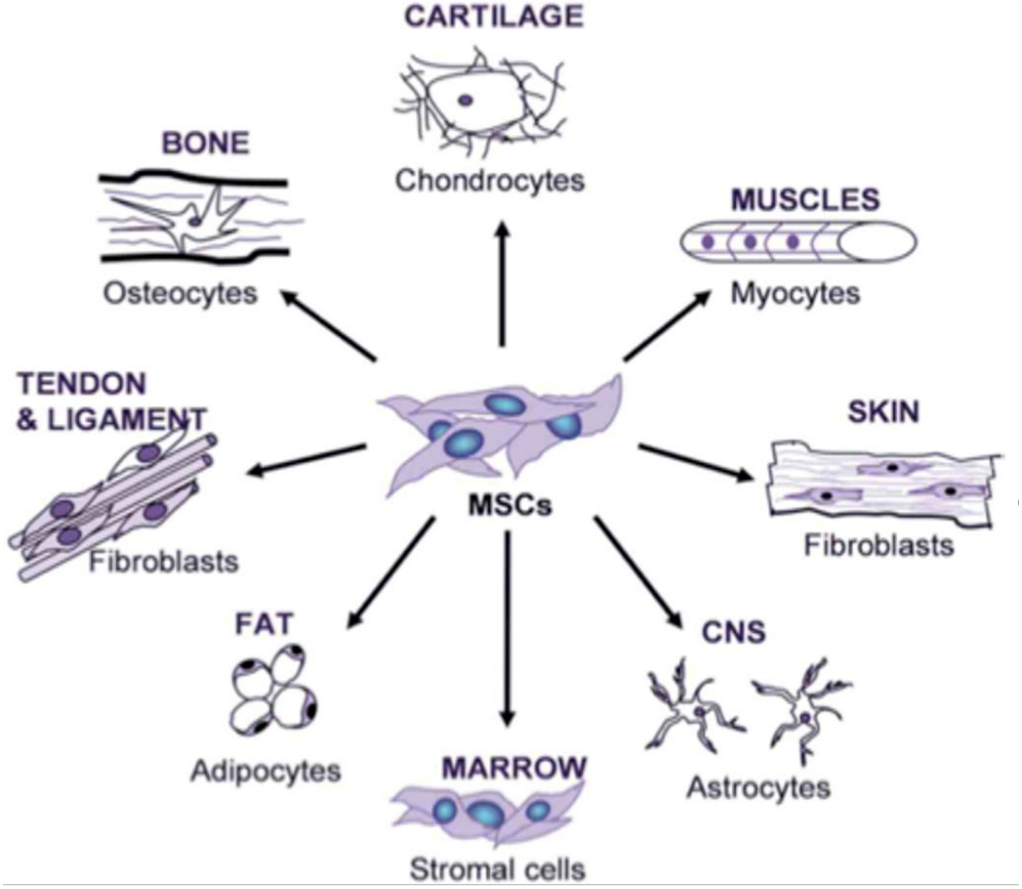

Figure 9: Adapted from Knee surgery clinic, showing the potential cell types that an MSC can differentiate into

definition of a MSC[1] (Dominici et al., 2006). As such it is now agreed that they are multipotent stem cell, that is, they can produce more than one type of specialised cell in the body, but not all types (see Figure 9) In addition, they can self-renew, dividing to produce more MSCs. Within the body they function to produce the chondrocytes, osteoblasts and fat needed for bone repair (Baksh, Song, & Tuan, 2004). Since they can be used to create different tissue types they are being extensively studied in the field of regenerative medicine.

MSCs have been used in clinical trials for bone repair since 1995 (Lazarus, Haynesworth, Gerson, Rosenthal, & Caplan, 1995). Osteoarthritis is the most common form of joint disease

[1] that it should adhere to plastic in standard culture conditions that it should express (95%+) CD105, CD73, CD90 and not express (2%+) CD45, CD34, CD14 or CD11b, CD79a or CD19, HLA-DR and should give at least three differentiated lineages: osteoblastic, adipogenic, chondroblastic

which causes joint pain and stiffness (ONS, 2013). Surgical intervention for osteoarthritis is very costly to the National Health Service and has a large impact on the patient in terms of their recovery time and their functional independence. Recent results of these clinical trials have shown that 80% of patients find that MSC based treatment improves their quality of life by alleviating pain whilst extending the life of their natural joints by 15±3 years (Hanifi et al., 2012).

Although the treatment has been shown to work there has been a debate in recent years about the true nature of MSCs, with some arguing that MSCs are not a single cell type but instead a collection of cells. There remains controversy surrounding MSCs as slight variation in the methods used to collect the cells can alter the differentiation potential of the cells leaving it hard to reproduce work. This has been compounded in recent years by studies that suggest that cells called MSCs are, in fact, a culture made up of several cell types (James et al., 2015). In addition to not fully understanding their nature, the differentiation potential of MSCs has recently been debated. The normal method to induce differentiation in MSCs is to culture them together with the cell type that they should differentiate into. The genotype of the MSC culture is tested both before and after this culturing to confirm that differentiation has happened (Levorson, Santoro, Kasper, & Mikos, 2014). However, some recent work has suggested that the MSCs do not differentiate at all, instead their presence enhances the proliferation of the cells with which they are cultured (James et al., 2015). In addition, there is another school of thought that suggests that the MSCs themselves do not encourage this growth, instead it is the proteins excreted by the MSCs that promote the growth (Bian, Zhai, Mauck, & Burdick, 2011; de Windt et al., 2015; Giovannini et al., 2010; Wu, Leijten, Blitterswijk, & Karperien, 2013).

The use of MSCs in tissue engineering is a current area of active research for many groups (Baksh et al., 2004; Curran, Chen, & Hunt, 2006; Hong et al., 2005a; K. P. Lam et al., 2013; Nöth, Steinert, & Tuan, 2008; Romanov, Svintsitskaya, & Smirnov, 2003a; Sachs et al., 2012; K. T. Wright et al., 2007). The reason the disagreement around the role of the MSC exists is because different researchers use different methods to determine the cellular make-up of their cultures. With some studies looking at two dimensional monolayers where the culture is adhered to a sheet of plastic (Bian et al., 2011; Dahlin, Ni, Meretoja, Kasper, & Mikos, 2014; Meretoja, Dahlin, Kasper, & Mikos, 2012), whilst others look at 3D structures of cells in freestanding pellets (Acharya et al., 2012; Giovannini et al., 2010). Other studies attempted to combine these two approaches by creating a 3D structure onto which the cells could be adhered, shown in Figure 10 (de Windt et al., 2015; Levorson et al., 2014; Meretoja et al., 2012). In addition to this each study defines whether the culture had been a success in producing cartilage from the MSCs in a different way. Some studies assumed that if the *extra cellular matrix* (ECM), a collection of extracellular molecules secreted by cells that provides structural and biochemical support to the surrounding cells and is very necessary in the formation of cartilage, had formed then the MSCs had differentiated (de Windt et al., 2015; Levorson et al., 2014). Other studies determined successful differentiation by the longevity

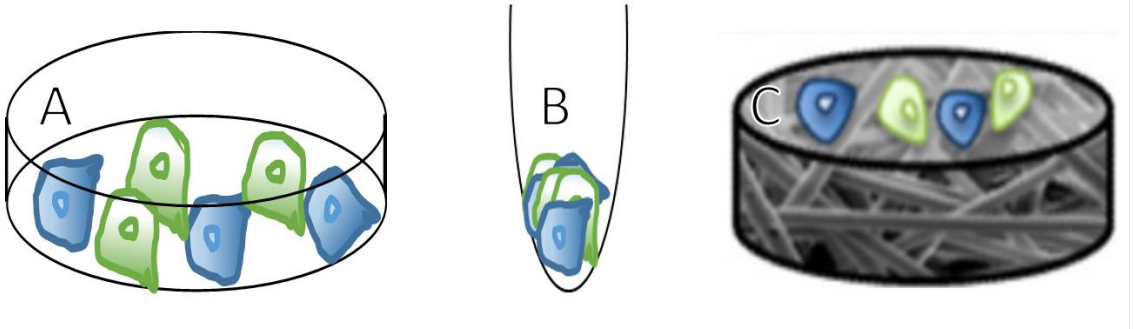

Figure 10: different methods of co-culturing stem cells. A) Cells grown in a 2D monolayers where the culture is adhered to a sheet of plastic at the bottom of the dish B) cells grown in a 3D structures of cells in freestanding pellets C) adapted from (Levorson et al., 2014) cells grown in a 3D structure onto which the cells could be adhered

of the culture (Acharya et al., 2012; Bian et al., 2011; Dahlin et al., 2014; Meretoja et al., 2012; Meretoja, Dahlin, Wright, Kasper, & Mikos, 2014).

What is common in all the above-mentioned work, is that they were looking at the culture as a whole rather than studying individual cells. Cell tracking is an approach that would allow the study of individual cells. One of the aims of this project is to build a set of biometrics which can be used to identify MSCs even in mixed cultures. From this it is hoped that it would be possible to see through the changes in morphology to determine whether the individual cells change shape. It is hoped that such a tool could be used by clinicians to see if the cells morphologies are linked to patient outcomes. For example, it could be seen that cultures with more motile cells lead to better outcomes and thus those with less motile cells would not be suitable candidates for this form of treatment. This would allow for more individualised treatment of patients.

Given the potential impact that MSCs may have on regenerative medicine as described previously, there is a growing need for automated tools to analyse and characterise the behaviours of these cells in vitro in an automated and high throughput fashion. Biologically speaking the morphology of cells is linked to their dynamic behaviour (Bertossa, 2011) and, as such, a quantitative characterisation of cell morphology (Bradhurst et al., 2008) could help to determine at which points cells are going through mitosis (cell division), apoptosis (programmed cell death) etc. Additionally, when culturing cells for clinical or research purposes, it is advantageous to be able to predict the fate of the MSC culture in a timely fashion; for example, to determine the long-term viability of the culture. One potential approach would be to monitor the early behaviours of the cell in order to accurately predict the fate of the culture (W. Li, Jiang, & Ding, 2012). The rapid advancement in computing storage and image capturing has made live cell imaging a valuable tool that allows for the observation of the culture over time.

Although the precise identity of MSCs remains a subject of on-going research, further understanding of the biological properties of the cells that are currently assumed to be MSCs will be greatly advanced by analysing the mechanisms that govern their self-renewal and differentiation potential.

Currently there is a divide between the laboratory based methods of understanding the use of stem cells and clinical best practice. Conventionally, most cell imaging based studies have used fluorescent markers to enhance the information given by the cells. This offers great insight into the functions of the proteins at molecular level and there are computer vision tools that have been created to deal with a number of data collection and cell tracking problems. Within a clinical setting, it is important that the fundamental biology of the cells is not altered, therefore the best available method to study the cells, fluorescent microscopy, cannot be used.

Whilst improvements in MSC based therapies for OA are evident (Baksh et al., 2004; Bradhurst et al., 2008; Curran et al., 2006; Hong et al., 2005b; Romanov, Svintsitskaya, & Smirnov, 2003b), the underlying reason that such treatment works on some patients but not on others is largely unknown. To facilitate clinical translation of our research in the science and biology of stem cells, it is crucial to investigate a practical alternative to fluorescent microscopy by developing similarly robust methods in phase contrast microscopy, a non-invasive imaging technology that does not rely on potentially phenotype-changing measures to study the cell. Additionally, most studies focus on end point assays, studies that just look at the state of the cells after a period of culturing rather than observing the culture throughout. This means that there is a distinct lack of a reliable approach for identifying different populations within the culture as it grows. Here, to meet both current and future clinical demands, there is a need for *(i)* novel cell-biological analytics and toolsets to enable a better

understanding of biology of MSCs and *(ii)* reliable, cost effective and predictable procedures for the in vitro manufacturing of these cells.

The challenges addressed in this thesis for MSCs look at finding a set of biomarkers that determine their characteristics with the aim to be able to identify an MSC in a mixed culture. This will be achieved through the use of a cell tracking algorithm. This should digitally label each cell and maintain a record of the changing morphology of the cell. From this computer vision and signal processing techniques can be used to see if there are any noticeable patterns that can be used to predict the behaviour of the culture.

2.1.2. Vesicles within back disk cells

The spine is made up of 26 separate moving parts. Before humans evolved to walking on two feet it would have originally been curved, however for the sake of improved balance it had to become S shaped (Wells, DeSilva, & Stock, 2012). A direct result of this is that the

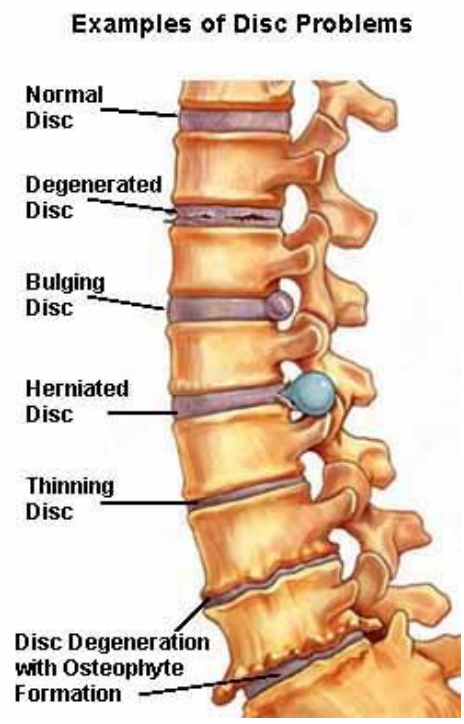

Figure 11: Back disk problems adapted from back surgery clinic

disks of the spine are under a vast amount of pressure which can lead to a number of problems illustrated in Figure 11.

With advances in regenerative medicine it is hoped that it will be possible to regrow back disks in a way that can alleviate the pain associated with their problems. In order to do this further understanding is needed of the cells that make up the back disks. One avenue of such research is on the *vesicles* within the cells.

In cell biology, a vesicle is a small *organelle* (constituent part of the cell) consisting of fluid enclosed by a membrane (see Figure 12). Vesicles can be viewed as the gut of the cell in that they perform a variety of vital functions in the maintenance of the cell including metabolism, transport, buoyancy control, and enzyme storage (Walsby, 1994). As such, they are particularly important for the trafficking of substances into and out of cells. For example, *lysosomes* are vesicles with enzymes which carry out functions to break down worn-out organelles, waste materials and substances/molecules that the cell may engulf. Thus, the absence of vesicles within a cell could lead to a build-up of waste substances which could undermine the proper functioning of the cell.

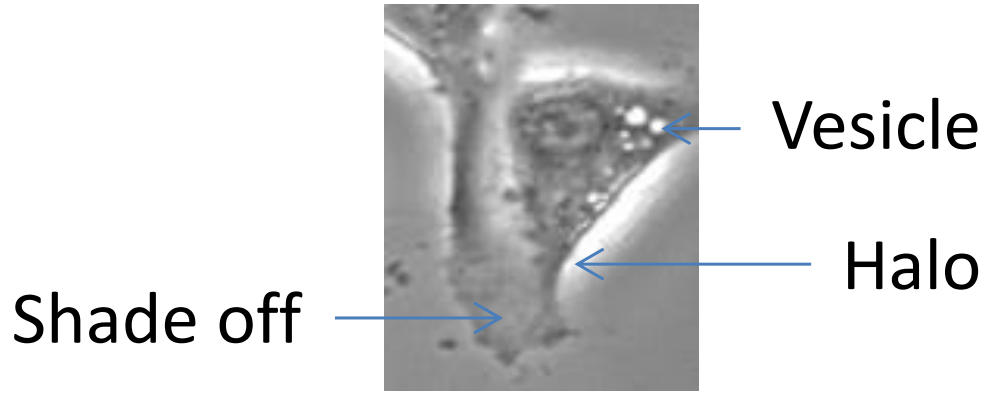

Figure 12: A back disk cell imaged with PC microscopy. Showing Vesicle on cell surface

Given this large array of functionalities, it should be apparent that the study of vesicles is becoming increasingly important in all fields of cell biology. At present, however, whilst many tools exist to track cells, none are capable of monitoring the vesicles inside individual cells particularly when the cells are unlabelled with fluorescent markers. This is important as recent work has shown that the presence on vesicles on the surface of the cell, as opposed to within it, where the vesicle would be expected to function, may be an indicator of imminent cell death (Brown, Richardson, & Lam, 2015; György et al., 2011). Vesicles within the cells cannot be seen by phase contrast microscopy. This was found in a study that induced back disk cell death with hydrogen peroxide. It was observed that visible vesicles, i.e. those on the cell surface, were present in greater number just prior to cell death.

It is possible to test whether an increase in surface vesicles leads to an increase in the chance of cell death but it would be a laborious process as the changing number of vesicles in each cell would have to be counted manually for all time frames across the experiment. In addition to looking at the number of vesicles automatically, it would be relatively simple to compare this to aspects of the cell biometrics and thus build a greater understanding of the behaviour of vesicles within a cell.

This project aims to create an algorithm that can quantify the changing number of vesicles on the cells throughout the time period of the culture. This will then be linked to the morphology of the cells at that time to see if there are any other predictors, apart from vesicle number, of programmed cell death.

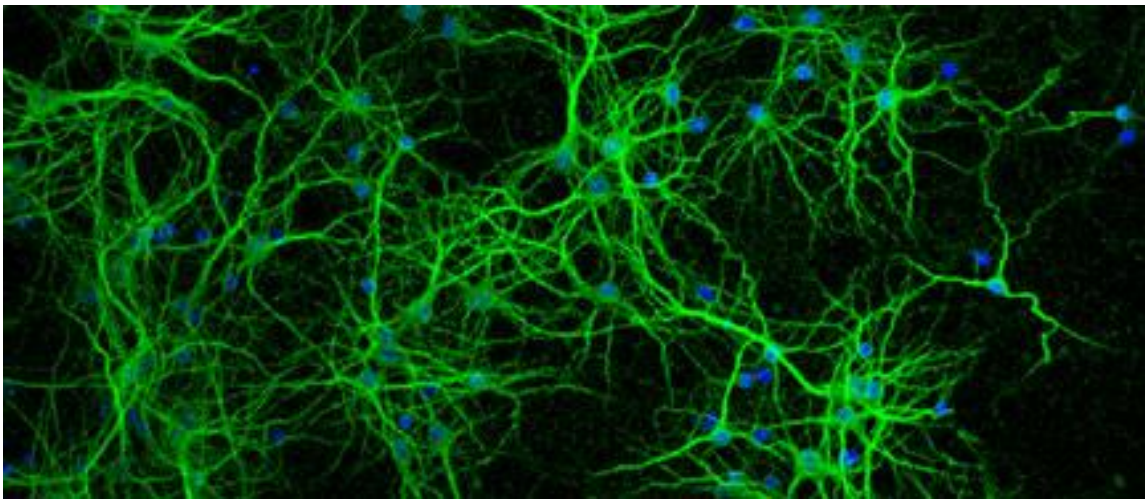

Figure 13: Fluorescently labelled hippocampal neurons in vitro

2.1.3. Hippocampal neurons

The core component of the nervous system in general, and the brain in particular, is the neuron or nerve cell. A neuron is an electrically excitable cell that processes and transmits information by electro-chemical signalling. Unlike other cells, neurons never divide, and neither do they die off to be replaced by new ones. A typical neuron possesses a cell body, dendrites (long, feathery filaments attached to the cell body in a complex branching dendritic tree) and a single axon (a special, extra-long, branched cellular filament, which may be thousands of times the length of the soma), shown in Figure 13 and Figure 14. Since, unlike other cell types, neurons do not divide to produce new cell types, neuronal damage is permanent. The brain, which is made up of neurons, is the most complex organ in a vertebrate's body. In a typical human, the cerebral cortex (the largest part of the brain) is

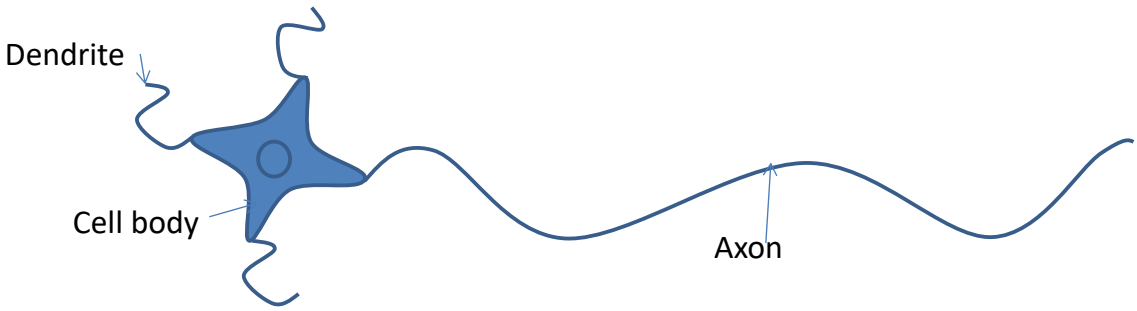

Figure 14: Showing a simplified version of the constituent parts of a neuron

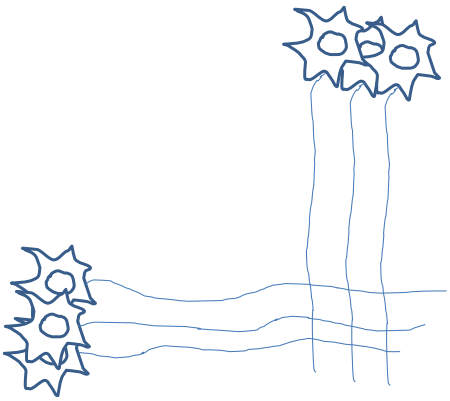

Figure 15: Simple 2D model of the hippocampus. The neurites grow out of the cell bodies and form collection of simple synapses where they cross.

estimated to contain 15–33 billion neurons (Pelvig et al., 2008). Despite being protected by the thick bones of the skull, suspended in cerebrospinal fluid, and isolated from the bloodstream by the blood–brain barrier, the human brain is susceptible to damage and disease. The most common forms of physical damage are closed head injuries such as a blow to the head or other trauma, a stroke, or poisoning by a number of chemicals that can act as neurotoxins, such as alcohol. Infection of the brain, though serious, is rare because of the protective blood-to brain and blood-to cerebral fluid barriers. The human brain is also susceptible to degenerative disorders, such as Parkinson's disease, forms of dementia including Alzheimer's disease (mostly as the result of aging) and multiple sclerosis.

The hippocampus is a major component of the brains of humans and other vertebrates. It plays important roles in the consolidation of information from short-term memory to long-term memory and spatial navigation. As such cellular damage within the hippocampus has been linked to several neurodegenerative diseases such as Alzheimer’s, epilepsy and schizophrenia. Remarkably, the hippocampal neuronal circuitry is quite basic when compared to other parts of the brain (Deng, Aimone, & Gage, 2010). At its simplest it can be described as a collection of simple synapses, the axons down which the electrical current flows, formed along 2-D laminar layers, as shown in Figure 15.

However, the brain is not a 2-D structure so it is more realistic to create a 3D version instead, suspended in a gel, as shown in Figure 16. Work has already been done to test the electrical firing of these neurons *in vitro* and has found that it mirrors the firing of the cells in hippocampus *in vivo* (Y. Yang, Wimpenny, & Ahearne, 2011). However, this work could not determine whether the cells were growing along the wires or towards the chemical that coated the wires, which needs to be understood to see how well the model can mimic the brain.

Cell tracking algorithms are a logical solution to determining the growth/trajectory of the cells, since they should be able to follow the growth of the axon and dendrites to determine which factor most encourages growth. Neurons are unlike the other cells mentioned earlier in this text, in that the neurons do not divide to form new cells. Instead the cell body would be expected to stay relatively sedentary whilst the axon and neurites would grow to form the sort of structures seen in Figure 15. Any algorithm developed for the tracking of the neurons must, therefore, take this into account and look at the position of the tip of the axon in relation to the cell body. The algorithms devolved here have the further problem that the structure is

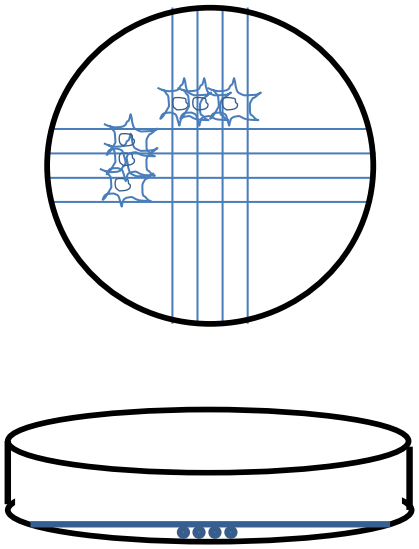

Figure 16: 3 D set up of hippocampal model.

inherently three dimensional, as shown in Figure 16, so the position of the cell body and axon tip in all three dimensions must be considered. Previous demonstrations of in vitro hippocampal networks have focussed on 2-D layers (Y. Yang et al., 2011) but due to the 3D nature of the model it will also be necessary to track in the z-plane. Algorithms for studying neurons have up until now only focused on single neurons and not on the complex multi-neuronal structure such as those shown in figure 15, so the development of software capable of looking at several neurons is necessary for the advancement of the research into these cells

2.2. Cell Tracking

Broadly speaking, previous methods developed for cell tracking entail two key steps: **(a)** distinguishing the boundary of the cells from the background and **(b)** tracking an individual cell across multiple time frames known here as *linking* the cell (Jaccard et al., 2013).

2.2.1. Confluence in cell culture monitoring

Whilst the measure of confluence is one that looks at the culture as a whole rather than at an individual cellular level, it is an important measurement of culture vitally and as such an algorithm that can measure it is needed for all cell types studied here. In addition, it has been found that some algorithms perform worse at higher confluences so having a method by which to measure it allows a greater understanding of the weaknesses of other algorithms.

Cell confluence or confluency can be defined as:

$$\frac{area\ (pixels)\ of\ the\ region\ of\ interest\ occupied\ by\ cells}{area\ of\ whole\ region\ of\ interest\ (pixels)}$$

This measurement is taken for a variety of reasons throughout the field of cell biology (Begg, McNally, Shrieve, & Kärcher, 1985; Chudley et al., 2012; Dor, Brown, Martinez, & Melton, 2004; Eslaminejad, Vahabi, Shariati, & Nazarian, 2010; Ross et al., 2000). For example, the

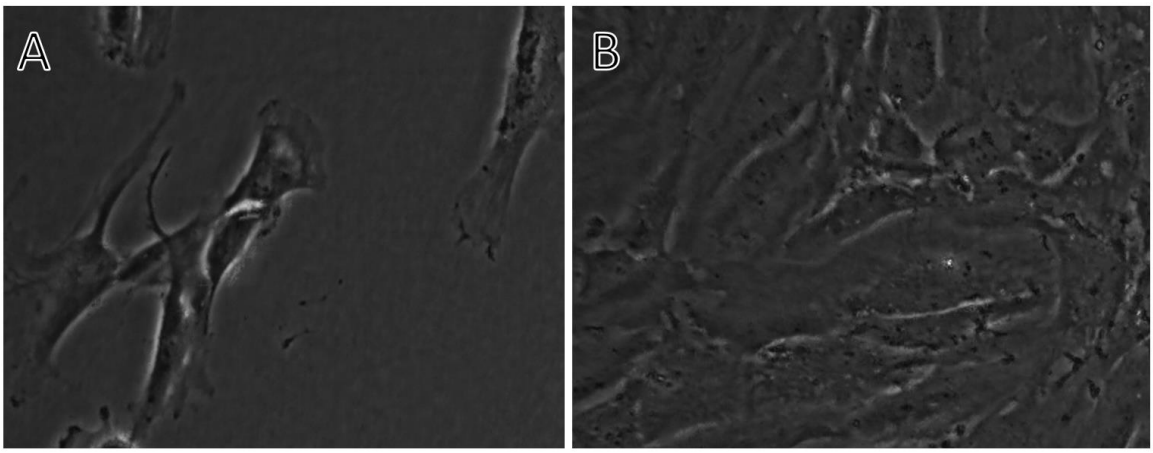

Figure 17: Showing MSCs at A) low confluence, 10% confluent and B) high confluence 100 % (right). In the lower confluence image the cells are more elongated and have more moral like processes. In the higher confluence culture the cells are fatter

rate of change of confluence can be used as a measure of growth of a culture, as a culture with a 40% confluence could be assumed to have twice the number of cells as a culture of 20% confluence. Accurate measurements of the confluence of a continuous culture over time can help to determine the growth rate of the culture. Additionally, methods used to obtain confluence in cell cultures can also be used as a first step in determining other morphological features of cells. Indeed, current approaches in measuring stem cell proliferation rely on estimating the doubling rate, i.e. finding the time it takes for the confluence to double (Jaccard et al., 2013).

In the case of cell tracking the confluence of a culture has to be taken into account as within a high confluence culture cells have a very different morphology, see example in Figure 17. In addition, the boundary between cells is less distinct than between cell and background, increasing the difficulty of distinguishing the cells from each other (section 2.1.1). At higher confluence assuming that a cell in a later image is in the same position as those is a previous image is more likely to result in mislabelling a cell as there are more neighbours. Currently available software (section 2.2.4) works best on low confluence cultures (< 10% confluence) and becomes less accurate as the confluence increases.

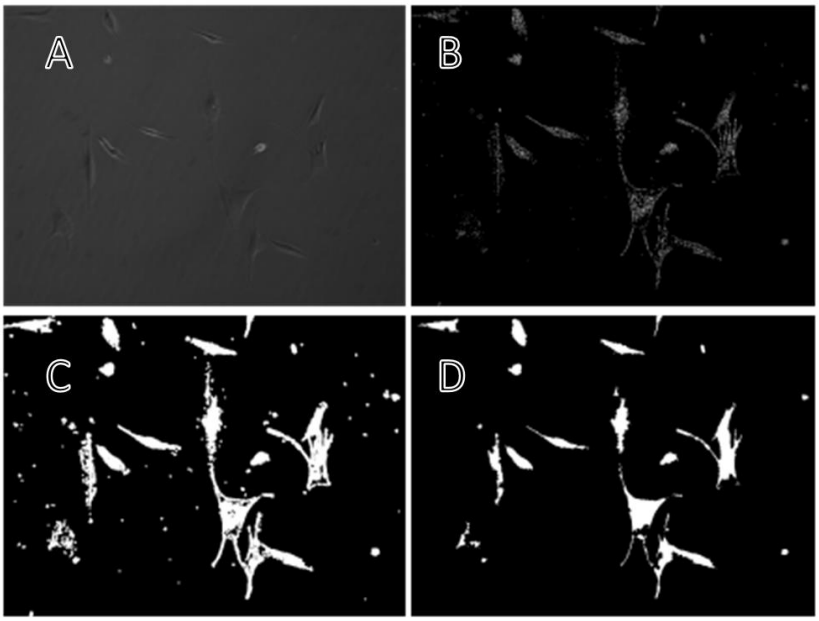

Figure 18: Showing the process of finding the location of cells in phase contrast. A) original image B) Canny Edge Detection C) Filling in the edges found by the Canny Filter D) removal of the debris, objects too small to be considered a cell

2.2.2. Distinguishing cells from the background

In computer vision a greyscale image, such as those used throughout the research presented here, are 'seen' by the computer as a matrix of numbers with each number indicating the intensity of the pixel as shown in Figure 19 The numbers range from 0 (black) to 255 (white), larger numbers are said to have a greater intensity.

Conventionally, there are two main approaches to distinguishing the boundary of cells: those that are based on *thresholding* (Jaccard et al., 2013; Whitehurst et al., 2011; Yin et al., 2010)

A) 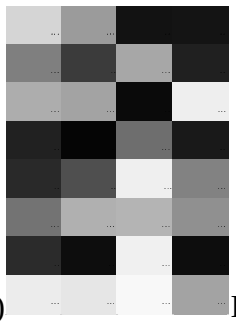 B)

214	156	19	21
128	60	168	33
174	164	11	239
34	6	111	26
42	80	240	131
116	177	181	145
44	14	241	14
237	231	249	164

Figure 19: A) an example of a greyscale image zoomed in so that the individual pixels can be seen B) the corresponding matrix of numbers seen by the computer

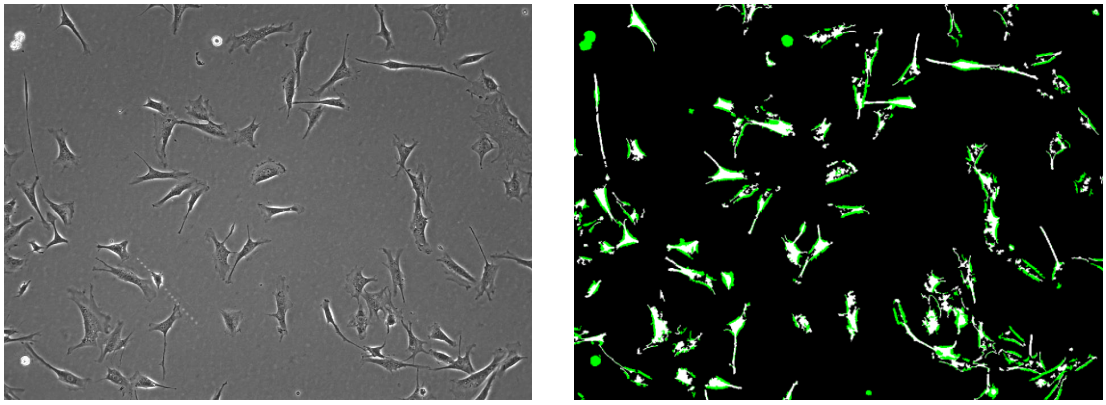

Figure 20: showing left: original image right: binary image with the halo effect in green

and those based on *template matching* (Adanja et al., 2010). In its simplest form, the former entails choosing a threshold such that any pixels above the threshold are cell and any below are background (Acosta et al., 2012; Jaccard et al., 2013; Kapur, Sahoo, & Wong, 1985; Lee, Yoon Chung, & Park, 1990; Yin et al., 2010). A more sophisticated method of thresholding utilises *Canny* edge detection to approximate outlines of the cells in the input image (Canny, 1986). This method uses a *two-threshold* technique. Rather than just selecting a number above which an area can be defined as cell it looks at the difference in the intensity of neighbouring pixels and assumes that a large difference is indicative of an edge. A mask covering each detected cell is then generated following a debris (parts of the image labelled as cell but not cell, these are smaller than the cell) removal procedure constructed using a particle filter (a filter that removes small labelled objects). Once the edges have been found the cell can be defined as the area within those edges. This above process is illustrated in Figure 18. Following successful edge detection, a binary image can be built up, whereby each non-zero connected component is considered an approximate location for the cell candidate, as shown in Figure 20.

The second approach to distinguish the positions of the cells involves finding the position of the foreground objects based on their expected appearance. This is typically achieved by the

construction of a cell template. An example from (Chen, Wang, Ozolek, & Rohde, 2013a) is shown in Figure 21. Whereby examples of cells are used to create a library of cells and from the objects found in an image matched to objects within that library. A variation on this does not use a library but instead finds the cells using either a collated set of features such as expected width and length, that best describes the cell (or objects) of interest. A simple example would be to say that all cells were circular and then create an algorithm that looked for all circular objects. Algorithms that use this technique, however, tend to be far more sophisticated and look instead for intensity patterns that are common to all cells. This approach relies to some extent on the user input which adds time and possible human error to the process.

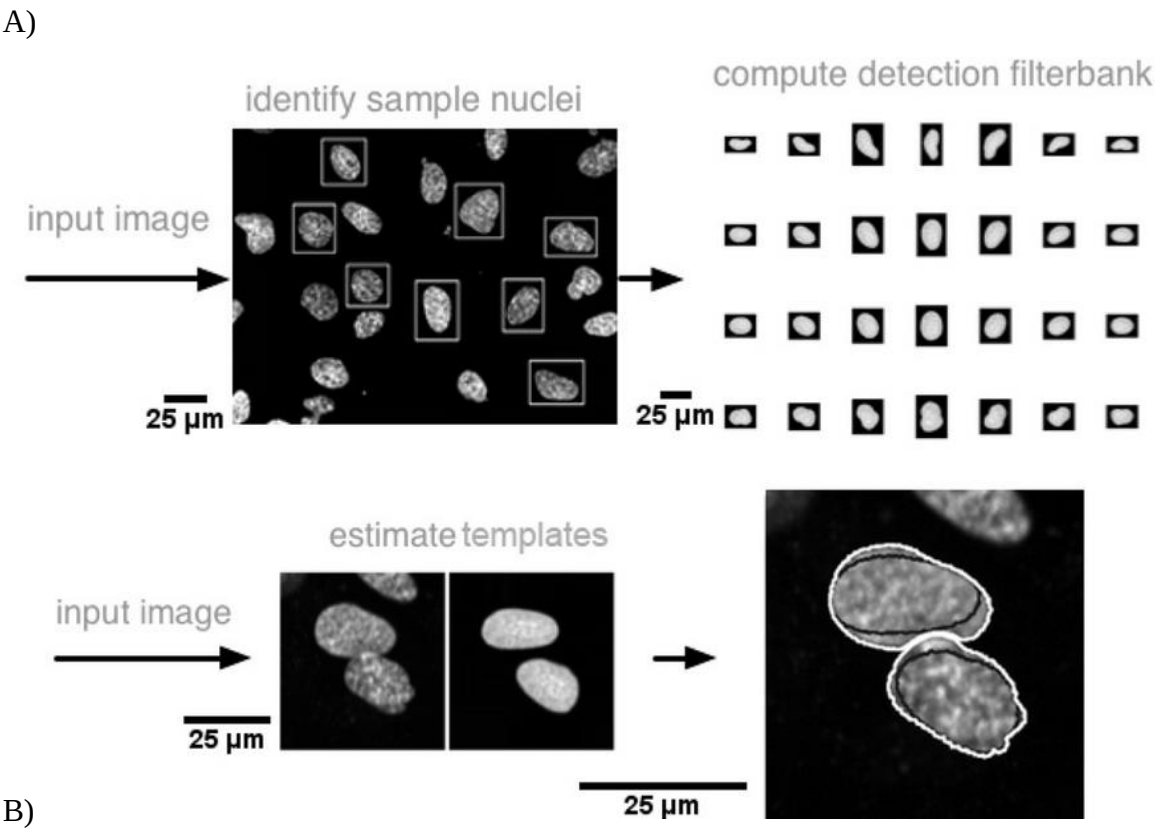

Figure 21: Overview template matching approach, adapted from (Chen, Wang, Ozolek, & Rohde, 2013b). Part A outlines the training procedure, where example cells are used to create a cell library Part B outlines the actual segmentation procedure which utilises the library to produce a rough segmentation, and then refines it using non-rigid registration based on the normalized cross correlation.

Since there are several types of cells studied for this thesis and MSCs in particular do not have a regular morphology, the work here mostly uses variations on the thresholding method. This has the additional advantage that these tend to take less processing power and so are more likely to be beneficial in more laboratory settings. A second advantage is that these algorithms could be expanded to more cell types.

2.2.3. Automated cell tracking

A simple method to link individual cells in successive time frames is based on the *nearest neighbour* principle. This tracks cells by identifying the nearest physical neighbour in the time dimention. In practice, this has a tendency to mislabel cells, especially when they are densely packed in a culture where cells frequently cross paths or even overlap. Alternatively, the linking of cells can also be achieved by a template matching method similar to that described earlier (Section 2.2.2) and entails matching up extracted features of the individual cells detected in consecutive time frames across the course of studying the cell. Here, feature matching depends on an error-free prior segmentation of the image, as any such errors can cause the cells to be incorrectly matched. Consequently, this technique is again most effective with high-contrast images such as those obtained via fluorescence microscopy. Furthermore, any large changes in morphology of a cell captured between consecutive frames may cause it to be labelled as a new cell in the following frame, thus rendering the associated track broken (Hand et al., 2009a).

2.2.4. Current software tracking cells in phase contrast microscopy

In the past 5 years, cell tracking algorithms have been increasingly developed for a vast array of uses. At their most simple these algorithms just provide an interface by which manual tracking (i.e. a user indicates which cell they are tracking in each successive frame) can take place, examples of such packages would be Braincells (Meijering, Dzyubachyk, & Smal, 2012) and Retrac (Hand et al., 2009b). Once the user has given the position and labelled all

of the cells Braincells and Retrac provide values for the number of cells, cell centroid positions, cell displacements and cell velocities. Whilst it is beneficial to have these numbers, the process of manually tracking the cells is very time consuming with a typical image series having at least six wells of 70 cells over 180 time frames all of which would need to be manually labelled.

More advanced tools find the location of fluorescently labelled cells. For example, a plugin for ImageJ (Schneider, Rasband, & Eliceiri, 2012a), Mtrack2 (Stuurman, 2003) , uses thresholding to locate the cells and feature matching to track their movement over time. There is an additional feature that allows for manual tracking. From either tracking method, it can give data on the number of cells, cell centroid positions, cell surface areas, cell displacements and cell velocities. Whilst this is a useful tool it has been shown to find and track a large number of non-excitant cells, with 40 non-excitant cells found in a culture of

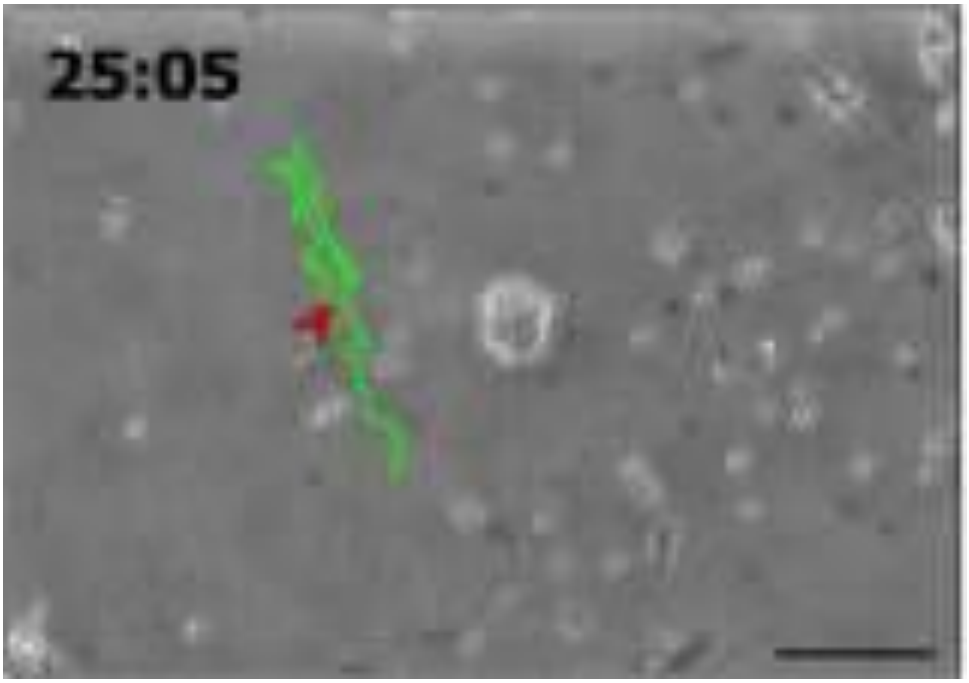

Figure 2119: Screen shot from manual cell tracking program Braincells. Once the user has given the position and ladled all of the cells Braincells provides values for the number of cells, cell centroid positions, cell displacements and cell velocities

153 real cells (Hand et al., 2009a). Such errors are problematic when trying to find common threads in the cells within the culture as such non-existent cells will skew the results.

2.2.4.1. Cell tracking software that uses thresholding

There exists currently, several free tools that can be used to monitor fluorescent cells both as single cells and also look at the cells in the context of the culture as a whole. Volocity 6 is a cross platform cell tracker that works only with fluorescently labelled cells. In this application, the position of the cells is first found using watershed thresholding, as discussed in 2.2.2. After thresholding, feature matching is used to track the cells through the series of images. From this it can generate values for the number of cells, cell centroid positions, cell surface areas (2D), cell volumes (3D), cell displacements and the cell velocities. Volocity works with fluorescent images as the background of these images is uniformly dark making the initial segmenting stage easier to perform computationally. There are other algorithms that work similarly to Volocity on fluorescently labelled cells including:

- MTrack2, an imageJ plug in that uses the watershed thresholding to detect the cells and feature matching to track them (Schneider, Rasband, & Eliceiri, 2012b).
- Imaris 8.3 uses edge detection to look at fluorescently labelled neurones in a culture, the growth of the neural tips is tracked with feature matching (Dray et al., 2015).
- Another method that makes use of the ImageJ was developed (Bradhurst et al., 2008), which made use of the change of pixel intensity gradient to localise individual cells and better define their shape. But did not attempt to track the cells from this.

Since much research is done using fluorescence there is a clear need for a tool that can work in this way, and since fluorescence provides greater contrast it is easier to create algorithms for. However, it is not suitable for the studies presented in this thesis as, as mentioned

previously, in clinical studies fluorescently labelled cells cannot be used so it is necessary to find a method that will work with phase contrast.

CellTrack (Sacan, Ferhatosmanoglu, & Coskun, 2008) is freely available software that works on PC images, introduced in section 1.5, as well as fluorescently labelled cells, introduced in section 1.4. The position of the cells is found using Canny edge detection methods and the cells are tracked by nearest neighbour matching. The number of cells, boundary positions, cell speeds, path length, cell area and cell deformation are found by the program in addition to the tracking of the cells. By not limiting itself to fluorescence it has more potential to be used in a wider context. However, the method cannot distinguish touching cells with no clear boundary and consequently cannot work in cultures of >20 % confluence in phase contrast cultures (Hand et al., 2009b). This is problematic as the cells studied for this thesis are grown in cultures ranging from 10-100% confluence. A similar system that works on phase contrast cells is Cell Tracker (Du, Marcello, Spiller, White, & Bretschneider, 2011), this uses a thresholding techniques based on the deviation of intensity from the background to segment the cells, followed by a feature based matching method that tracked the cells. Whilst this could find the cells better than cell track it was still only able to find the correct position of 42 of the 156 cells, identifying the remaining cells as background (Hand et al., 2009b). This is not ideal for studying the outcome of the whole culture as is intended here.

All the methods mentioned here use thresholding based methods to distinguish the cells from the background and both have demonstrated that it is possible to use this method to some degree of success. Nevertheless, they cannot be used in the process of tracking the cells that are frequently used in this thesis as they either rely on fluorescent imaging, which is not always possible in clinical trials or they cannot distinguish individual cells in clumps.

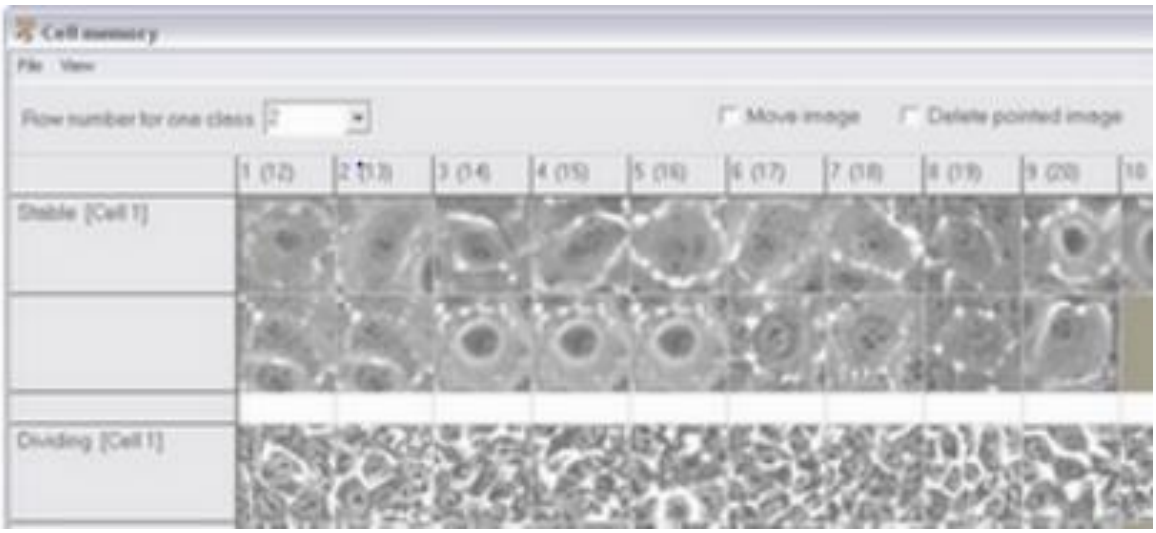

Figure 22: Screenshot from image analysis tool. A cell template library for use in the cell segmentation in Cell IQ analyser

2.2.4.2. Cell IQ analyser

This section looks at a method that uses template matching to segment the cells. Cell IQ analyser is a commercially available software that tracks cells in phase contrast and fluorescence. The Cell IQ analyser software is used in conjunction with the Cell IQ imaging software. The analyser allows users to open the images taken previously from the live cell imaging microscope and stitch together images of adjacent regions and create a video of the culture through time.

In addition to this functionality Cell IQ analyser has the ability to categorise and track the cells based on a sample library (see example in Figure 22). The library could consist of different cell types (which would be useful in a co-culture) or regions of cells (for example the cell body and axons of a neuron) from which a protocol can be constructed to identify the cell types/regions throughout the study. Once a suitable library has been created the cells in the culture can be labelled and tracked. The advantage of this method is that this technology is not specific to any one type of cell and so can be used for a variety of studies. By building a library of 100-150 cells of each type it is possible to use the inbuilt tools to track the cells and measure certain morphological features of the cells.

Cell IQ uses nearest neighbour analysis for the tracking or a combination of nearest neighbour and template matching. The maximum distance the cell could have moved between successive timeframes is user defined. From this the program creates a map of cellular trajectories and a rose plot showing the number of cells that moved in each direction. The analysis of cell movement is completed with graphs showing the cell movement over time.

The output of the Cell IQ analyser can be more accurate than the other methods mentioned but the accuracy depends on the library created by the user. Cells with rapidly varying morphologies, such as MSCs, have lower accuracy ratings (Tarvainen et al., 2002). Consequently, it is important to spend time creating a good library. It takes on average 5 iterations of a library to track the culture to a good enough degree of accuracy where it can recognise most of the cells and not create too many false positives (K. P. Lam, Dempsey, Collins, & Richardson, 2016). This process has to be repeated for each different culture, even those using the same cell type, so whilst less time consuming than manual tracking, it can still not be considered fully automated.

An aim of this thesis is to create an algorithm capable of tracking and monitoring several cells types with minimal manual input. Thus, the template matching thresholding technique described here is not suitable for this purpose as here the quality of the user inputted library is indicative of the quality of the results generated. This is problematic as creating a library is time consuming and has to be done for each culture, even if two cultures use the same cell types.

All of the PC based algorithms described in section 2.2.4. only work on two dimensional images, however not all cultures are best described in two dimensions so in addition to being

able to track cells in two dimensions it would also be ideal if it was possible to create an algorithm that works in three dimensions.

2.2.5. Cells in three dimensions

Automated focusing is an important requirement for automated microscopy since a microscope must capture images of cells as they grow in cultures for up to a week. As stated in section 1.6 part of this project looks to define the cells spatiotemporal characteristics, one of these would be the appearance of the cell in 3D. Thus, robust techniques are needed to determine the height and z-position of the cell. A potential use for this is looking at adherence, whether or not the cells will attach to the plastic at the bottom of the culture dish. MSCs are adherent cells that grow as a monolayer (i.e. they do not overlap) on the bottom of an artificial substrate such as a petri dish or 24 well plate of cultures (Romanov et al., 2003a). These cells do not proliferate when they are not attached to the artificial substrate and are just floating in the culture medium. In order to study the proliferation of these cell it is necessary to first ascertain whether they have adhered (Smith, Lam, Collins, & Richardson, 2013a).

Depth from focus/defocus is a computational vision technique which estimates the depth of a 3D surface of an image from a set of two or more images of that scene. In practice in microscopy this works by taking a stack of images and selecting the pixels that have the highest focus value on each plane and using them to produce the image in 3D, as shown in Figure 23 (Smith, Lam, Collins, & Tarvainen, 2012; Tarvainen et al., 2002). In combination with live cell imaging this technique allows the observation of phenomenon such as apoptosis, programmed cell death, and cell migration, the movement of cells, over the time period of the study. It is also possible to observe the behaviour of individual cells within a

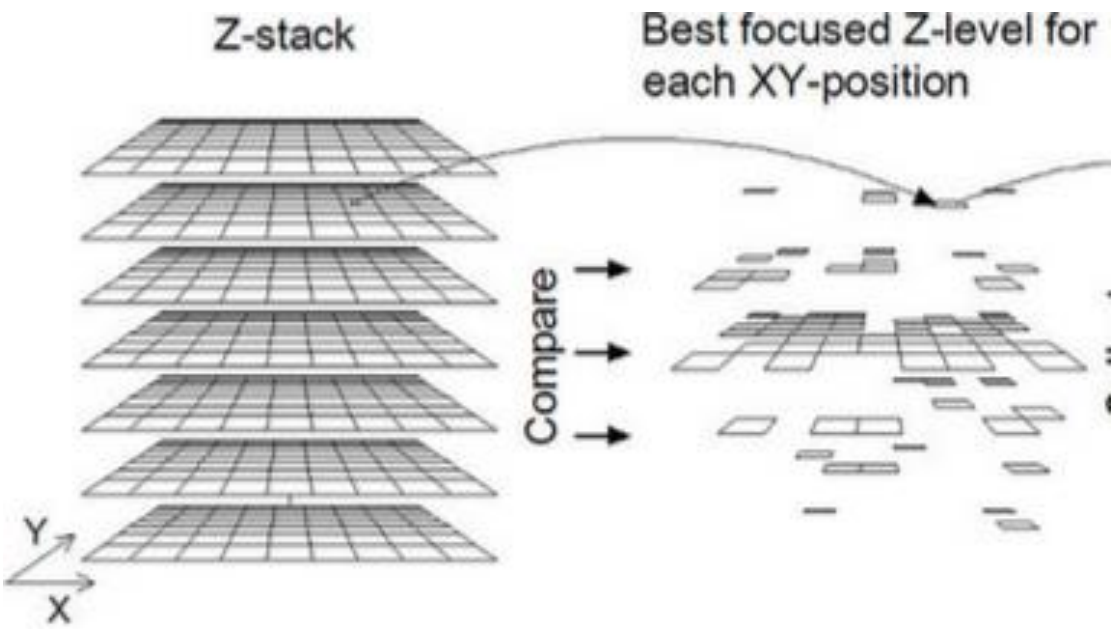

Figure 23: Adapted from (Tarvainen et al., 2002), finding the z position of each pixel

culture. From this it can be observed that there are available techniques to measure the depth of the cells but they have not yet been applied to a full culture over an extended time period.

2.3. Remarks

The advancement in microscopal techniques has naturally been followed by an advancement in computational methods to deal with the vast amounts of data that the new live cell imaging microscopes are generating. Due to the computational problems that are inherent in phase contrast microscopy there has been less progression in this subject. As such there is a need for a project that focuses on this aspect of imaging especially because such microscopes are cheaper and so more widely represented within laboratories. The work in this thesis focuses on the single cell within the culture, and the interactions of the single cell with neighbouring cells. The following chapters, 3-8, show the computational and biological methodology used to achieve this, and the results obtained from these.

3. Searching for Mitosis in a Flash

This chapter covers the first algorithms that were created to study the behaviour of the cells. Within this chapter, the cells studied are MSCs (described in section 2.1.1), however the algorithm forms the basis of the algorithms used to study back disc cells and neurons. This chapter specifically seeks to address the objectives 1, 2, and 4 detailed in section 1.7.

The main contribution of this section is the creation of a mitosis finding algorithm. Within this section the algorithm does not track the cells but it does form the basis of the tracking algorithm in chapters 6-8. In addition, the method used to find the location of the cells is used in all subsequent chapters on all cell types.

3.1. Experimental Background

All the research generated by this thesis comes in the context of ongoing clinical trials at the RJAH orthopaedic hospital in Oswestry. The context of this chapter is within a trial into the use of MSCs as a treatment for osteoarthritis. Osteoarthritis is the most common form of joint disease which causes joint pain and stiffness (ONS, 2013). Surgical intervention for osteoarthritis is very costly to the National Health Service and has a large impact on the individual in terms of recovery time and functional independence. Clinical trials have begun of a procedure to try and repair the damage caused by osteoarthritis by taking MSCs from the bone marrow of the patient and growing the culture in the laboratory in a co-culture with the chondrocytes, so that the MSCs would differentiate into chondrocytes and the resultant could be injected back into the affected knee. Recent clinical trials have shown that 80% of patients find that MSC based treatment improves their quality of life by alleviating pain whilst extending the life of their natural joints (Bajada, Mazakova, Richardson, & Ashammakhi, 2008). The focus of the work presented here is the culturing of the cells whilst in the laboratory. The current challenge facing researchers is to identify the biological

reasons why this treatment fails in 20% of the cases tested, as demonstrated by the ongoing clinical trials at the RJAH. A reason that these studies show a differing prognosis could be that the MSCs are not differentiating into chondrocytes as predicted. Stem cell differentiation, where the cell changes from a stem cell to another type of cell, occurs at mitosis or cell division. A second possibility is that the cultures were not growing enough cells for the patients so a method of estimating the cell count was also required

In order to study the differentiation of the cells a protocol first needs to be developed to detect when the cells are going through mitosis, in order that the differences can be studied before and after. The study presented in this chapter investigates methods for automating two elements of the procedure that occur during the stage of the trial while the cells were being grown in the laboratory:

1. Locating mitosis events in MSC based cultures based on the morphology of live cells.
2. Measuring the confluence of the cells to determine the health of the culture which can act as a substitute for a cell count.

The current best practice for identifying stem cell differentiation is based on studying whole populations after a period of time and determining the proportion of cells that has changed. By identifying mitotic events as they happen, the individual cells can be tracked alongside the rate of differentiation throughout the experiment, leading to a greater understanding of the mechanics and behaviour of stem cells. Additionally, in a clinical context, a label free imaging environment (i.e. not using fluorescence) is also required, necessitating the use of PC microscopy in the form of live cell imaging techniques coupled with integrated incubator platform to maintain and monitor the cells over an extended period of time.

Cell confluence is indicative of cell growth and is typically estimated by the percentage of cell coverage of a region of interest in the substrate over which cells become well attached

to the plate that they are being cultured on. This is currently an estimation from an individual looking at the culture, since this relies on individual estimation it is inherently inaccurate and incomparable between experiments. In addition, constantly monitoring the growth of a cell culture is a time-consuming task that would be suited to automation. As such, a principal requirement is that the algorithm developed would be amenable to real time analysis.

3.2. Methods

Section 3.2 describes the methods used to find the mitotic events and measure the confluence. 3.2.1 details how the cells were collected and their treatment before the experiment, 3.2.2 describes the imaging of the cells and 3.3.3 presents the algorithm generated from these experiments.

3.2.1. Cell Collection and Preparation

The cells used in this study were MSCs that had been monitored previously by staff at RJAH hospital who were looking at differing rates of viability between cell cultures. The MSCs used in this study were harvested patients undergoing spinal fusion in the treatment for lumbar degenerative disorders (n=5; aged 29–53 years). They were kindly collected by spinal surgeons from the Centre for Spinal Disorders and sent to the spinal studies research laboratories for processing (both based at the Robert Jones and Agnes Hunt Orthopaedic Hospital Orthopaedic Hospital, Oswestry, UK).

The cells were then maintained in the standard method for the laboratory: Once the cells had been isolated from a patient they were plated in cell culture flasks in order than they would proliferate enough that a culture could be studied. To achieve this plating, the cells were first spun at 900 *g* for 20 minutes[2] to form a pellet of cells removed from the fluid. From this pellet, they were plated onto 175 ml cell culture flasks at a seeding density of 20×10^6 cells

[2] over Lymphoprep (Fresenius Kabi Norge AS, Oslo, Norway)

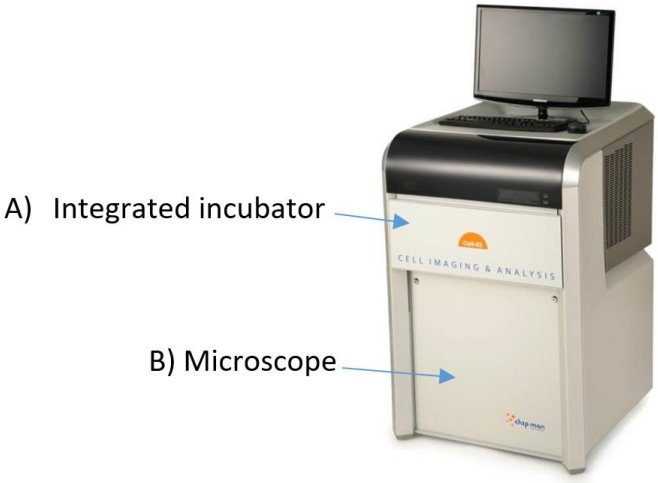

Figure 24: Cell-IQ platform containing: A) an incubator that allow for the user to specify the temperature and CO_2 % of the air around the cells being imaged. B) A phase contrast light microscope with fluorescent capabilities

per flasks. They were given a feed that provided them with all of the nutrients that they would need to proliferate and antibiotics to prevent infection in the culture[3]. After 24 hours, non-adherent, and therefore dead, cells were removed, and the adherent cell populations were cultured in monolayer and were maintained in a humidified atmosphere of 5% CO_2 at 37°C which is necessary to maintain the cells healthily. When the cell reached 90-100% confluence, estimated by a researcher, the cells were removed from the flasks and re-pelleted and re-seeded in other flasks at a seeding density of 20×10^6 cells per flask, as MSCs stop proliferating at 100% confluence. For the imaging, the cells were once ageing pelleted and this time they were re-seeded on a 12-well plate at a density of 10000 cells/cm^2 in the same medium needed to feed the cells.

3.2.2. Imaging

The experiments were carried out on the Cell-IQ platform, a multimodal microscopy system which uses phase contrast and multichannel fluorescence microscopy, providing automated

[3] Dulbecco Modified Eagle's Medium (DMEM/F12) supplemented with 10% foetal bovine serum (FBS) and 1% penicillin and streptomycin (P/S) (Invitrogen Life Technologies, Paisley, UK).

imaging in 2-D or 3-D cultures, shown in Figure 24. The integrated incubator allows for the maintenance of the cell whilst they are being imaged as it can maintain a humidified atmosphere of 5% CO_2 at 37°C as in the preparation in section 3.2.1. It is also designed to accommodate analyses of two standard plates (12 well in this instance) simultaneously, allowing quantitative cellular parameters to be measured non-invasively from the long (up to a week) time-lapse image sequences.

3.3.3. Algorithm development

The first step in identifying cell mitosis is to identify the positions of the cells themselves as described in section 2.2.1. A two-step technique was used here, the first of these is a rough segmentation was performed to find the approximate position of the cells (section3.3.3.1), the second is a fine segmentation to more accurately be able to determine the cells shape section (3.3.3.2). The major problems associated with PC microscopy segmentation, as detailed in section 1.5, are the two artefacts: (a) the halo which is manifested as a bright ring in the image around the cell, and (b) the shade off, which is often displayed as notable reduction of contrast moving from the centre of larger cell objects toward their edges. An example of these artefacts is given in Figure 7.

Various computational methods have been developed to overcome these artefacts (Bradhurst, Boles, & Xiao, 2008; de Boer et al., 2012; Jaccard et al., 2013; Yin, Li, Kanade, & Chen, 2010). This study builds on the work of (Bradhurst et al., 2008), which made use of the change of pixel intensity gradient to localise individual cells and better define their shape. Our algorithm significantly extends the work and is based on well-defined characteristics of dividing cells during mitosis; that is, before the division they contract and form a circular football like shape shown in Figure 25. These events are manifested in PC microscopy as bright flash double halos as a direct consequence of the rapid changes in surface structure and height of the cell (Paucker, Cantell, & Henle, 1962). Using such

characterising features as the ‘bright flash’ and circular properties of the cells as they divide, shown in, Figure 24.a computational method to pinpoint these events has been developed

3.3.3.1. Rough Segmentation

A rough segmentation was performed by utilising Canny edge detection to approximate outlines of the cells in the input image (Canny, 1986). This works on two basic assumptions: firstly, those large intensity gradients are more likely to correspond to edges than small intensity gradients. Secondly, important edges should be along continuous curves in the image.

The Process of Canny edge detection algorithm can be broken down to 5 different steps:

1. Apply Gaussian filter to smooth the image in order to remove the noise
2. Increasing the width of the Gaussian kernel reduces the detector's sensitivity to noise, at the expense of losing some of the finer detail in the image. The localization error in the detected edges also increases slightly as the Gaussian width is increased. Find the intensity gradients of the image.

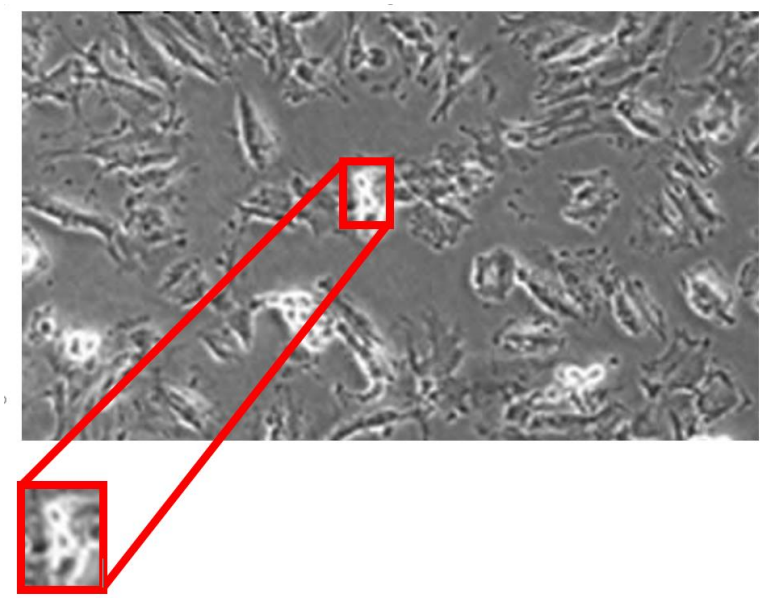

Figure 25: Showing an MSC culture imaged with a PC microscope. The cells have the double halo artefact making them brighter than the surrounding cells due to the fact that they have formed a more ball like shape during division

An edge in an image may point in a variety of directions, so the Canny algorithm uses four filters to detect horizontal, vertical and diagonal edges in the filtered image. The edge detection operator returns a value for the first derivative in the horizontal direction (Gx) and the vertical direction (Gy). From this the edge gradient and direction can be determined: by the equation

Equation 1

$$G = \sqrt{G_x^2 + G_y^2}$$

Equation 2

$$arctan(y / G) = tan -1 (y / G) = atan2(x, y)$$

3. Where G can be computed using the hypot function and θ is the angle between the two arguments. The edge direction angle is rounded to one of four angles representing vertical, horizontal and the two diagonals (0°, 45°, 90° and 135°). Apply non-maximum suppression to get rid of spurious response to edge detection

   Non-Maximum suppression is applied to "thin" the edge. After applying gradient calculation, the edge extracted from the gradient value is the algorithm for each pixel in the gradient image is:

   i. Compare the edge strength of the current pixel with the edge strength of the pixel in the positive and negative gradient directions.
   ii. If the edge strength of the current pixel is the largest compared to the other pixels in the mask with the same direction (i.e., the pixel that is pointing in the y direction, it will be compared to the pixel above and below it in the vertical axis), the value will be preserved. Otherwise, the value will be suppressed

4. Apply double threshold to determine potential edges

   After application of non-maximum suppression, remaining edge pixels provide a more accurate representation of real edges in an image. However, some edge pixels remain that are caused by noise and colour variation. In order to account for these spurious responses, it is essential to filter out edge pixels with a weak gradient value and preserve edge pixels with a high gradient value. This is accomplished by selecting high and low threshold values. If an edge pixel's gradient value is higher than the high threshold value, it is marked as a strong edge pixel. If an edge pixel's gradient value is smaller than the high threshold value and larger than the low threshold value, it is marked as a weak edge pixel. If an edge pixel's value is smaller than the low threshold value, it will be suppressed. The two threshold values are empirically determined and their definition will depend on the content of a given input image.

5. Track edge by hysteresis: Finalise the detection of edges by suppressing all the other edges that are weak and not connected to strong edges.

   . Usually a weak edge pixel caused from true edges will be connected to a strong edge pixel while noise responses are unconnected. To track the edge connection, blob analysis is applied by looking at a weak edge pixel and its 8-connected neighbourhood pixels. As long as there is one strong edge pixel that is involved in the blob, that weak edge point can be identified as one that should be preserved.

It was found early on that whilst this produced a better estimation of the cell edges than other edge detectors, it did not encompass the whole cell so an extra stage of processing

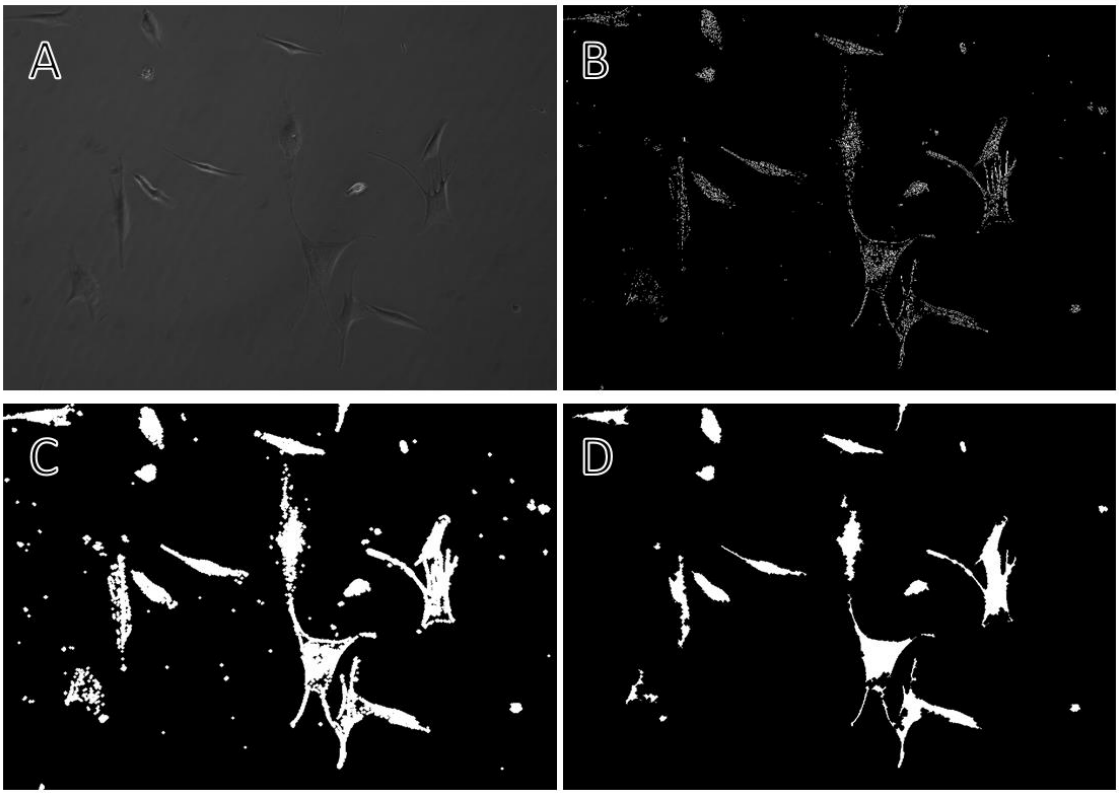

Figure 26: Process of segmenting the cells A: original phase contrast image of MSC culture. B: edges found with Canny edge detection. C: edges dilated so that the whole cell is found. D: final rough segmentation of cells

dilated the lines so that more gaps would be filled. Using the two-threshold technique of the Canny edge detector, the problem of shade off (Figure 7) becomes less as this allowed for the finding of the edges of the cell not surrounded by the halo that do not have such high contrast with the background. Thus, a more accurate estimation of cell edges amongst other (irrelevant) objects including debris in the culture could be performed. A mask covering each detected cell is then generated following a debris removal procedure constructed using a particle filter, i.e. removing the smaller objects. Hence, the output produced by combining these steps yields a binary image, whereby each non-zero connected component (white object) is considered an approximate location for the cell candidate, as shown in Figure 26. Since Canny edge detection only considers intensity gradients it will count the halo as part of the cell (Canny, 1986). This is a major drawback

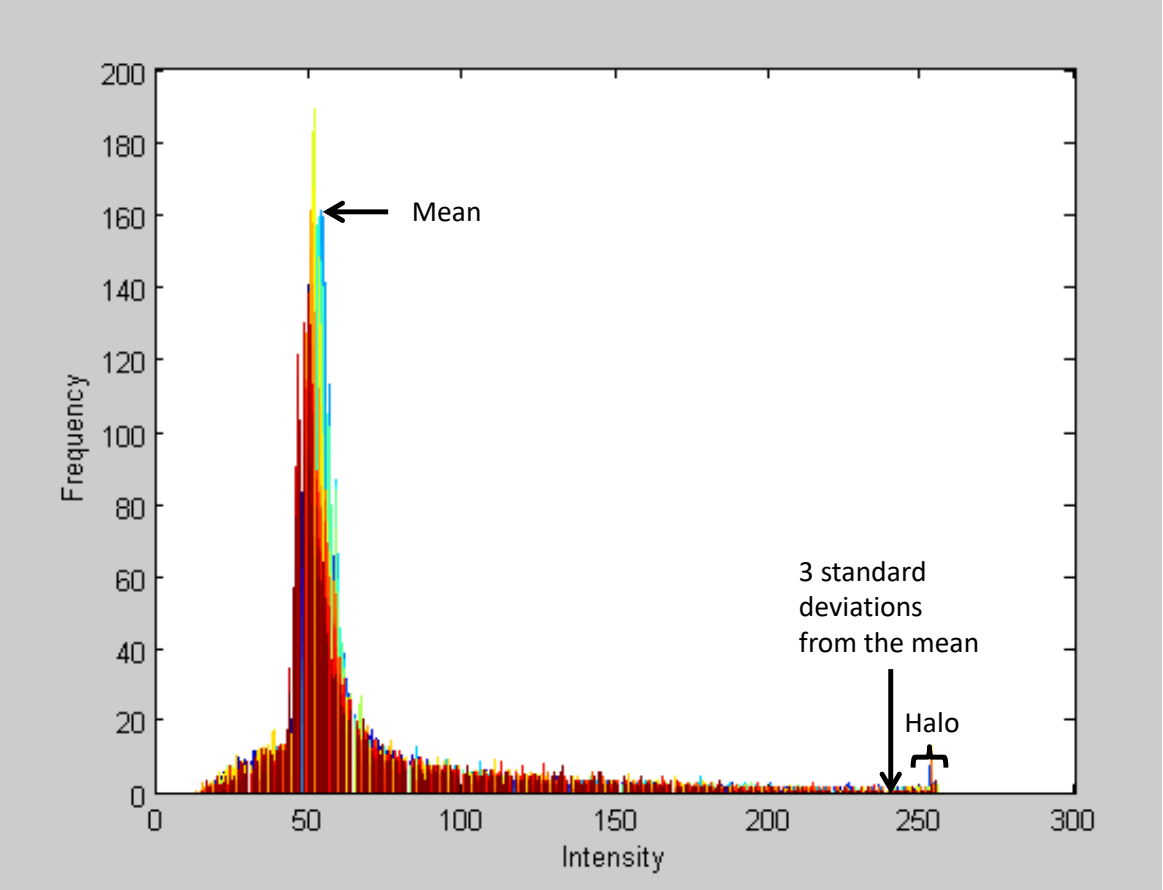

Figure 27: Plot used to determine the intensity of the halo for the purpose of removing the halo during the segregation phase of the image processing. This shows Intensity histogram of every pixel over 5 experiments showing the range of intensities that make up the halo

as this adds up to an extra 30% to the estimation of the size of the cell (Jaccard et al., 2013).

3.3.3.2. Fine Segmentation

To find a more accurate position for the cells the effects of the halo, show in Figure 7, have to be considered. As can be seen the halo is represented by a bright border at the edge of some of the cells. To define the halo, the average background intensity was calculated. Initially the value used to define the halo was just taken to be the highest intensity of 255 since it was assumed that the entire halo intensity was always at the highest end. However, histograms of the pixel distribution across 3 separate repeats of 5 different experiments, shown in Figure 27, found that this was not consistently the case. Therefore, the value of the

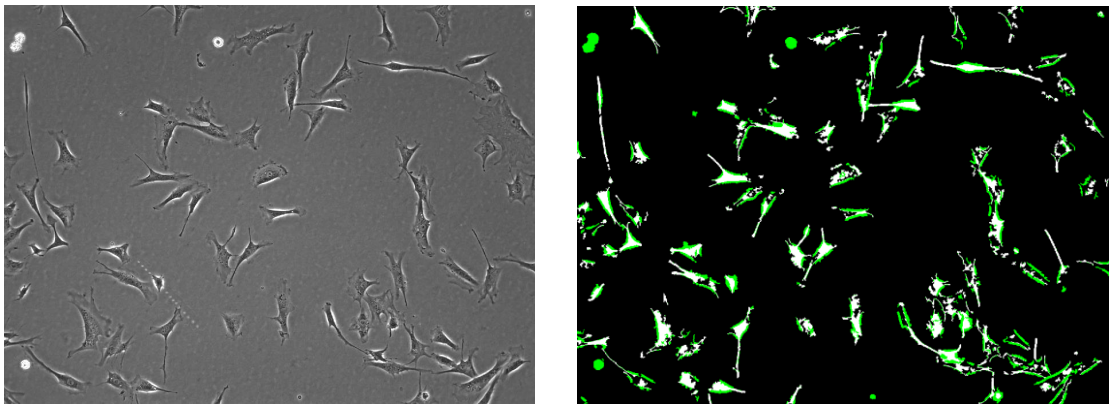

Figure 28 : left: original image right: binary image with halo to be removed in green

halo was taken to be any intensity higher than three standard deviations above the mean. As it can be seen from Figure 27 that such a value includes the whole of the halo but none of the cell represented by the first peak.

Using this value, the halo was then removed from the cell mask and the resulting image was kept so that cells containing the double halo, as shown in Figure 27, could be added back to facilitate detection of mitosis events at a later stage.

3.3.3.4. Accounting for the double halo

Cells such as those shown in Figure 28 are deemed to have a double halo, where two bright rings are noted. A double halo typically occurs in PC microscopy when a cell forms an egg-yolk like shape by curling up on itself. This event signifies mitosis (cell division) so it is important that such cells are included in our studies. The removal of the halo method described in section 3.3.3.1 has the effect of removing the double haloed cells.

Initial attempts at removing the halo artefact surrounding the cell whilst not removing those with the double halo, assumed that the actual cell was thicker than the halo artefact, so most of the white object from Figure 25 was actual cell and not artefact. Consequently, this early algorithm included only those parts of the image that had a thickness of more than 40 pixels. This was found to also include some of the halos of cells in close proximity to each other so

Figure 29: rounded cell showing double halo artefact

another method had to be found. This second method took into account the circular property of the cells in order to find their locations. This is done by using a *Circular Hough Transform* based algorithm for finding circles in images (Ballard, 1981) as the sensitivity of this method can be scaled to include cells that form a nearly perfect circle.

The Hough transform is a technique which can be used to isolate features of a particular shape within an image. Because it requires that the desired features be specified in some parametric form, the classical Hough transform is most commonly used for the detection of regular curves such as lines, circles, ellipses, etc. The main advantage of the Hough transform technique is that it is tolerant of gaps in feature boundary descriptions and is relatively unaffected by image noise.

The Standard Hough Transform uses the parametric representation of a line:

Equation 3

$$\rho = xcos(\theta) + ysin(\theta)$$

The variable ρ is the distance from the origin to the line along a vector perpendicular to the line. Θ is the angle of the perpendicular projection from the origin to the line measured in degrees clockwise from the positive x-axis. The range of theta is $-90° \leq \theta < 90°$. The angle of the line itself is θ+90°, also measured clockwise with respect to the positive x-axis.

The Hough Transformation is a parameter space matrix whose rows and columns correspond to ρ and θ values respectively. The elements in the Hough Transformation represent accumulator cells. Initially, the value in each cell is zero. Then, for every non-background point in the image, ρ is calculated for every θ. P is rounded off to the nearest allowed row in the Hough Transformation. That accumulator cell is incremented. At the end of this procedure, a value of Q in Hough Transformation (r,c) means that Q points in the xy-plane lie on the line specified by θ(c) and ρ(r). Peak values in the Hough Transformation represent potential lines in the input image.

For in the specific case used here the objects that are searched for are perfect circles.

This enables the image mask to be updated and refined with prospective candidates of mitotic cells still to be identified. The sensitivity that needed to be used was found empirically.

3.3.3.5. Finding the Dividing Cells

The finding of Mitotic cells was based on the work done for finding cell confluence. The mitotic cells can be identified as those which display a figure of eight pattern (two double halos close together) as shown in Figure 30. This is found by measuring the distance between

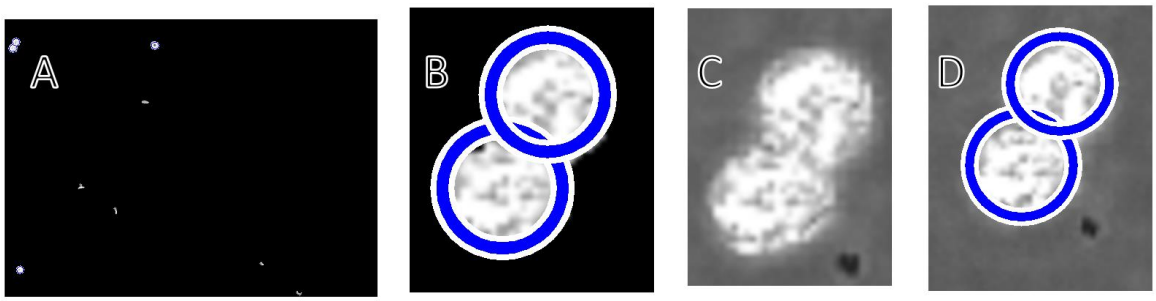

Figure 30:(a-d): Showing the identification of double halo cells Left to Right, a) mask with all of the large (>150 pixels) part of the halo left showing the identification, b) zoomed in showing the identification of the mitotic cells c)+d) showing the identification in phase contrast without the mask

all the double haloed cells and by determining if it is greater than the length of the two radii in question. The areas where this is the case are defined as the regions of interest (ROI). In live cell imaging where real-time analysis is beneficial, it is important that earlier/previous images in the sequence be examined (via *back tracking*), to eliminate potential false positives where there is only one cell within the identified ROIs (as opposed to two cells coming together and forming a 'mitotic' shape).

3.3.3.6. Calculating confluence

Once a binary mask had been build up containing all the cells, including those that were dividing the confluence can be calculated with:

$$\frac{total\ area\ of\ cells\ (pixels)}{total\ area\ of\ frame\ (pixels)}$$

Equation 4: Confluence

3.3.4. Algorithm

The input image is an all-in-focus phase contrast image containing the cells at a single time point. To determine the location the cells the following processes are performed

1. Find the edge of the cells using the Canny edge detection. This creates a black image with the outlines in white. This was used with a Gaussian filter of size 5x5 with a σ of √2. The upper and lower threshold values were selected dynamically by the MATLAB algorithm.
2. Dilate the edges by 2 pixels to ensure proper connection.
3. Fill in the cells location by filling in regions in contact. Creating a black background with the approximate locations of the cells in white.
4. Erode the edges by two pixels to account for step two, the area is now considered to be a rough estimation of the location of the cell.
5. To clean up the image, the small particles (area <= 300 pixels) and holes (area <= 256 pixels) were removed by applying a particle filter to the thresholded image of the region of interest. The area of the particles and holes to be removed was determined manually by measuring their average sizes across a range of typical images. At this stage, the output of the image was a black and white mask.
6. Determine the value of the halo, by finding the value three standard deviations above the mean intensity of all the pixels of the input image.

7. Remove the halo from the cells by removing any pixels that are brighter than the value from step 5.
8. Apply a Hough transform to the removed piles to see if any are round, (and hence displaying the double halo artefact) these are then returned to the original image.
9. Finally, the double halo artefacts are excited to see whether they are in close proximity and thus dividing.
10. Confluence is measured by finding the number of pixels that represent cells on the mask and then dividing that number by the total number of pixels (equation 1).
11. The number of mitotic events were then recorded. The output of this from the algorithm was a table of the image number (time sequence) and the number of mitotic events on that image. This was compared to a manual count of the same to generate the identification rate and the number of false positives shown in table 2.
12. The output of the confluence measure was a table of the image number (time sequence) and the percentage coverage of the image in question.
13. To test this, the results were compared to the results of just using the Canny edge detection and the Phantast model developed by (Jaccard et al., 2013). In addition, the results were compared to the results of 11 slides that were found by drawing the area that contained the e cells by hand. This was done using the CROIEditor (Jun, 2013), which allowed the ground truth to be constructed manually via measurements taken from freehand drawings overlaid on the all-in-focus images.
14. To compare the results the mean difference between the computationally gathered results and the ground truth was found.

3.3. Results

The results section is here divided into two with 3.3.1 looking at the effectiveness of the mitosis finding algorithm and 3.3.2 comparing the results of the confluence measuring algorithm to other similar algorithms.

3.3.1. Finding mitosis

The results obtained are analysed and compared with earlier work on identifying ROIs based on spatiotemporal analysis (Huh et al., 2011), and the work of Bradhurst et al. (Bradhurst et

al., 2008) which identified the individual cells by means of the surrounding bright halo of each cell. In particular, our investigation assesses the accuracy and real-time capability of detecting the onset and duration of a mitosis event. Results show that the method presented is considerably faster whilst achieving comparable accuracy with the other two approaches.

Based on the results obtained to date (using five 72-hour long image sequences), it was found that all three methods were able to accurately locate the dividing cells, with over 98% accuracy, in cultures of up to 75% confluence shown in Table 2.

Beyond the edges of the cells could not be determined.

Table 2: Identification of mitosis in cultures of varying confluence

Confluence (%)	**Number of Dividing Cells per Image**	**Identification Rate (%)**	**False Positives**
7-8	0-1	100	0
12-15	0-7	100	0
20-34	0-3	100	0
20-50	0-7	98	0
30-75	0-12	95	0

In comparison to the analysis used in earlier work by (Smith, Lam, Collins, & Richardson, 2013b), this method has the distinct advantage that it is not reliant on the availability of the whole image sequences (offline) and, as such, offers the potential for real-time analysis. Furthermore, whilst the work of Bradhurst et al. produces a good representation of the position of the cells from which the mitosis can be inferred, their procedure is comparatively slow, requiring an average of approximately 40 minutes to process/analyse a single image with the typically long image sequence; viz. ~500 images over the 72-hour period, compared to the 2.6 seconds/frame to process a single image with this method.

In summary, further studies into the effectiveness of MSC as a treatment for OA are needed to better understand why treatments are more effective on some patients than others. One

crucial area for investigation concerns the development of a reliable procedure for detecting mitosis in real time within live cell cultures, as the current normal approach to pinpoint the occurrences of cell division by manual observations are, at best, time consuming. An automated algorithm which makes use of the change in intensity and morphology of the cells as they go through mitosis has been developed. In addition to achieving greater accuracy, early results show that the proposed algorithm offers the distinct advantage that it is amendable to real-time implementation.

3.3.2. Measuring confluence

Traditional methods of measuring cell confluence (i.e. the percentage of the growth surface covered by cells) involve inherently subjective estimation. Here, measuring cell growth and (thus) assessing cell quality in monolayer cultures are usually achieved using standard imaging techniques such as phase contract microscopy which monitors several parameters simultaneously. However, most current computational methods have been developed for fluorescent imaging primarily for ease of segmentation. The major advantage of accurate confluence measurements is the facility to compare how the confluence changes across an experiment. In this work, the algorithm developed was used to look at the doubling rate of MSC over time. These results are designed to highlight the real-world applications of using real-time confluence measures for a variety of data. Three separate methods, two developed for this thesis, of finding the confluence are measured here on a culture as it grows over the course of 52 hours.

1. Canny edge based techniques, a quick method of obtaining confluence for a monolayer culture, as a rough segmentation method described in section 3.3.3.1.

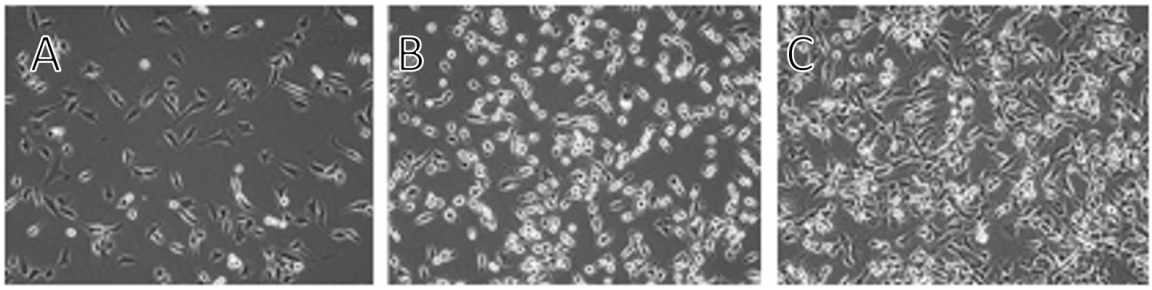

Figure 31: Showing the growth of MSC culture left to right: A) at start B) at time point 45(33 hours in) C) and at the end point 52 hours after the start. The increased confluence is from the extra cells formed through mitosis.

2. Method as described above (section 3.3.3), including the rough segmentation, fine segmentation and accounting for the halo, that provides more accurate data just using the Canny based method.

3. PHANTAST a phase contrast confluence finder created by (Jaccard et al., 2013) that does account for the halo around the cells but does not take into account the double halo artefact of the dividing cells or the shade off.

In addition to looking at algorithms for tracking the cells the confluence of the cells was calculated by hand. This was achieved by using the MATLAB ("MATLAB and Statistics Toolbox," 2012) based tool CROIEditor (Jun, 2013), which allowed the ground truth to be constructed manually via measurements taken from freehand drawings overlaid on the phase contrast images. From this the confluence could be calculated as in section 3.3.3.6. Due to the time-consuming nature of such analysis this was only done for every 10 frames of imaging. The three algorithms and the hand measurement were run on the cells which were the same cells as those used for the mitosis experiment as shown in Figure 31 the results were found to be as shown in Figure 32. From Figure 32 it can be seen that the method proposed in this project comes in between the results of the other methods to which it was compared. The figure shows the confluence calculated for the cells by each of the three

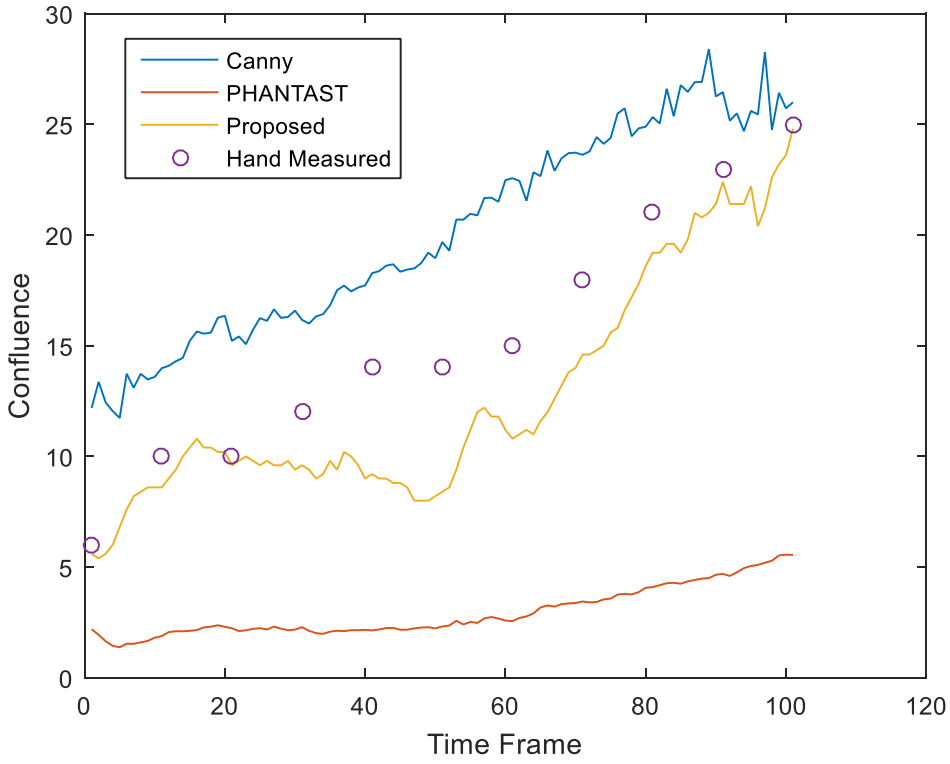

Figure 32 Showing the change in confluence measured of the stem cells by the three different techniques. Each unit on the x-axis represents 44 mins.

algorithms. It was found that the mean difference between the Canny edge detection method and the hand measured method was 4.6 ± 0.5 %, between the method and the hand measured method was 2.8 ± 0.5 % and between the PHANTAST method and the hand measured method 12.2 ± 1.4 %. As would be expected, it is shown that the Canny edge detection method consistently gives a greater reading of confluence than the other two methods. This is expected as it does not remove the halo around the cell so the prediction of the cell area is consistently higher than reality. The PHANTAST gives the lowest reading of the three as would be expected since it has no mechanism to count the cells with a double halo so is likely to underestimate the size of the culture. When compared to the hand measurements the proposed method was the closest of the three methods tested. Nevertheless, it should be noted that the proposed method still falls consistently below the measure of the hand measurements, especially within the 10-15% confluence range. This discrepancy is due to

the assumptions of where the cell ends, the proposed method would not expect it to have any cell under the halo artefact, however where the cells are close to each other there is a possibility that that could happen.

A similar trend in growth rate was observed in Canny and the model proposed here, whilst the PHANTAST method showed a significantly lower rate of growth. This can be seen in Figure 31, that the culture does grow in confluence but maintains a large number of cells that display the double halo meaning that they are not counted in the PHANTAST model.

The advantage of the Canny edge is that it provides an extremely fast method (<0.2 sec/frame) of obtaining an approximate value of confluence. For very low confluence (<15%) the accuracy (when compared with the hand measured methods) will be given a significantly greater value (+10%) due to the fact that this method includes the halos around the cells which account for a greater proportion of the overall image. Once the cells reach 20-25% confluence the results become more accurate when averaged over time (due to the halo effect there seems to be less variation in the first method, this is because in this instance small areas between cells can be counted as cells when the gaps are filled in).

Due to the fact that it takes into consideration the halo effects the second method is more accurate (closer in value to the hand measured method), but more time consuming (2.6 sec/frame) to process, this is shown by the higher levels of differentiation seen in the areas of higher confluence. The 2.6 second calculation times is in no way inhibitory to real time analysis (in this instance the time frames represent a 16-minute time interval).

The method proposed by (Jaccard et al., 2013) (orange) takes a comparable length of time to the second method (3.8 sec/frame) but removes all of the double halo artefacts that are common before mitosis and in curled up cells.

Since the Canny and the PHANTAST method have a common error throughout, all three methods do show the underlying trend of the data, that there is a slight increase in confluence (~1.5%) over the time period given (44 hours). From this, doubling rates can be obtained that would have comparable accuracy to the current literature and would have the potential for use in any form of live cell imaging as an automated way of determining when cells need to be passaged. Nevertheless, there can be an advantage to knowing the precise confluence of a region of interest in which case it is important that the result is neither over estimated, as with the Canny edge detection keeping the halo, nor underestimated, as with the removal of the double halo from the PHANTAST. The method proposed here is an improvement on both of the other methods but still slightly underestimates the confluence of the culture.

3.4. Observations and further work

This study focuses solely on a single culture of MSCs and uses the morphology to determine one stage, mitosis, within the cell cycle. This idea is in itself is not a novel one, but it builds on previous attempts at this by taking into account the need for real time analysis. Whilst differentiation does occur at mitosis, not every instance of mitosis is an instance of differentiation. The major result of this study is that it provided the techniques used in this thesis to find the location of the cells detailed in chapters 4, 6 and 7 as well as some early work on the importance of morphology.

The work on confluence can be applied more generally as confluence is a common measure used when maintaining cells and determining their growth. As such it is used in later experiments as a common measure. The implications and impact of this study are further discussed in chapter 9.

4. A Computational Approach to Quantifying Axon Regeneration in the Presence of Mesenchymal Stem Cells

This chapter makes use of the confluence algorithm from Chapter 3 and details the generation of the first algorithm used to study neurons. Within this chapter, the cells studied are MSCs (described in section 2.1.1) and neurons (described in section 2.1.3). Within this study these cells are co-cultured with the biological objective of understanding how they interact. This chapter specifically seeks to address the objectives 1, 2, and 3 detailed in section 1.7. The main contributions of this chapter are the creation of an algorithm that provides an automated method to determine whether the cells had adhered and an algorithm that quantifies neural complexity.

4.1. Introduction

This study looks at two types of cells, MSCs and neurons. It is based on previous work that looked at whether the presence of MSCs would allow neurons to grow on chemical growth inhibitors (K. Wright, 2013; K. T. Wright et al., 2007). This was being investigated because transplantation of bone marrow stromal cells has shown to encourage functional recovery in animal models of spinal cord injury (SCI) and recent clinical trials suggest possible recovery also in humans. However, there are two fundamental barriers to the development of new and improved MSC-based treatments exist:

1. The general lack of cost-effective strategies to boost the number of MSCs in vitro in order to meet clinical and research demands.
2. The absence of understanding of the mechanism and condition for these improvements.

To overcome these barriers novel computational toolsets are required to quantitatively assess and characterise spinal cord motor neurite interactions MSCs in an in vitro SCI model (K.

Wright, 2013). These analyses may begin to unlock the mechanisms responsible for the growth and regeneration of neurons, which are believed to be responsible for the functional improvements noted after cell transplantation for treating lesions to the central nervous system. Since PC microscopy is the primary imaging technique for the long-term monitoring of the spinal motor neurite outgrowth an accurate and robust method for its evaluation is a crucial prerequisite for implementing such toolsets. The work presented in this chapter focuses on creating a quantitative image analysis for live cell studies, which examined the interaction of MSCs with neurons based on an established in vitro nerve growth model in the presence of substrate-bound extracellular molecules that are known to inhibit axonal regeneration (K. Wright, 2013).

The algorithm developed for this was, in part, based on the algorithm described in chapter 3. However, it required substantial modifications in order to be able to look at the morphology of the neurons, as they behave in a different way to MSCs since they grow rather than reproduce.

4.2. Methods

Section 4.2 describes the methods used to measure the growth of neurons when co-cultured with MSCs in the presence of a growth inhibitor. 4.2.1 details how the different cell types were collected, their treatment before the experiment and how they were co-cultured with a growth inhibitor, 4.2.2 describes the imaging of the cells and 4.2.3 presents the algorithm generated from these experiments.

4.2.1. Cell preparation

The cells used for this study were human MSCs and chick neurons. The neurons were cultured alone, both with and without the growth inhibitor, and were co-cultured with the

MSCs with and without the growth inhibitor. This was done to ascertain the role of the MSCs in overcoming the inhibitor.

4.2.1.1. MSCs

The MSCs used in this study were harvested individuals undergoing spinal fusion in the treatment for lumbar degenerative disorders (n=5; aged 29–53 years). They were maintained as described in section 3.2.1.

4.2.1.2. Neurons

Spinal cords were dissected from Day 4.5 hybrid brown chicks by staff at the Robert Jones and Agnes Hunt Orthopaedic Hospital, Oswestry, UK. These were then digested in 20 μL of trypsin (2.5% wt/vol; final concentration of 0.05%) in PBS (Invitrogen Life Technologies) for 15 minutes at 37°C while agitating frequently. The trypsin supernatant was removed and replaced by 900 μL of neuronal culture medium (NCM; L-15 culture medium supplemented with 1% [vol/vol] insulin, transferrin, and selenium, 1% [vol/vol] P/S [L-15/ITS-X/P/S medium; Invitrogen Life Technologies], 1% [vol/vol] horse serum, and 1.5 mg/mL of glucose) (Sigma-Aldrich, Poole, UK) and 100 μL of 4% (wt/vol) bovine serum albumin (Sigma-Aldrich). The spinal cord tissue was homogenized using a pipette, and spinal cord motor neurons were isolated by density gradient centrifugation at 500 *g* for 15 minutes over a warmed 1.5 mL cushion of 6.8% (vol/vol) Nycodenz (Serva, Heidleberg, Germany). Dissociated cells were seeded into 24-well tissue culture plates (Co-star, Corning Inc, NY, USA) pre-coated with nerve-permissive and nerve-inhibitory molecules (see in the following sections) in NCM supplemented with 0.4% (vol/vol) N2 supplement and 10 ng/mL of basic fibroblast growth factor (bFGF) (Invitrogen Life Technologies) at a seeding density of 3×10^5

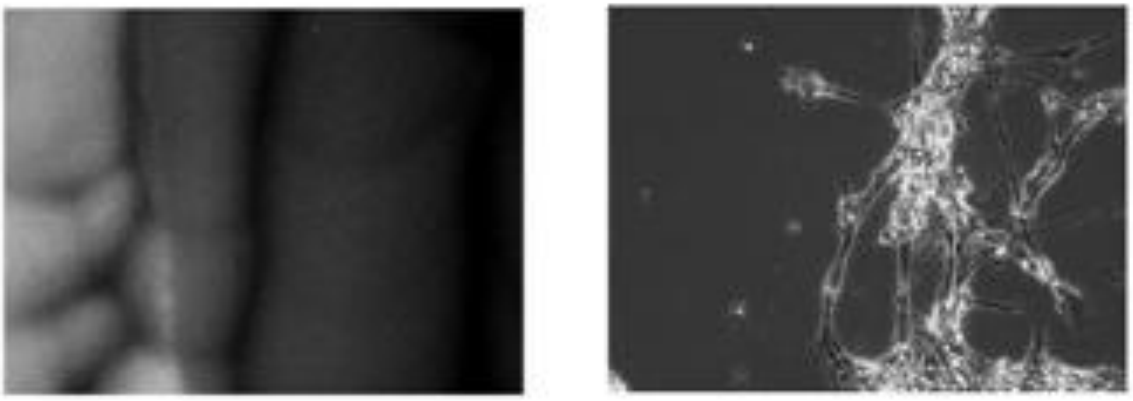

Figure 33: Left: fluorescently labelled inhibotor. Right: Nueires growing on uninhbiated side. From this it can be seen that the nurons are much less likely to grow on the part of the plate that is coated with the inhibitor

cells per well and were maintained in a humidified atmosphere of 5% CO_2 at 37°C for 72 hours.

4.2.1.3. Co-Culturing with growth inhibitor

This experiment sought to investigate and compare the behaviours of neurites in different environments, by coating half of each well with a fluorescently labelled inhibitor; Figure 33, where it can be seen that the well was divided into two sections; a) the inhibitor treated, and b) control/untreated parts respectively. The work presented in this chapter sought to combine elements of advanced imaging technologies and image analysis algorithms to describe axonal regeneration in an objective and quantitative manner when compared with current methods. The inhibitor was labelled, rather than the cell, to maintain the fundamental biology of the cell as discussed in section 2.1.

4.2.2. Imaging

The cells were imaged using a motorised microscope that captures multiple images at different heights, providing a z-stack of images which can be used to select the most in-focus pixels at the appropriate depths/planes via the generation of a 2.5-D surface map shown in

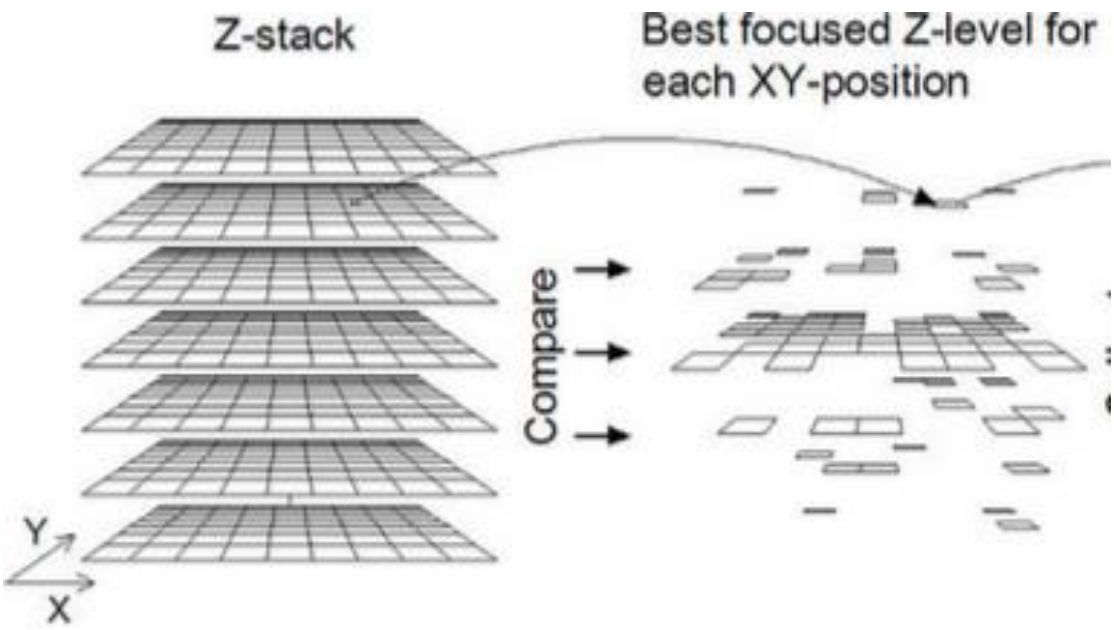

Figure 34: Adapted from (Tarvainen et al., 2002), finding the z position of each pixel. Each pixel of each level in a z-stack is analysed to find out which pixel is most in focus. The level on which the pixel is most in focus is found to be indicative of the level at which the object of interest is positioned/

Figure 34 (Tarvainen et al., 2002). As the image focus for each pixel depends on the position of the camera relative to the cell surface, thus depth/movement of the cells in the culture may be indirectly observed by measuring the corresponding image focus within the z-stack. In other words, as the number of cells that enters the same image plane increases, the focus measure for that particular plane also increases. This is particularly useful for assessing the degree to which the cells/features have settled within the culture, since cells that are found lower in the well indicate their high affinity to the substrates and, as such, suggest that they are most likely to successfully adhere to the substrate. The location of the growth inhibitors was examined using fluorescent microscopy. All other images were viewed in PC microscopy, where images including the z-stack were taken at 16-minute intervals over a 72-hour time period using the Cell-IQ® system manufactured by CMT (Finland) Ltd. (Tarvainen et al., 2002).

4.2.3. Algorithm development

The algorithms developed for this study aim to see whether the neuron has grown and how complex that growth is. To achieve this depth studies were first conducted to see whether the cells had adhered to the plastic, then the confluence of the cells was measured and finally the complexity was quantified.

4.2.3.1. Cell growth

The first result that could be considered biologically meaningful here was whether the cells, the length of the neurons and number of MSCs, had grown. The measure used to define this was confluence, the total area of the image covered by the cell. Cell confluence is indicative of cell growth and is typically estimated by the percentage of cell coverage of a region of interest in the substrate over which cells become well attached. Computationally, this entails detecting and subsequently segmenting cell objects before they are counted. This was done using the method described in section 3.3.3. Once the cell area had been defined the confluence was calculated as the ratio of total cell area to total image area as chapter 3. However, in this experiment there are in effect two areas of interest, the area of the image covered by the fluorescing growth inhibitor and the non-covered part. As such it was necessary to define the confluence twice, once for each area. This was done by specifying further image masks based on the corresponding florescent images, from which the locations of both the treated and untreated parts of the culture were identified.

4.2.3.2. Normalised variance (NV)

NV is the range of difference of pixel intensities from the mean of the intensity of the whole frame. An area that was more in focus would be expected to have a higher NV value. From the MATLAB ("MATLAB and Statistics Toolbox," 2012) implementation perspective, the z-stack images (as shown in Figure 34) are reshaped to a matrix A of size $X \times Y \times Z$, where $X \times Y$ is the width x height of the image I and Z is the number of planes. The SVD equation

can be defined as $A=USV^T$, where the left-rotation vector U obtained is used to project the original image data, S is an $X \times Y \times Z$ diagonal scaling matrix and V^T represents the transpose of the right-rotation vector. In doing so, we may calculate the sum of squared errors between the projected image and the observed image Formula. We determine the z-plane that has the least residual, or maximum energy, for a given pixel $I(X, Y)$ in the z-plane providing a measure that estimates the 'best' depth level for each pixel location (X, Y). The depth map is reconstructed from these calculated z-levels. By finding the NV value for each pixel an estimation of the height of each pixel can be built up as shown in Figure 34.

4.2.3.3. Complexity measurement

Neurites have a remarkable diversity of different branching patterns which vary greatly in length, thickness, and network topologies (K. Wright, 2013; K. T. Wright et al., 2007). To date, the characterisation of this bio-structural complexity has been largely based on subjective assessment. The algorithms developed in this work sought to significantly improve the way in which such complexity could be assessed beyond the broad description using typically the mean length of neurites and number of axonal branches of the biological system. Here, automated image analysis with time-lapse video microscopy has been used to quantify important aspects of their growth and differentiation, by applying the mathematics of *Fractal Geometry* which can provide an objective description of the morphological complexity apparent in axonal growth and regeneration.

A fractal is a natural phenomenon or a mathematical set that exhibits a repeating pattern that displays at every scale. It is also known as expanding symmetry or evolving symmetry. An object is considered to be fractal if it displays self-similarity, i.e. it can be split into parts, each of which is (at least approximately) a reduced-size copy of the whole. Within the context of neurons, it is used because the dendrites that branch off of the axon can be viewed

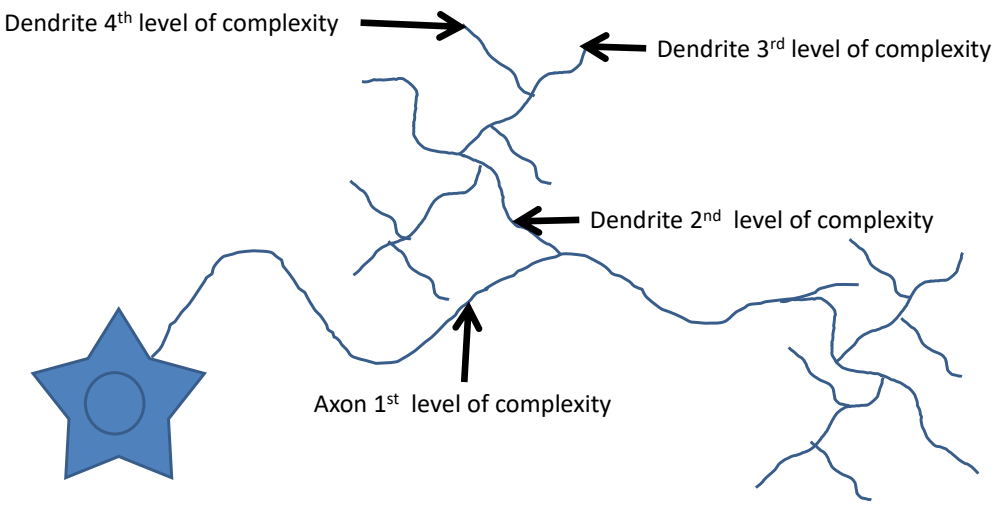

Figure 35: simplified diagram of a neuron showing levels of complexity as defined by fractal geometry

as small axons in themselves in that there can be further branching off of these, a simplified version of this is shown in Figure 35.

Indeed, the *fractal dimension* (D_f) has been shown to be useful for quantifying the irregularity and shape complexity in systems which appear to display scaling correlations (between structural units) over several orders of length or size such as trees and crystal structures (K. Lam & Richardson, 2012). To calculate this dimension for a fractal, imagine this fractal lying on an evenly spaced grid, and count how many boxes are required to cover the set. The box-counting dimension is calculated by seeing how this number changes as we make the grid finer by applying a box-counting algorithm, an example for the coast of Britain is shown in Figure 36. The complexity is measured here in the form of *box counting*. The algorithm counts the number of boxes needed to cover the dendrite/axon at a given box scale. The scale is changed, and the process is repeated. The fractal dimension of an object, also known as the Hausdorf–Besikovich dimension, is computed as the ratio of the change in the log of the box count to the change in the log of the box size.

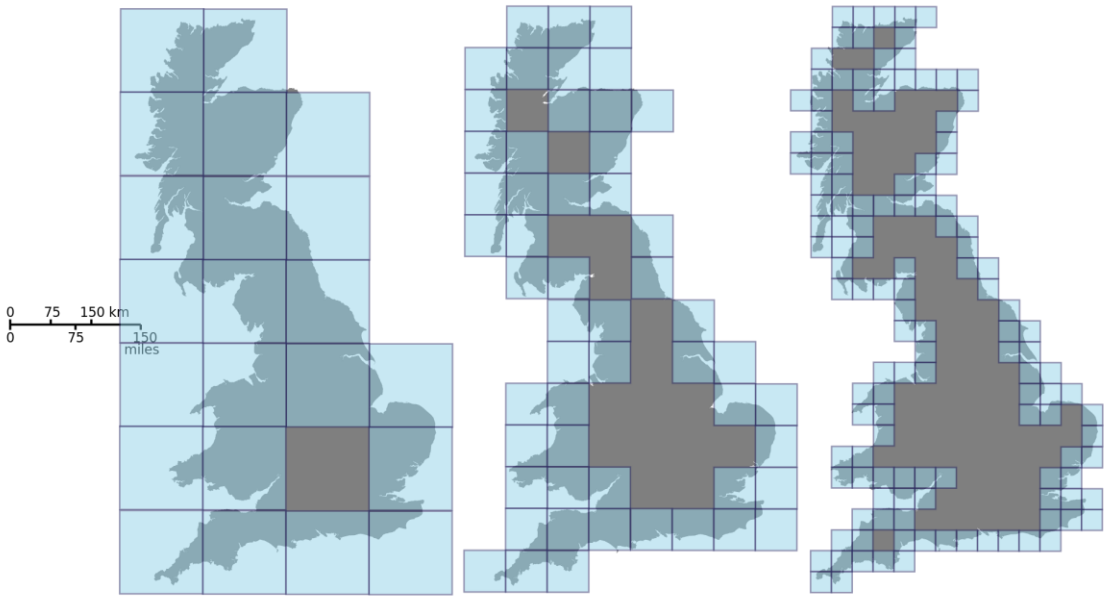

Figure 36: Covering of a fractal curve (here the coast of Britain) by grids of decreasing sizes. To measure the Box-counting dimension, we count how many squares contain parts of the curve.

As such, the branching dynamics of spinal cord neurites have been evaluated using fractals, to determine the correlation between branching *complexity* and the quantity of substrate-bound extracellular molecules which are known to inhibit axonal regeneration in growth.

4.2.4. Algorithm

This work required two types of input. The first of these was the z-stack of images that will be used to determine the depth of the cells and thus whether they have adhered to the surface of the plastic. The second is the all-in-focus phase contrast image that will be used to determine position of the cells in the x,y plane. (NB, it is possible to derive the second of these from the first if desired)

1. The depth of each pixel was determined using the NV method that assumed that a pixel was most in focus at the point that it had the most variance compared to the cells around it.
    a. Therefore, the NV of each pixel was calculated for each level of the stack.
    b. The NV was compared at each level of the stack and the pixel with the highest NV was thought to represent the correct depth of the object represented by that pixel in the culture
2. The second part of this algorithm was finding the position of the cells in the x,y plane.

a. The first stage of this was to find the outline of the cells. For this purpose, Canny edge detection was used. This was used with a Gaussian filter of size 5x5 with a σ of √2. The upper and lower threshold values were selected dynamically by the MATLAB algorithm of the
b. Unlike the cells in chapter three neurons are not contained within 'blobs' so for the purpose of determining the position of the cells it was assumed that the cells exist between two sets of parallel lines.
    i. To determine if the lines were parallel an Improved Hough transformation was performed on the image generated form the application of the Canny edge detection.
    ii. The area containing the cells described by filling in the area between the parallel lines.

3. The cell was then thinned down to one pixel thick. This skeleton therefore represented the area at which the cell was deemed to lie.
4. The first measurement make was the confluence. This was found by finding the number of pixels described as cell in 2bi and dividing that number by the total area of the field of view.
5. The complexity of the neurons was found from the skeleton of the neurons described in 3. This was done by finding the minimum number of boxes that would be required to cover the whole of the neurons. This started by applying the box size of 1x1 pixel and seeing how many boxes that would require then doubling the box width of the box - (so next investigating the 2x2 box size) the width of the box was repeatedly doubled until only one box was needed to cover the whole are.
6. From this a graph of box size against number of boxes was plotted.

7. The Df was then found to be the gradient of the graph, it is computed as the ratio of the change in the log of the box count to the change in the log of the box size. A lager Df would indicate a more complex structure.
8. The Df was calculated for each frame and the result was plotted against time so that the change in complexity could be vied,

4.3. Results

The results here are divided into two - the complexity of the neurons with the cultures and the confluence of the neurons both with the growth inhibitor and without.

4.3.1. Complexity measures

The complexity analysis provides a summative measure of neuronal outgrowth based on Df, which augments the commonly adopted approach to counting the number of adhered cells and branch points that have extended neurites. To compute Df, the cell bodies were removed from the image before the desired neurites/features were extracted (by thresholding). The remaining neurites were then eroded to one pixel wide where applicable as shown in Figure 37.

For the purpose of this study it is assumed that a greater level of neural complexity is represented by a greater Df. Figure 38 summarises the results obtained from all three studies (Treated with neurocan, Treated with Nogo-A and Treated with MAG). From Figure 38 it can be readily observed that the co-cultures form more complex neurons and thus it would follow that the processes of the MSCs allowed for the neurons to overcome the neurosupressant. In the case of Nerocan and MAG from the beginning the sample was able to surpass the complexity of the single culture. The complexity at least levelled with (Nogo-A) the spinal cord control sample; (ii) in all cases, the MSC co-culture has a notable increase in complexity throughout the early cycle of each experiment, most notably in the Nogo-A

experiment. This would be expected as the neurons grow more dendrites and are hence have more complexity. However, it can also be seen that all of the results are within error of each other. Whist the trends are what would be expected, the error on the fractal dimensions is too great (roughly 10% of the result) to draw any meaningful conclusions from the data.

Figure 39 summarises the results which are completely in line with those obtained from earlier investigation (K. Wright, 2013). In particularly, it was shown that the cells treated with Neurocan and Nogo-A had a significant increase in coverage when co-cultured with MSCs, whilst the increase in the presence of MAG is modest; see hashed bars in the 39. Likewise, in the absence of co-cultured MSCs, there are noticeably fewer cells detected in the treated part of the image in both Neurocan and Nogo-A studies. Furthermore, as previously reported in (K. Wright, 2013), the inhibitory effects of Neurocan and Nogo-A

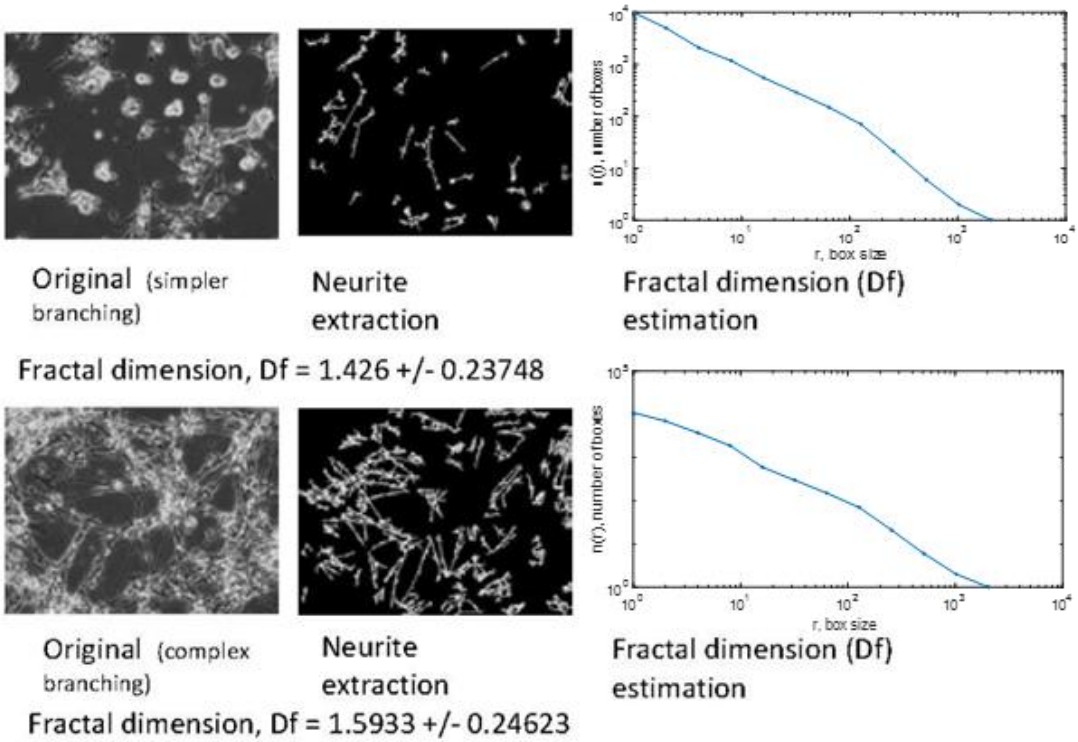

Figure 37: Illustration of the fractal analysis of a simple neurite system (top) and a more complex system (bottom). From left to right: the original image, the extracted neurites and a fractal dimension estimate with the box size on the x-axis and number of boxes

were countered by the addition of MSC whilst MAG does not appear to inhibit neurite adhesion in the presence or absence of MSCs.

4.4. Observations and further work

This chapter has described the use of quantitative live cell imaging technologies in our recent studies of novel co-culture assays developed to identify cell mediated activities, whereby human MSC were seen to promote neurite outgrowth in an in vitro SCI model. The investigation has required the development of advanced image analysis techniques to better understand the complex interactions between the cells in such systems. In particular, the fractal dimension was demonstrated to be a useful indicator of axonal shape complexity, providing a single numeric value that corresponds well with the general notion of complexity or shape irregularity of the feature boundary by virtue of the characteristic power-law scaling of fractal geometry. The attraction of fractal analysis lies in its ability to quantify aspects of the development of biological systems, and in doing so providing us with a new tool to objectively quantify the effect of changes in environment and parameters on growth. However, the results shown here demonstrate that there is too much error to make the use of this method without first reducing the error. In addition, the fact that neurons within the body are not a two-dimensional structure but instead form a complex three-dimensional structure, is not considered, so some of the complexity will come from the fact that the neurites are crossing rather than branching. The next chapter looks at a method that such structures can be imitated in the laboratory and presents methods for analysing the images that this produces. The implications and impact of this study are further discussed in Chapter 9. this technique practical in the short term.

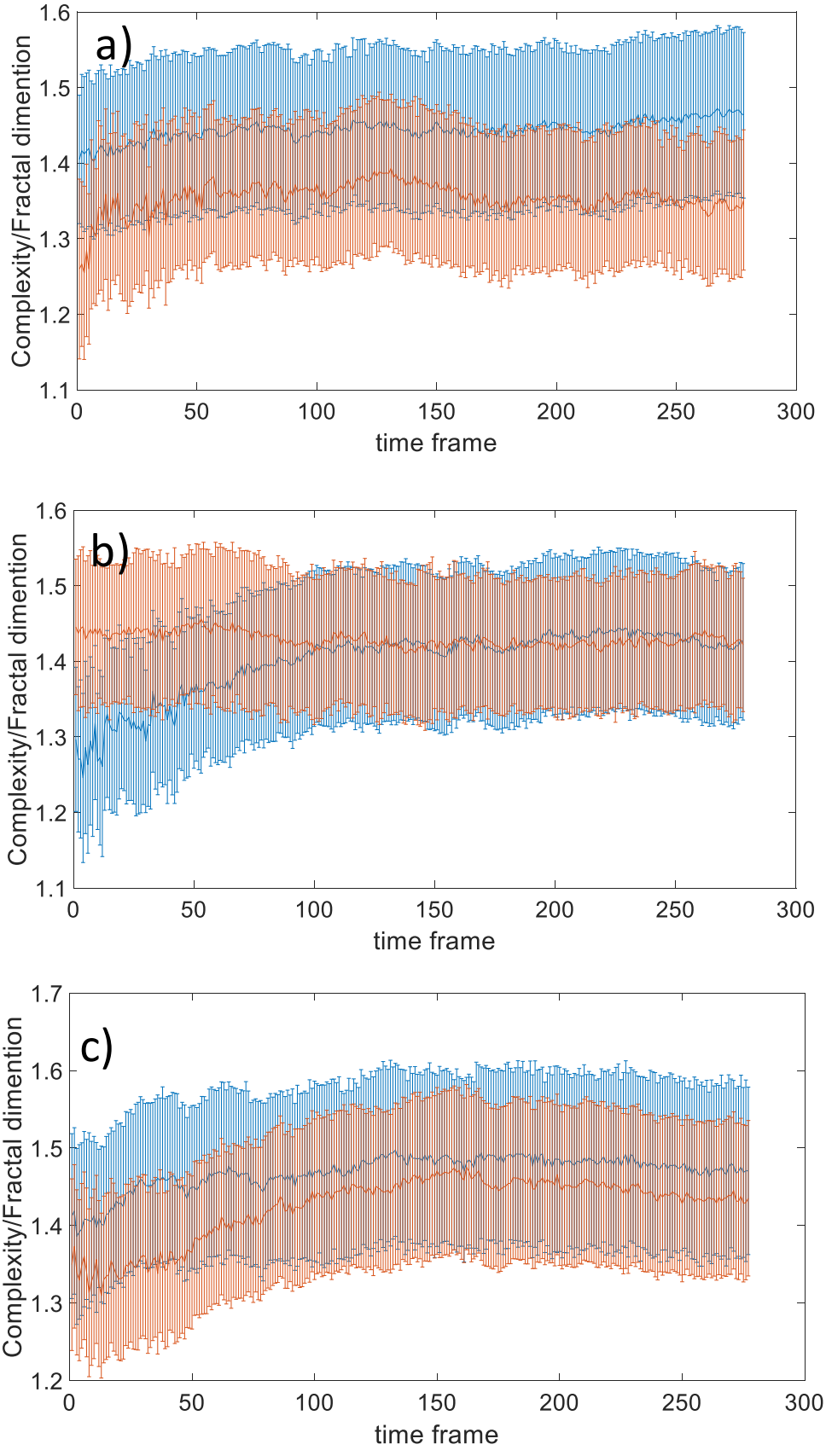

Figure 38: Changes in neurite complexity over time showing the difference between the neuron-MSC co-culture (blue) and the neuron culture (red). From top to bottom (a)-(c): (a) Treated with neurocan, (b) Treated with Nogo-A and (c) Treated with MAG

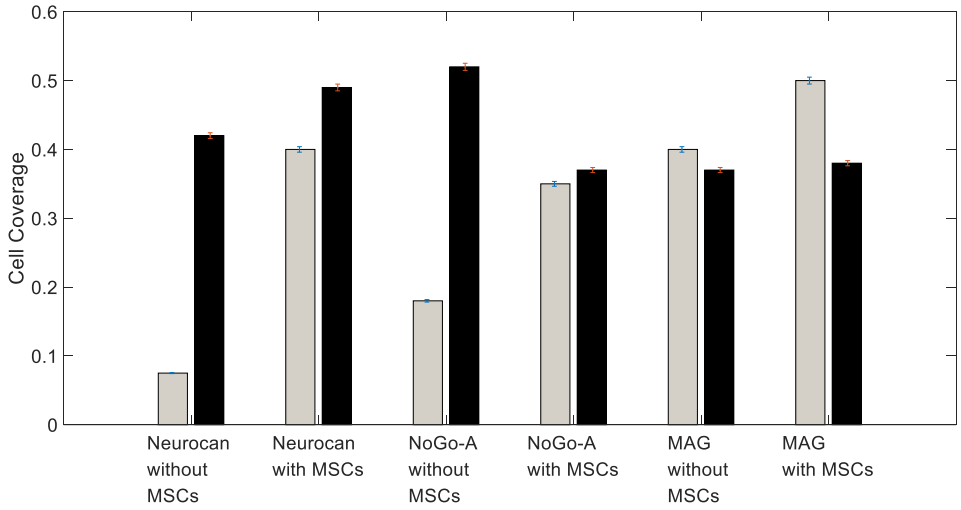

Figure 39: Comparing cell confluence (0–1, 1 = full coverage & 0 = no cell) in treated (grey bar) and untreated (black bar) regions of the images respectively for the individual experiments.

5. 4-D Hippocampus Measurements of Neurite Growth In Vitro

The work presented here looks at the hippocampal neurons (described in section 2.1.3). Unlike the previous studies this work looks into the movement of neurons along a scaffold to more closely mimic the behaviour of such cells in the brain. This increases the range that the cell has to be observed in the z-directions. This chapter specifically aims to address objectives 2 and 5 as detailed in section 1.7. The main contributions of this section are the use of an algorithm that aims to find the depth of the neurons as they grow and from this show that the neurons grow along the scaffolds rather than towards the cell adherent.

5.1. Introduction

The work presented in this chapter does not look at confluence as was done before instead an attempt was made to use the same method of segmenting the cells, however it was found that it was not possible to perfectly distinguish the cell from the scaffold along which it was grown. The biological purpose of the investigation described in this chapter was to determine whether neurons are compelled to grow in a direction because of topographical cues or whether the cell adherent polylysine could be used to dictate the movement of the cells by acting as a chemoattractant.

5.2. Methods

Section 5.2 describes the methods used to track the depth of the neurons as they grew across nanofiber scaffolds. 5.2.1 details how the scaffolds were made, how the cells were collected and how the cells and scaffolds were seeded into the gels. 5.2.2 describes the imaging of the cells and 5.2.3 presents the algorithm used to determine the location of these cells in three dimensions.

5.2.1. Plate set up

Polylactic acid nanofiber was produced by an electrospinning technique following a protocol established in previous studies (Y. Yang et al., 2011). The aligned nanofiber meshes were mounted on a round glass coverslip either in uniaxial or orthogonal alignment to provide the supporting ECM/scaffold. The assembled nanofiber scaffolds depicted in Figure 40 were sterilised and then coated by polylysine overnight and laminated for 4 hours. E19 rat embryo was isolated from placenta. The middle brain was dissected out and hippocampus region tissue was collected. Approximately 10,000 hippocampus cells per scaffold were seeded with neutobasal medium supplemented by B27, L-glutamine and antibiotics for culture up to 7 days at 37 ^{o}C and 5% CO_2. Three experimental conditions were tested, with neurons seeded on:

1. The nanofiber layers with no separation between them, allowing cells to be seeded 1 mm from the crossover of the fibres as depicted in Figure 40a (Blue).
2. Nanofibers separated by aluminium foil of thickness 10μm. Cells were seeded on both layers of nanofibers about 1 mm from the crossover as shown in Figure 40b (Green).
3. A collagen-based gel ~75 μm above the nanofibers as depicted in Figure 40c (Red).

5.2.2. Imaging

The investigation was carried out on the Cell-IQ platform (Tarvainen et al., 2002) a multimodal microscopy system which uses phase contrast and multichannel fluorescence microscopy, providing automated imaging in 2-D or 3-D cultures described in 3.2.2. The equipped high precision motorised Z-stage of the automated microscope allows the

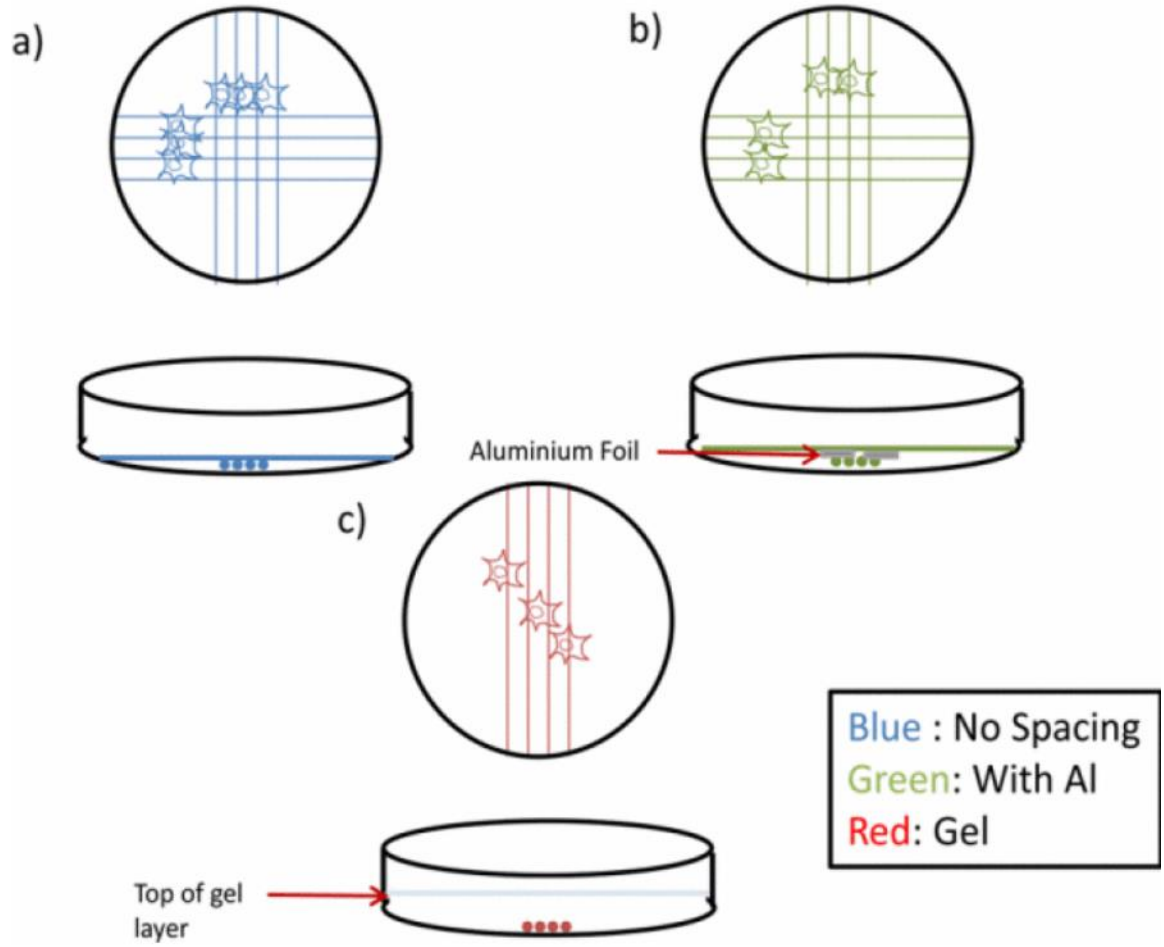

Figure 40:Top down (above) and side on view (below) of the experimental setup of the hippocampal models. A) Two layers of nanofibre directly on top of each other. B) Sample contains two layers of nanofibre on top of each other separated by 10 µm thick aluminium foil. C) One nanofibre layer covered by ~75 µm of gel. The cells are seeded on top of the gel over the microfiber. In all cases, the nanofibres were coated with polylysine.

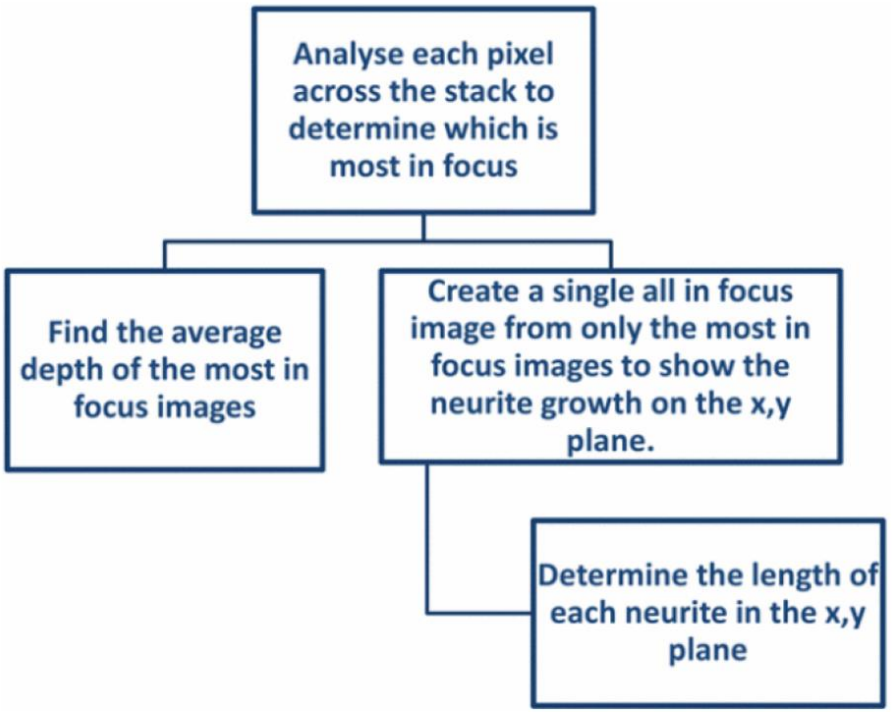

Figure 41: Summary workflow of the computational procedure adopted previously.

acquisition of 3D image stacks, with a minimum measured volume (voxel) which is characterised by an anisotropic (x,y,z) resolution at $0.18 \times 0.18 \times 0.4 \mu m^3$.

5.2.3. Computational Methods

An important requirement of the algorithms developed for this work is to accurately determine within the 2-D field of view (FOV) the position of the individual neurites as they moved in the z-axis over the course of each experiment (Smith et al., 2012). Here, images of the cells were captured using automated microscopy with a high precision Z-stage (0.4 μm), from which a series of 89 images were focused at different heights, collectively forming a so-called z-stack of images. The z-position of the individual cell/feature can then be estimated using the multi-scale focus estimation procedure described in (Smith et al., 2012). The cell organelles are analysed by means of the most in focus pixels whereby their dynamic locations (x,y,z,t) can be determined. The computational procedure has been used successfully in previous studies of mesenchymal stem cells, offering a first ever

demonstration using 4-D time lapsed videos to characterise neuronal proliferation at the site of adhesion (Smith et al., 2013a; K. T. Wright et al., 2007). This is summarised in Figure 41.

5.2.3.1. Depth from focus

To facilitate detailed examination of the neuronal cell/ECM interactions in which complex topographical and biochemical cues of the environment can be present, a scalable quantitative procedure for measuring neurite extension and characterising axonal formation within the 3-D continuous culture must be developed as described in section 5.1. This was achieved by taking advantage of the limited depth of field of the phase-based microscopy systems, where images are retrieved with discernible quality differences given the relatively narrow depth of field or in-focus limits; that is, cell object/features captured at different depths from the camera may appear out of focus if they are away from the focus plane. Using the widely documented computer vision technique of shape-from-focus (SFF) (Nayar & Nakagawa, 1990), several measures of quality of image focus (or focus depth measures) have been studied to best compute the in-focus image frame for a particular point in the image space (Duthaler & Nelson, 2005a; Pertuz, Puig, & Garcia, 2013). An important step in applying the SFF technique in this study thus entails the focus depth computation of each scene point for every image frame in the z-stack of the focusing sequence. That is necessary in order to generate the all-in-focus image as described in section 4.2.3.2.

To help characterise the neurite outgrowth across the nanofiber meshes, the two focus measures adopted in this study compute the averaged most in focus depth positions for the field of view, where movement of the cell objects/features could be monitored by tracking changes in the image focus within the z-stack. That is, as cell/features enter an image plane, the focus measure for that particular plane increases accordingly. Here, the NV was used as it was used previously to track cells in section 4.2.3.2.

Using this the position of the neurite cells in the z-direction can be estimated for each time frame, given that a high variation in pixel intensity in a predefined neighbourhood is attributed to a sharper image focus. This in turn helps estimate the neuron growth in the z direction. More importantly, the results obtained could also determine whether the neurites were taking advantage of the extra degree of freedom afforded by the 3-D scaffold and/or the gel support.

Computationally, NV assumes that the neural cell bodies, once seeded to the substrate/ECM, remain largely in the same position over the course of the experiment, (thus) expecting that any measurable depth changes are solely the result of the growth of the neurites. To further test this, the commonly used Sum-Modified-Laplacian (SML) operator, defined in equation 1, was also used as a separate focus/depth estimator for assessing the neurite outgrowth (Naylor et al., 2012; Pertuz et al., 2013). A principal advantage of SML is that it provides an

in a textured image (typical of microscopy imagery) can be determined (Naylor et al., 2012).

Equation 5

$$\nabla^2_{SML} I = \left|\frac{\partial^2 I}{\partial x^2}\right| + \left|\frac{\partial^2 I}{\partial y^2}\right|$$

Here, the analysis of the neurites in the (x,y) plane was achieved by using the CROIEditor (Jun, 2013), which allowed the ground truth to be constructed manually via measurements taken from freehand drawings overlaid on the all-in-focus images as described above; i.e. images created from the most in-focus pixels computed across the z-stack of images as shown in Figure 42.

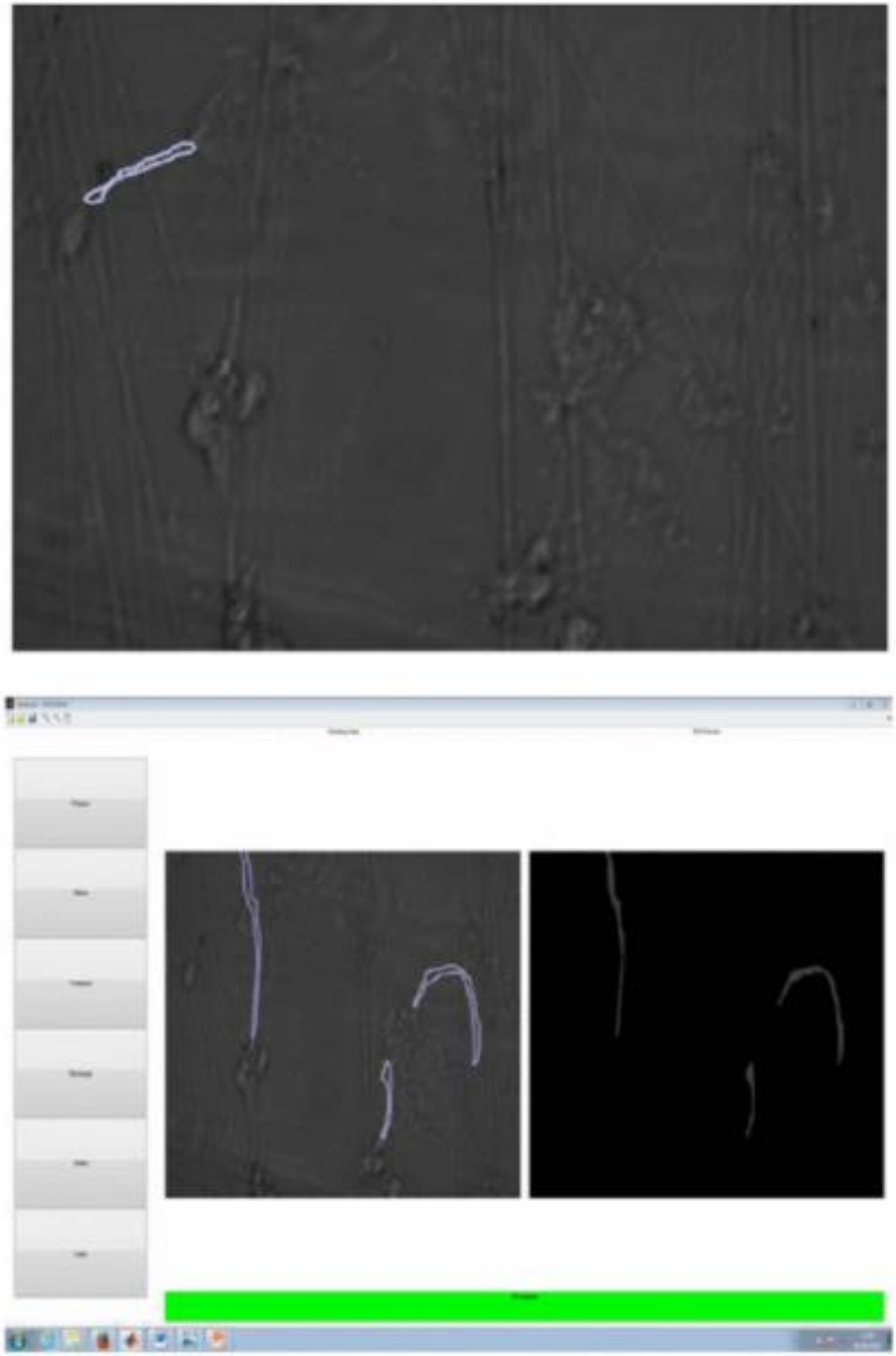

Figure 42: A) Top: The neurite boundary is demarcated and highlighted in light blue colour. B) Bottom: The neurites identified (left figure) are individually filled to produce a binary mask identifying their respective locations and areas covered in the FOV (right figure)

5.2.4. Algorithm

1. The inputs for this algorithm is the z-stack of images generated at a resolution of $0.18\times0.18\times0.4\mu m^3$ to determine the depth of the cells and the all-in-focus image generated by the Cell IQ2 machine to determine the position of the cells in the x-y plane.
2. The z-position of the individual cell/feature can then be estimated using the multi-scale focus estimation procedure described in (Smith et al., 2012).
3. The position of the cells in the x-y plane was determined by hand. This was done using the CROIEditor (Jun, 2013), which allowed the ground truth to be constructed manually via measurements taken from freehand drawings overlaid on the all-in-focus images
4. The depth of the cells was then found using the NV and the SML to estimate the position of the most in focus pixel.
    a. First the focus of each pixel on each plane was found by comparing it to the intensity of the surrounding pixels - this difference was calculated as per equations 3 and 4.
    b. The greater the difference between the pixels the more in focus the pixel was found to be. Each pixel could therefore be ranked from 1-80 (the number of frames) as to which would give the greatest focus and thus depth of the object being imaged.
    c. The average depth
5. This was compared with the SML.
6. These results are studied in detail by means of the correlation matrix, to examine the similarity or patterns displayed in the respective sequence of the computed focus/depth measures obtained by the two estimators.
7. The length of the neurons in the x-y plane was calculated by eroding the cells as found in step 3 to a single pixel of width. The length was then calculated as the total number of pixels related to that specific cell.

5.3. Results

Previous work utilising standard 2-D imaging technologies has shown that neurites respond well to the nanoscale topographical cues within 3-D scaffolds (Y. Yang et al., 2011). However, crucial questions remain as to the extent of such influence over that of the

attachment factors. This study was designed to address these questions, specifically by analysing high-resolution (40x lens) spatiotemporal data that could capture minute dynamic details of the complex yet regular hippocampal neuronal networks. In particular, the data would allow us to quantify such details via the dynamic measurement of (i) length; (ii) width; (iii) motility (how far they moved) and (iv) complexity (e.g. neurite connectivity), in the presence of different cues, both chemical and topographical, presented within the 3-D scaffold. The procedure developed locates the cell/features of interest within the 3-D culture, by computing the depth at which the FOV was most in focus. Here, the algorithms adopted analysed and quantified such growth using the 3-D locations of the most in focus pixels estimated for each time frame, particularly along the z-direction where growth was anticipated. By examining such focus/depth changes, it was also possible to explain the effects of the attachment factor (polylysine) on the direction of neurite outgrowth and (thus) its role on axon formation.

5.3.1. Estimating the Focus

From a 3-D imaging perspective, studying minute structural details of the neurite outgrowth necessitates the use of the highest numerical aperture (NA) objectives available. Computationally, a principal challenge in monitoring live cells at high NA values is that the depth of field decreases rapidly with the square of NA, making it extremely difficult yet important to maintain focus during image acquisition when high quality/resolution measurements are desired. This is compounded in extended time-lapse experiments where interesting, spatiotemporal (4D) events such as cell growth, differentiations or axon extension take place over significantly longer time scales.

Figure 43 depicts the changes in the estimated focus in terms the sampled depth (in μm) of the z-stacks of the image sequences over the course of the three experiments. In (a), the shift in focus is evident in the experiment where cells were moving down within the nanoscale

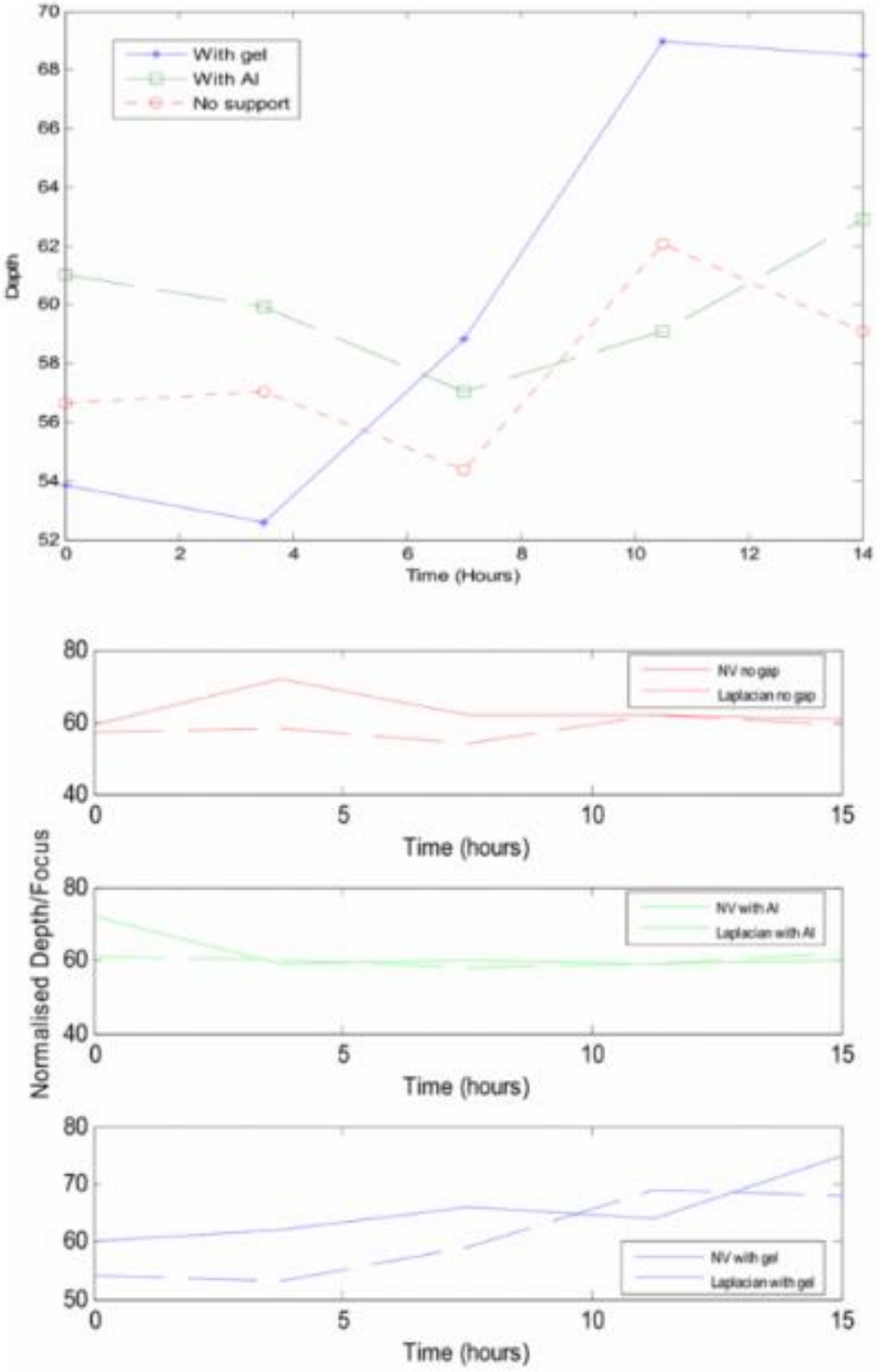

Figure 43: (a)-(d): (Top to bottom) (a) Mean estimates for the focus/depth of cell features during the course of the three experiments: Red-cells were seeded on top of the gel with polylysine laced nanofibres ~75μm directly underneath them. Blue-cells were seeded directly onto the two nanofibre layers with no spacing between them. Green-Cells were seeded onto the two nanofibre layers which are separated by a 10 μm gap. (a) Focus/depth estimations using the NV algorithm. (b)-(d) Results obtained by the SML

ECM, demonstrating the overall positive response by the neurites under the influence of the attachment factor (poly-lysine) in preference to other topological cues present in the 3-D scaffold. By monitoring the amount of downward movement of the computed depth throughout the three experiments, the effect of polylysine on neurite outgrowth could also be determined, particularly with respect to its role in promoting adherence and hence the direction of growth in the 3-D scaffold. Here, the results show that the cells seeded on the gel display a distinctively larger movement than those seeded directly onto the polylysine coated nanofibers where the gel is absent. The amount of such movement computed is also consistent with the visual inspection of the all-in-focus images collated as the previously described ground truth (discussed later).

As noted in Section 5.2.3.1, the measured depth change using NV was accounted for by the neurites outgrowth and/or their movement in the FOV, given that the nanofibers were held in place and that the neural/cell bodies were assumed to be largely stationary. The

	Fig 4a (red) with NV	**Fig 4a (red) with SML**	**Fig 4b (green) with NV**	**Fig 4b (green) with SML**	**Fig 4c (blue) with NV**	**Fig 4c (blue) with SML**
Fig 4a (NV)	1.0000	**0.6174**	-0.0283	-0.3758	0.1438	-0.1170
Fig 4a (SML)	**0.6174**	1.0000	-0.3604	-0.5096	-0.4143	-0.2324
Fig 4b (NV)	-0.0283	-0.3604	1.0000	**0.7953**	-0.2304	-0.0393
Fig 4b (SML)	-0.3758	-0.5096	**0.7953**	1.0000	-0.4708	-0.4597
Fig 4c (NV)	0.1438	-0.4143	-0.2304	-0.4708	1.0000	**0.6806**
Fig 4c (SML)	-0.1170	-0.2324	-0.0393	-0.4597	**0.6806**	1.0000

Table 5: Correlation matrix (RPQ=RQP) showing the respective sequences (p and q) of the computed focus/depth results as shown in fig. 4(b)-(d). The largest positive coefficient for each column/row is highlighted in bold typeface

assumption was further validated by using the SML operator as a second/reference estimator for the best in-focus positions within the z-stack. The results are presented in Figure 43(b)-(d), with normalised focus/depth to facilitate direct comparisons with the NV estimator (shown as dotted lines in the individual experiments). These results are studied in detail by means of the correlation matrix, which was constructed in Table 6 to examine the similarity or patterns displayed in the respective sequence of the computed focus/depth measures obtained by the two estimators. As expected, the estimated depth positions by the NV and SML operators for the individual experiment are highly correlated, attaining a coefficient value of 0.6147 (red), 0.7953 (green) and 0.6806 (blue) respectively for the three experiments. Likewise, the correlation of the results obtained between individual experiments are either absent (with rpq close to zero) or strongly inversive (with rpq yielding large negative values), with SML producing a stronger relationship in nearly all cases.

5.3.2. Neurite Length Measurements

The associated changes in the neurite length can be computed more accurately given the dynamic (3-D) estimation of the focus/depth position over the course of the individual experiments. Here, the CROIEdtior was used to help determine the length of the individual neurites, allowing the ground truth to be produced manually by demarcating the (2-D) position of the individual neurites appearing in the all-in-focus image computed for each time frame. This is illustrated in Figure 43a.

The original aim of this work was to be able to create an algorithm that could track the neurites automatically. However, whilst testing the algorithm it was found that the nanofibers were always picked up as neurites and so the data on neurite depth was inaccurate. In order to obtain accurate data and to test whether it was possible to determine the depth of the neurites in the z-axis with NV, the position of the neurites on the x-y plane was found by hand. Figure 44, shows a mask created by these hand drawings. This process was supported

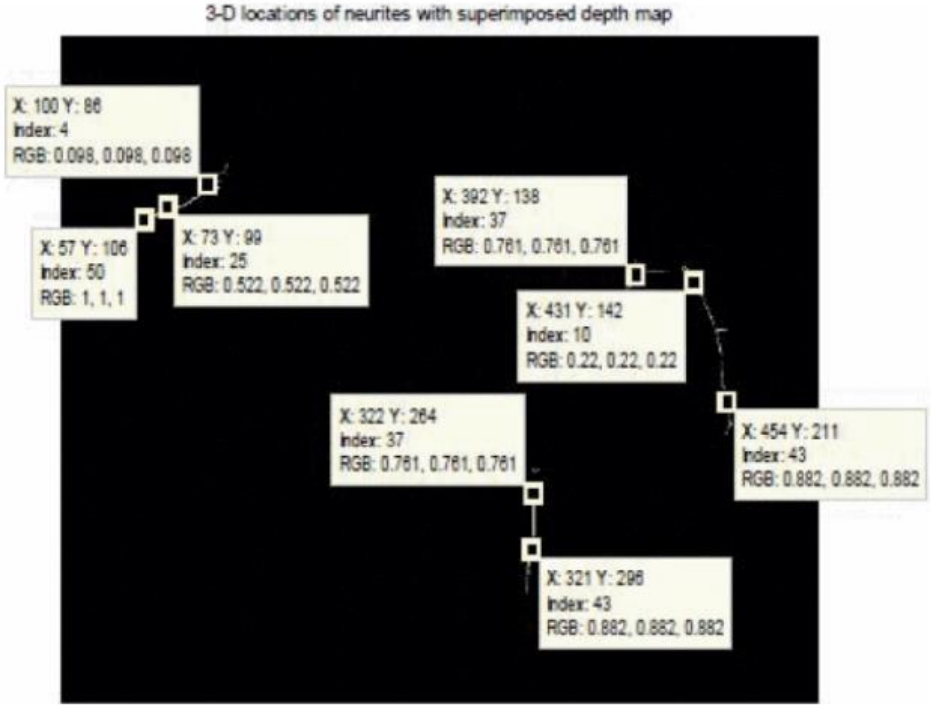

Figure 44: The mask shown in Figure 40b was superimposed onto the indexed depth map obtained for the all-in-focus image described in section III. The data-tips shown illustrate the computed (x,y,z) locations for each labelled neurite in the ground truth image generated at each time frame. The total length of a neurite was computed using the sum of the piecewise linear approximations between successive points (x1,y1,z1) and (x2,y2,z2).

by a frame by frame comparison of the (same) image over the entire course of the experiment, which helped determine the reference position of the statically constructed scaffolding nanofibers within the FOV. Once the neurite boundaries had been labelled, a morphological reconstruction procedure was then developed to enable the production of the binary mask that filled only (non-zero) connected components of the neurite objects; see Figure 40b. Finally, a morphological procedure allied to object thinning was applied to the non-zero object/components of the resulting binary mask, allowing skeletisation of the individual neurite from which its length could be computed by tracking the full run of the connecting pixels (in 3-D). The latter was achieved by superimposing the ground truth mask onto the depth map previously computed for the all-in-focus image as described in section III. This procedure is summarised in Figure 44, where the ground truth mask generated in Figure 42 was overlaid on the corresponding (indexed) depth map.

5.4. Observations and further work

Using innovative imaging and data analytics, this work on developing advanced/4-D models of the hippocampal circuitry, where a laminar 3-D network of orthogonally orientated nanofibers was studied within a 3-D collagen gel matrix. The results presented here provide demonstrable evidence that the neurites are projected towards the attachment factor even when the connecting neuron cell bodies are seeded directly above the polylysine coated nanofiber. Further work can involve the refinement of the algorithms developed which can (1) automatically and accurately locate the neurite outgrowths in 3-D and, hence, (2) quantify in detail the extent to which they are influenced by the different attachment factors as well as their concentrations. This will in turn help elicit the complex interplays between the chemical hints and topographical cues within the (3-D) nano-scale constructs, which are barely understood to date.

Several comments are in order. First, the findings of the neurite growth assay (Figure 43a) are far from conclusive, given the inevitably different neurite lengths calculated at the start of the imaging experiments; i.e., at t = 0. Second, the allied change in neurite growth rates (Figure 43b) suggests that the neurites in the collagen gel were growing at a higher rate (2.25μm/hour) than those seeded directly onto the nanofibers (0.5 μm/hour). This result can be understood by the unidirectional chemical cues existing in experiment 3 (solid line) and the lack of topographical cues. Evidently, the neuronal cell growth was more dispersed and, thus there were fewer competitions overall for cell nutrients in the disparate areas where the cells were growing. Third, the neurites in all three experiments showed a converging trend in growth rate which was manifested as a rapid decline in neurite projection, suggesting the complete depletion of surface attractant somewhat expectedly at the same time point when t=7; i.e. after 7 hours. The findings of this study are further discussed in chapter 9.

6. On tracking of spinal disk cells

This chapter makes use of the some of the algorithm from chapter 3 and builds on it to track the cells and quantify the vesicles within them. Within this chapter, the cells studied are back disk cells (described in section 2.1.2). This chapter specifically seeks to address the objectives 1 and 4 as detailed in section 1.7. The main contributions of this section are the creation of an algorithm that segmented the cells through their entropy, tracked the cells as they moved through the culture and quantified the vesicles at each time point. With this the biological conclusion that there are more vesicles on smaller cells was found.

6.1. Introduction

In cell biology, a vesicle is a small organelle within a cell, consisting of fluid enclosed by a lipid bilayer membrane. Vesicles perform a variety of vital functions in maintenance of the cell-including metabolism, transport, buoyancy control, and enzyme storage (Walsby, 1994). As such, they are particularly important for the trafficking of substances into and out of cells. For example, *lysosomes* are vesicles with enzymes which carry out functions to break down worn-out organelles, waste materials and substances/molecules that the cell may engulf. Thus, the absence of vesicles within a cell could lead to a build-up of the waste substances which could undermine the proper functioning of the cell. Given this large array of functionalities, it should be apparent that the study of vesicles is becoming increasingly important in all fields of cell biology. At present, however, whilst there are many cell tools exist to track cells, few, if any, is capable of monitoring the vesicles inside the individual cell particularly when it is unlabelled.

6.2. Methods

Section 0 describes the methods used track the back-disk cells and quantify the vesicles within them. 0 explains new method of segmenting the cells from the background, 0 describes how the NV was used to track the cells and 0 presents the algorithm generated that quantifies the vesicles on the cells that are being tracked.

6.2.1. Segmentation based on entropy

A new segmentation method that uses textural context to distinguish cells from the background is presented in this chapter. This is a principal contribution of this thesis, namely the application of the mathematical framework of entropy to cell tracking. This method is used to further enhance the feature finding method described in chapter 3. This builds on the traditional cell tracking method which combines the two-step approach to segment and link/label cells as described in section 1 above. In addition, this chapter explores the required data analytics, needed for quantitative analysis of vesicles of the individual cells following tracking.

Entropy is the measure of disorder; it is mostly associated with thermodynamics where it represents the unavailability of a system's thermal energy for conversion into mechanical work. In the context of image processing it represents how dissimilar a group of pixels are. A group of pixels with greatly dissimilar intensity, such as at the edge of a cell would have a high entropy, whereas a group of pixels with similar intensity such as the background would have a low intensity.

The key objective of the cell-tracking algorithm developed is to compute the locations of the individual cells in each image/time frame and connect (each cell to) its successive positions in the image sequence captured over the course of an experiment. Using entropy measurements, the individual cells are segmented from the background of an image from

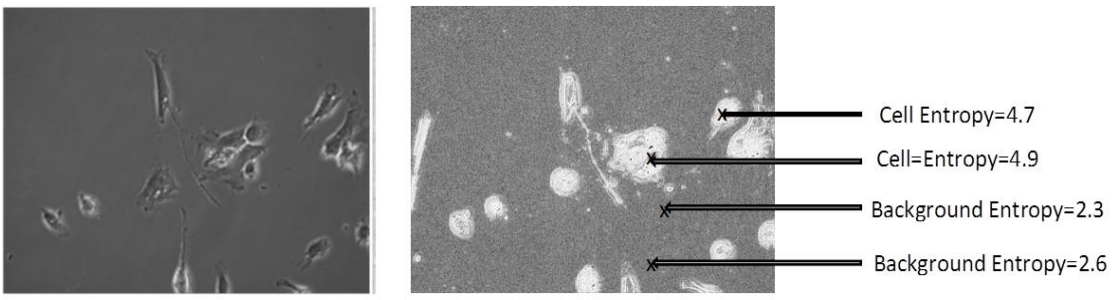

Figure 45: (Left) A PC image at 20X magnification of back disk cells in 20% Foetal Calf Serum. (Right) The corresponding local entropy map which shows low values of local entropy in grey and high values of local entropy in white. It should be noted that cells a are identified as objects in the foreground with relatively high entropy values.

which the location and area of each cell could be estimated. Such measurements are subsequently used to compute the texture-based feature vector for each cell, enabling it to be connected or mapped to the same cell in successive images where the required mapping is obtained by developing a cross correlation procedure applicable to consecutive frames of the image/time sequence.

The first step used in this paper is to find the entropy of every pixel in relation to its local region, in the predefined 5x5 kernel, resulting in a map as shown in Figure 45. The entropy is calculated as:

Equation 6

$$-\sum p.* \log_2(p)$$

Where p represents the relative histogram count (i.e. the probability) as described by Gonzalez et al (Gonzalez, 2002). (NB. The entropy of an 8-bit image/region is 8, where p = probability of occurrence of each symbol/value btw 0-255)

Figure 45 illustrates how the local entropy is used to split an image into two distinct pixel areas: those with low entropy representing the background and those with high entropy representing the cell/objects. A relatively simple thresholding method can then be used on

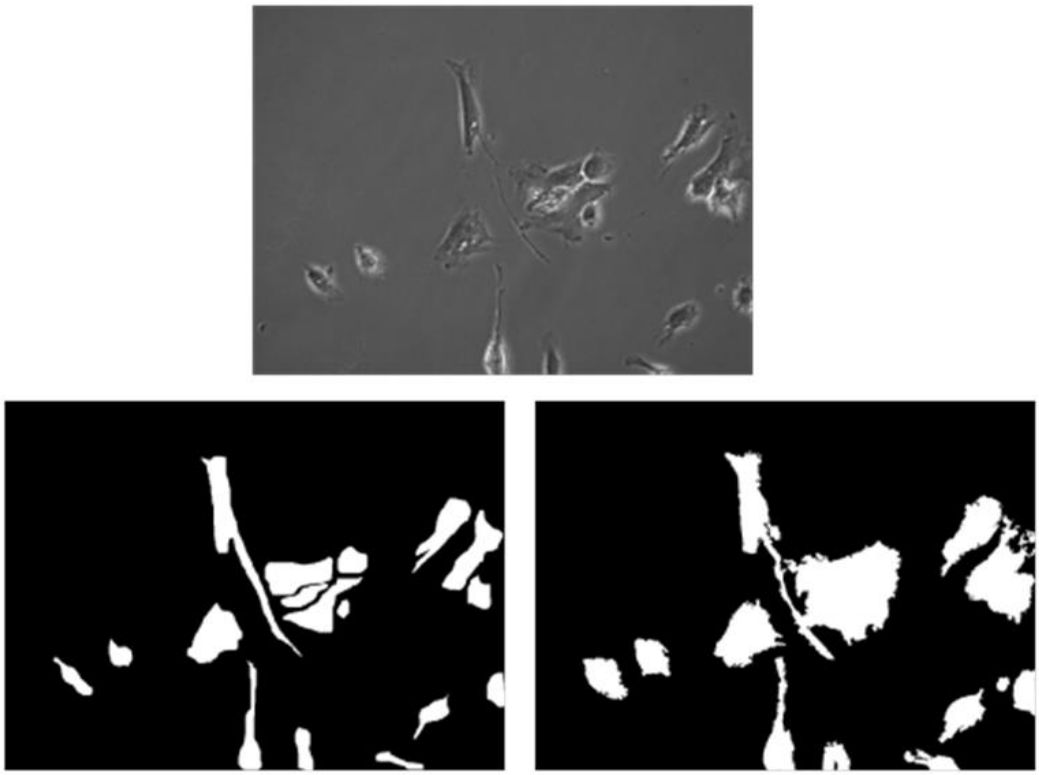

Figure 46: An example of the entropy based segmentation method showing (top) a PC of the back disk cells used in this study (20% Foetal Calf Serum). (Bottom left) Cells found by template matching, here the position of the cells if found using Normalised Cross Correlation, a form of template matching done in 2-D spatial frequency plane, to compare with the previous image. (Bottom right) Cell positions found by applying a threshold to the local entropy map as shown in Fig.1.The final position of the cells was found to be the average of these two images shown here on the bottom row

the entropy map without having to perform image segmentation whereby pixels with entropy values less than or equal to three are considered as background. The value of three was found empirically over the course of several tests to consistently act an appropriate threshold. The advantage of this methods over simple segmentation is that the brightness of the image does not affect the threshold value. More importantly, a key advantage of this method over the Watershed-based segmentation technique is that the halos associated with the individual cells are completely removed; as such, structures consist of pixels which have low local entropy values. Therefore, the method is consistent with the basic principle of entropy encoding for which data streams are compressed without loss of information. An example of this segmentation approach is demonstrated in Figure 46.

6.2.2. Cell tracking

In this chapter, the linking stage of the algorithm is divided into two steps. The first of these is to find a *cell value* for each cell. The vector component utilises the entropy found for the cell in the segmentation state of the algorithm and complements this with other textural features, namely smoothness and intensity as found across the whole cell, and the position of the cell to develop a feature vector for each cell. This is then multiplied with a weighting vector to form a single cell value for each cell. The weighting vector gave a value of 10 for the intensity of the cell, since this would be most noticeable by eye. The smoothness of the cell was given a weighting of two as the smoothness changes quite rapidly as a cell moves whilst a five was used for the entropy. Once every cell across the time series has a cell value they are compared against the cell value in the previous frame to see if any possible links can be made. It has been found empirically that for the cells used in this experiment the cell value did not change by more than ±0.2 in any consecutive frame, thus a list of possible links was developed.

Whist this process was happening one cell is allowed to map to more than one cell in the next frame and equally to no cell at all, this allows for cells that may have migrated from the field of view. If a cell is found not to link to any cell it will be assigned a new label and the tracking of the cell will begin from that point.

It should also be noted here that this initial list of mappings that links the individual cells of the current image to those obtained in the previous frame is incomplete and/or non-unique, often due to the fact that cells (new or otherwise) could enter into or move out of the current field of view. In the case of a new cell moving into the current frame, a new label must be added to the list, while any cells that have moved out from the previous frame must be withdrawn (but not removed from the current list else a different cell may be assigned their label). To address this and other anomalies arising from the ambiguity of the similar feature

scores that are within the predefined value of ±0.2, the initial list of cell assignments must be refined to facilitate a one-to-one mapping of the individual cells obtained between any two consecutive frames. Here, two approaches could be adopted; namely, the *sum of absolute difference* (SAD) (Richardson, 2003)and *Normalised Cross Correlation* (NCC) procedures, which are both described below.

The first procedure based on SAD considers the intensity changes across the pixels representing an individual cell in the current frame and find the best match from the preceding frame. It works by constructing a template that covers the 2-D region of the individual cell of interest and finding the best match for this template/region in the preceding image frame. The latter is achieved by computing the minimum of the sum of the absolute pixel-by-pixel differences of all possible regions covered by the template within the preceding frame**.** While the SAD procedure is conceptually simple to implement, it could present a major computational bottleneck in practice as the SAD calculation must be performed for each pixel of the image for which the minimum (and hence the best match) is to be found (Wong, Vassiliadis, Cotofana, Ce, & Tudelft, 2002). More importantly, any significant changes in morphology of a cell captured between consecutive frames may also render such a procedure completely inadequate to correspond cells between frames (Hand et al., 2009b).

Alternatively, the NCC method seeks to address much of the shortcomings of the template matching based procedure of SAD by using the FFT (Fast Fourier Transform) based convolution technique in the 2-D Fourier domain; see (Feng Zhao, Qingming Huang, & Wen Gao, 2006). The technique is particularly attractive as it is computationally efficient method of implementing correlations with several orders of magnitudes faster for relatively large target and search images, and has previously been used in a number of image tracking

applications (Feng Zhao et al., 2006; Norman & O'Reilly, 2002; Tsai & Lin, 2003). Mathematically, the NCC is defined below:

Equation 7

$$NCC = \frac{\sum_{x,y}[f(x,y) - \overline{f_{u,v}}][f(x-u, y-v) - \bar{t}}{\sqrt{\sum_{x,y}[f(x,y) - \overline{f_{u,v}}]^2 \sum_{x,y}[f(x-u, y-v) - \bar{t}]^2}}$$

where f*(x,y)* is the search image, $\bar{t}$ is the mean of the intensity of the target/image template and $\overline{f_{u,v}}$ is the mean of *f(x,y)* in the region of interest under the template. *x* is the position of the cell in the x-axis, *y* is the position in the y-axis, *u* is the displacement in the x-direction and *v* the displacement in the y-direction.

As described in (Feng Zhao et al., 2006), the NCC procedure was shown to be able to generate the best position of the target image *t* in *f* (x,y) - the search image (in the preceding frame) from which a cell that has an appearance very similar to it could be located. This was observed in the experiments/data.

6.2.3. Vesicle quantification

The final yet important objective of the proposed method concerns the quantitative analysis of vesicles that are present in the individually tracked cells over the course of our experiments. Here, given that the vesicles of interest are most noticeable by their extremely bright appearance within each tracked cell (see Figure 10), a relatively simple thresholding procedure has been applied to facilitate generation of the relevant 2-D masks for the relevant cell in order for quantitative measurements such as size and number of the detected vesicles can be obtained.

It should be noted that further studies of vesicles concerning automated analysis of the size and distribution of vesicles are beyond the scope of this study and thus, has not been covered in this thesis.

Finally, as with the cell tracking algorithm presented here, the results obtained for this chapter have also been validated against the ground truth that was obtained by using the vesicle counts generated manually using the freehand drawing tool (CROIEditor) (Jun, 2013)

6.2.4. Algorithm

1. The entropy of each pixel was determined by calculating the entropy of the 5x5 pixel region around a pixel from the equation 5. The entropy map of the image was then plotted in a region of the size of the original input image. Here the intensity of the pixel represented the entropy rather than the image intensity of the input images.
2. From this entropy plot the cells were then found using the same edge detection methods described in Chapter 3.
    a. Find the edge of the cells using the Canny edge detection. This creates a black image with the outlines in white. This was use with a Gaussian filter of size 5x5 with a σ of $\sqrt{2}$. The upper and lower threshold values were selected dynamically by the MATLAB algorithm.
    b. Dilate the edges by 2 pixels to insure proper contention.
    c. Fill in the cells location by filling in regions in contacting. Creating a black background with the approximate locations of the cells in white.
    d. Erode the edges by two pixels to account for step two, the area is now considered to be a rough estimation of the location of the cell.
    e. To clean up the image, the small particles (area <= 300 pixels) and holes (area <= 256 pixels) were removed by applying a particle filter to the thresholded image of the region of interest. The area of the particles and holes to be removed was determined manually by measuring their average sizes across a range of typical images. At this stage, the output of the image was a black and white mask.

3. Textural feature (entropy, smoothness, etc) of each cell, identified by being a single frame were then found.
    a. Entropy was found by taking the average entropy from the parts the entropy plot found in step 2.
    b. The smoothness of the cell was found by finding the variance of the intensity of the pixels that make up that cell. This was calculated as

Equation 8

$$S = \sqrt{\frac{\sum(x-\mu)^2}{N}}$$

Where x is the intensity of a pixel μ is the mean intensity of all pixels in a given cell and N is the number of pixels that make up that cell. Cells with a smaller S value have a greater level of smoothness.

    c. The mean intensity of the cell.
4. Each cell found on the first image was given a unique label to facilitate the tracking.
5. The most likely candidate for cell matching was then found by SAD. This was done using the MATLAB.
6. The same features are found for every cell in each image in the sequence.
7. The position of each cell was defined as the position of the centre of the cell. Thus, each cell was given x, y coordinates in relation to the top left of the image frame.
8. The most likely candidate for cell mating was then found by taking an area of the target frame 100 pixels around the coordinates of the centre of the cell location form the previous frame. The SAD was then found for each set of possible locations within this area.
9. The region with the smallest SAD was then examined to see if:
    a. It contained a cell
    b. If the mean intensity, entropy and smoothness of that cell was within 10% of the original cell.
10. If both a and b in step 9 were not met then the search moves to look at the region with the second smallest SAD.
11. Use NCC to generate the closest position in the target frame and compare to the SAD to confirm the final position.

12. Each cell should maintain its unique label throughout the time frames examined. Any new cells entering the field of view are given a new unique label. If a cell leaves the field of view it is no longer tracked.
13. The intensity variance across the cells in each frame is then examined to look for the number of vesicle within a cell. The vesicles were found by finding a group of over exposed pixels in the cell region, between 15 and 100 pixels in size.
14. The mean intensity, entropy, smoothness, x and y coordinates of the cells are then recorded alongside each cell's unique labels to track the changes in the cell over time.
15. In addition, the following was recorded for each cell. Features of the cells were identified by
    a. Area - total number of pixels
    b. Perimeter- number of pixels that make up the edge of the cells
    c. Orientation- angle between the major and minor axis
    d. Aspect ratio- minor divided by major axis length
    e. Circularity - per equation 2
    f. Displacement (length) change in central pixel location
    g. Displacement (angle)- change in orientation with relation to an arbitrary x axis
16. The cells were then divided into three cell types, those with less than three vesicles, those with three to 10 vesicles and those with more.
17. Differences in the morphology of the cells was compared to the number of vesicles by plotting bar graphs of the means and standard error on the mean.
18. The change of the cells over time was investigated with scatter plots of number of vesicles vs time.

6.4. Results

To help study the changes in the number of vesicles over time closely, a computational workflow must be developed to automate tracking and analysing potentially thousands of cells captured using high-throughput time lapsed microscopic imaging technologies. The tasks at hand are complex, involving principally the previously presented tracking algorithm which sought to locate the cell/features of interest within the culture, by computing firstly, the position of the individual cell and secondly, the relative locations of vesicles identified

in each of the individually tracked cells over the course of our studies. Specifically, the techniques developed help to quantify such physical movements within the field of view, by separating from the image background the individual cell in the entropy space where the locally measured entropy was also added to the texture-based feature vector, dynamically constructed as a descriptor for each cell across the time lapsed image sequence. Coupled with the NCC procedure which was designed to operate in the frequency domain (primarily to improve run-time efficiency), such a descriptor enables individual cell to be tracked and, importantly, analysed for the presence and development of vesicles over time.

To facilitate the development of the complex workflow described above, several tests have been devised to help develop/validate the proposed tracking algorithm that was accompanied by closely allied data analytics specifically designed to analyse vesicles development over the course of our study. These tests have been implemented using a manually constructed ground truth (GT) set which can be defined as follows:

- For cell segmentation; the GT consists of the manually obtained location of each cell selected.
- For cell linking; the GT consists of the complete mappings of the individual cell over successive time frames.
- For vesicle quantification; the GT consists of the manual vesicle counts for the individually tracked cell over the selected time frames.

6.4.1. Validations

The results obtained by the automated cell segmentation of cells were compared with the relevant GT set (consisting of a total of 87cells), where it was found that 87% of the cells were labelled correctly, 5% were incorrectly labelled as cells (i.e. false positives) and (8%) were without a label (i.e. false negatives). These results were further compared to those generated by the Cell Tracker, a freely available software platform that combines the

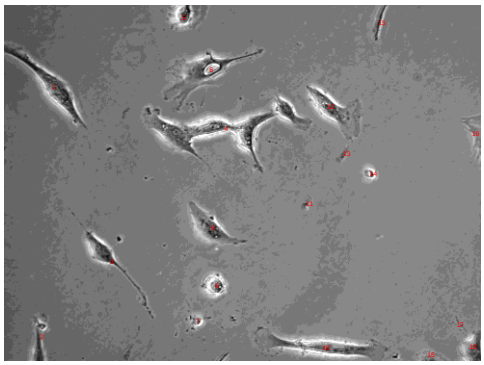

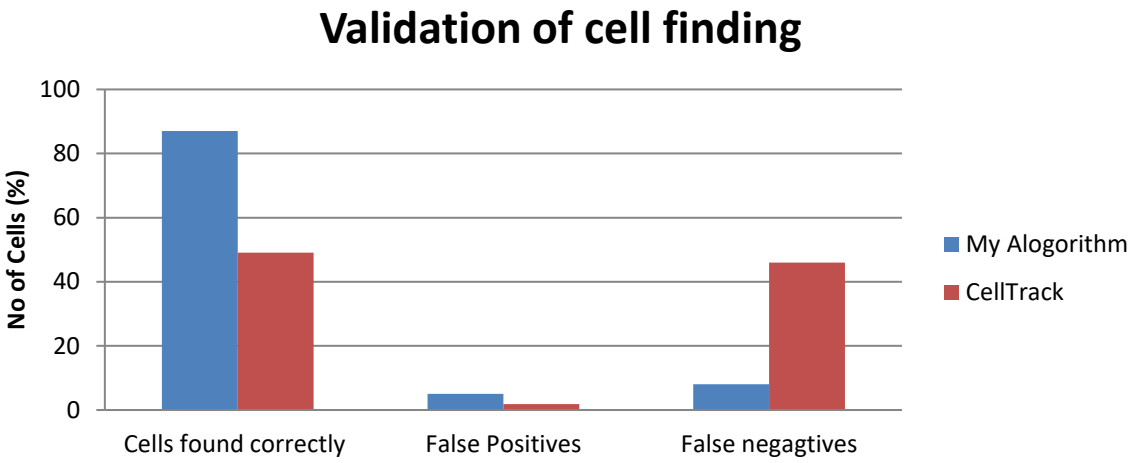

Figure 47: Validation of cell finding from the local entropy maps shown in Fig. 1. (Top) Shows the cells with their assigned label showing where the algorithm has found the centre of the cell to be, it is to be noted that the large group of cells has only been assigned one label as to the algorithm it looks like one cell. (Bottom) shows the how well the cells in the test group (n=73) were found in the first images (where cell tracking could not be used). It was found that 87% of the cells were found and labelled correctly in our algorithm when compared to manual results and just 49% of those using the cell track, 5% of the cells labelled were found to be background or debris incorrectly labelled as cell, a worse result than the 2% of the cell track. Of the 87 cells labelled manually 7 (8%) were not labelled by the algorithm, including those cells where a large group of cells were labelled as one cell, whilst this applied to 46% of the cells with the cell track.

techniques of particle filtering and active contours technique to determine the relative position of the nucleus and cytoplasm of the individual cell. Using the same test data and GT set, the cell tracking platform was only able to correctly label 50% of the total number of cells, although with fewer false positives (2%) when compared with the proposed algorithm (5%) shown in Figure 47.

It was found that the cells were tracked accurately $p<0.05$. This figure was found from the null hypothesis that assumed that the cells would not be tracked from the first image in the linked series to the tenth. It was decided to test to the tenth image as this was done in the cell

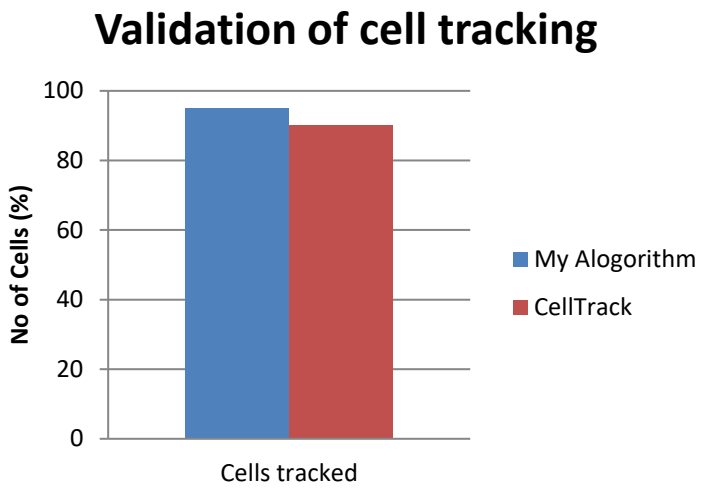

Figure 48: Validation of Normalised Cross Correlation tracking algorithm. It was found that most of the cells (n=73) were tracked accurately ($p<0.05$, students t-test) when compared to those tracked manually. Figure depicts the percentage of cells that the tracking algorithm matched the cells tracked manually. It is evident that whilst some of the cells could not be tracked the majority could. It is to be noted that the cells were miss-tracked when the cell being tracked was more than 50% occluded by the other cells.

tracking comparison paper by (Hand et al., 2009a). This test was carried out across several sets of cells that were imaged in separate wells of a 24 well plate. Only cells that were correctly identified in the first image were used in this test so that the results of the image tracking did not depend on the results of the initial segmentation. Cells were deemed to have been tracked correctly if they retained the same numerical value between the first and the 10^{th} image when compared to the manually derived values. The graph in Figure 48 shows the results of the validation, from this it can be seen that 87% of the cells were correctly label and tracked through the first 10 frames when compared to the manual labelling. It should be noted that the cells were miss-tracked when the cell being tracked was more than 50% occluded by the other cells. The result found is comparable to the results found using the Cell Track software that tracked 89% of the cell correctly. However as discussed above, the Cell Tracker software was only able to identify 49% of the cells correctly so there was a smaller starting pool from which to draw these cells.

6.4.2. Vesicles

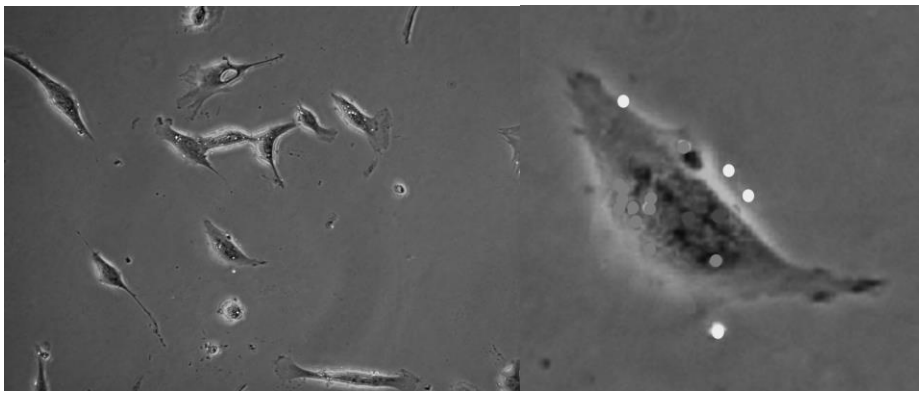

Figure 49: A exampe of showing (top) a PC image at 20X magnification of back disk cells in 20% Foetal Calf Serum, with vesicles found by the algorithm highlighted in white. (Bottom) a close up of a cell showing in grey the number of vesicles (n=17) correctly identified by the proposed algorithm. The that were not identified by the proposed algorithm are shown in black were and false positives are shown in white (with n=4)

The second requirement of the algorithm was that it could find the vesicles. The vesicles found are highlighted on a single time sequence image are shown in Figure 49 with the vesicle found in white. A close-up of one cell in this image gives an indication of the number of identified vesicles (n=17) that are false positive (n=4) and false negatives (n=2).

This last but important study was designed in a biological context to investigate vesicle development in back disk cells over time, the algorithm developed and the results generated are a contribution of this thesis. Specifically, it sought to capture minute dynamic details of these cells with a 20x lens to facilitate quantitative analysis of vesicles present in the individual cell.

A key objective of the developed algorithm was to facilitate generation of biologically meaningful measurements of back disk cells that are based on automated quantitative studies of vesicles developed in these cells over the course of an experiment. As proof of principle, the data analytics were constructed so that they would (i) enable vesicles to be identified reliably within the individually tracked disk cells across successive time frames, where (ii)

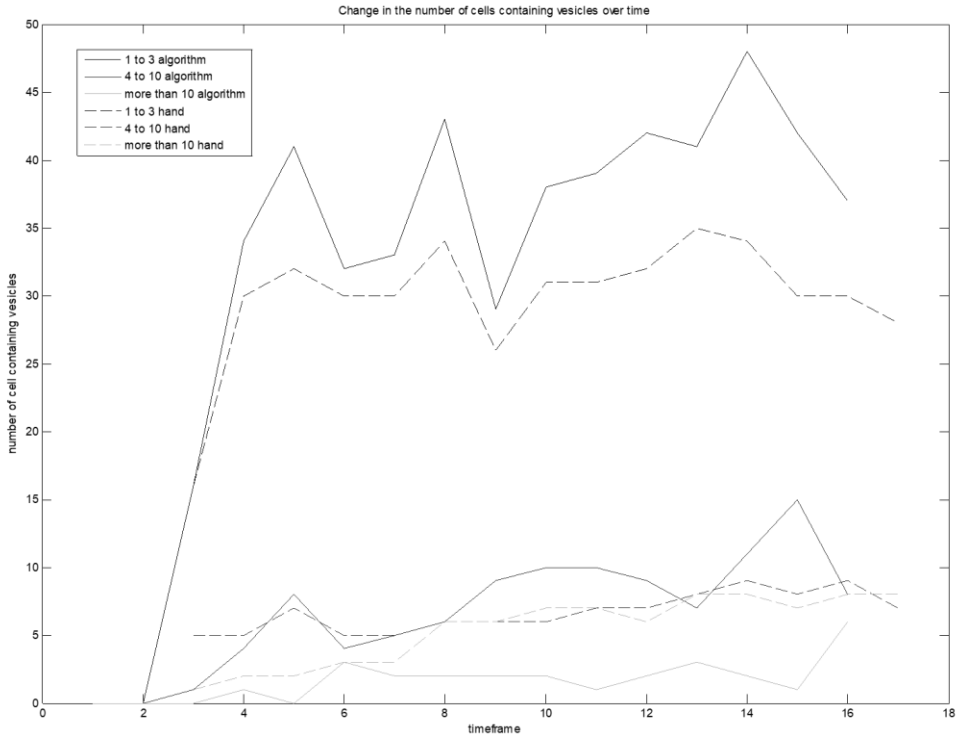

Figure 50: total number of vesicles per cell as found manually (dashed line) and by the algorithm (straight line). In this graph the vesicle count has been split in three types of vesicle count those cells with <3 vesicles (dark top line) those cells with 3-10 vesicles (middle dark line) and those cells with more than 10 vesicles (grey line). This was done to see how the algorithm dealt with different concentrations of vesicles.

the statistical distribution of back disk cells could be characterised based on a simple yet biologically relevant analysis of vesicles present in these cells. In three distinct groups, such as in the graph of Figure 50. This was done by splitting the cells in to three groups depending on the number of vesicles contained within: namely, cells with fewer than three vesicles were in the first group, 3-10 vesicles in the second and over 10 vesicles in the final group. It was found that the algorithm and the manual count broadly matched the values found manually and taken to be the ground truth with p=0.001 and the maximum difference between the cumulative distributions, D, is 0.7143 as measured by the Kolmogorov-Smirnov Comparison of Two Data Sets cells that contained less than three vesicles, with the algorithm (solid line) getting a slightly higher count than the manual method, this higher count accounted for by the false positives as shown in Figure 47. However, there were too few

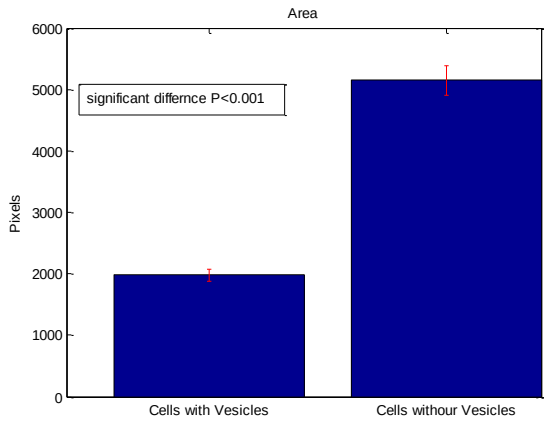

Figure 51 A statistical distribution illustrating the mean size of the cells that contain vesicles and those that do not. It was found that of the cells measured (n=302) there was a significant (with P<0.001) difference in size between those cells that contained vesicles and those that did not.

cells, (less than 10), in the two larger categories (3-10 and more than 10) for any statistically significant conclusions to be drawn. This shows that whist the algorithm can detect the vesicles within cells with low number of vesicles, more work needs to be done with a much higher number of cells ~n=750 to determine its usefulness for the cells with a high number of vesicles. The significance of this result comes from the fact that it is now possible to see that after an initial fast rise in the number of vesicle containing cells (i.e. originally there were some cell that did not contain any visible vesicles but after a period of time they did) there does not seem to be much change in the number of vesicles per cell.

The next test was designed to investigate the biological significance of cell morphology over the number of vesicles developed in disk cells. To test this, the cells were split into two groups; those without vesicles and those with more than three vesicles. Those with 1-3 vesicles were discarded to eliminate the likelihood of false positives generated by the proposed tracking algorithm and thus should not affect the results. The results as shown in Figure 51 show that it is the smaller cells that contain the vesicles, with P<0.001 in the applicable students T-test on the mean value of the size in pixels of the cells. This result is

of particular interest. Until now, the relatively simple study of the effect of cell sizes on vesicles development has not been possible without performing the measurements by hand.

This result is particularly of interest as to obtain an accurate measure of size of the cells by hand would be too laborious so up until this point the morphology of such cells could not be determined.

A final application of such an algorithm is to look at how the number of vesicles changed overtime in individual cells. The results for the number of vesicles in 87 cells are shown in Figure 52.

It can be seen in Figure 52 that the number of vesicles in the experiment for every cell is initially zero, in the cells with vesicles this then grows with the first 90 minutes before fluctuation at a relatively stable number. These fluctuations are expected as the vesicles

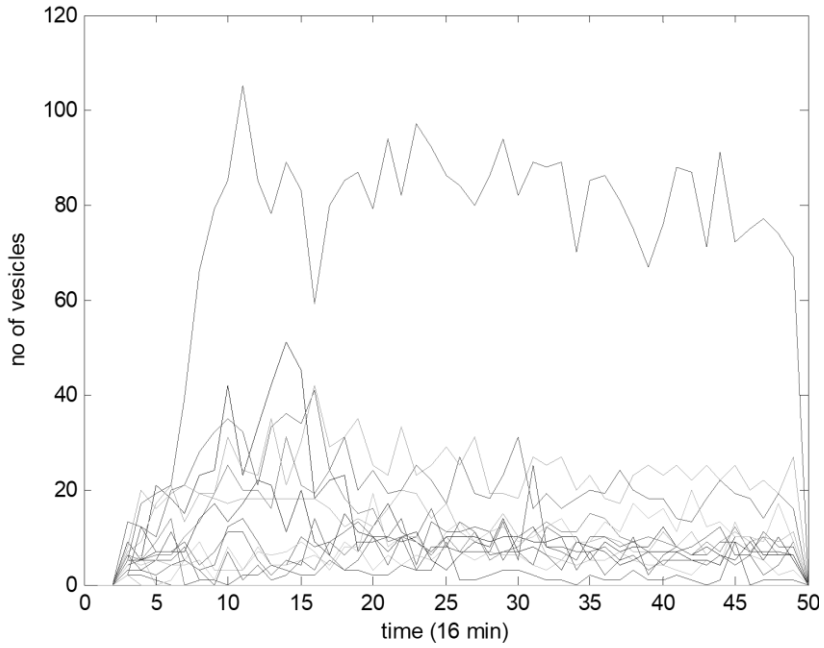

Figure 52: showing the changing number of vesicles in individual cells (n=87) over the course of a 13 hour experiment in a glucose rich environment. It is to noted that most of the cells (n=79) have less than 10 vesicles per cell throughout the experiment and that most of these (n=68) have less than three vesicles per cell.

move from the top of the cell, where they are visible to the microscope, to other parts of the cell, where they are not.

6.5. Observations and Further Work

The results show that algorithm can be used to effectively track cells in phase-contrast time-lapse microscopy images within a time frame that is amenable to real time analysis. Under the specific tracking conditions examined here, software developed using local entropy achieved a better rate of successes in finding the initial positions of the cells than CellTracker, thus allowing the development of a cell tracking algorithm that is not dependant on user input. Using a mixture of Normalised Cross Correlational and a textural based weighted tracking system an effective method of cell tracking was developed, as shown by comparison to manual tracking methods. It was considerably faster than manual tracking, leading to the possibility of real time analysis. Furthermore, there was a good result from the vesicle tracking algorism that successfully identified 87% of the vesicles within the cells. The main power of this algorithm is that it has the potential to deliver a large amount of data from which many different biological conclusions can be drawn. As the finding of the initial positions of the cells is done automatically no user input it required. The findings of this study are further discussed in chapter 9.

7. Tracking chondrocyte movement in 3D gels

This chapter makes use of the depth algorithm used in chapter 5 and couples it with the tracking aspect of the algorithm from chapter 9. Within this chapter, the cells studied are chondrocytes. This chapter specifically seeks to address the objectives 1 and 5 as detailed in section 1.7. The main contribution of this section is the combining of the two dimensional and three-dimensional tracking to see the behaviour of the individual cells in the culture.

7.1. Introduction

The work in this chapter looks at chondrocytes. This is done as, in clinical settings, chondrocytes are differentiated from MSCs for the purposes of cartilage repair. Chondrocytes are the only cells found in healthy cartilage. They produce and maintain the bone and the bone structures. The loss of cartilage leads to arthritis in joints.

Recent work on the chondrocytes in 3-D shows that a gel can be used to form an effective extracellular matrix. In phase contrast microscopy, as used in this experiment, there is no effective gold standard for measuring the position of the cells within a gel. In order for this to come about the imaging properties of these gels needs to be investigated. The resultant data would enable us to track the cells as they moved and formed bonds within the gel, and ultimately detect the effect of different treatments on cellular migration and structure formation in three dimensions. The contribution here was to identify the gel type that was most suited to 3-dimentional analysis in phase contrast.

7.2. Methods

Section 0 describes the methods used to track the chondrocytes as they move in three dimensions. 7.2.1 describes how the cells were harvested and seeded in the gels, 7.2.2. details

how the cells were imaged in order to be able to obtain the three-dimensional data necessary for the experiment. 7.2.3 describes the algorithms that determined the depth of the cells. 7.2.4 Presents the algorithm generated that tracks the cells as they move through the gel.

7.2.1. Plate set up

The cartilage isolated from the bone marrow was seeded in four well culture plates at low density (4000 cell/cm^2) in culture medium in an equal volume mix of ham's F12 medium and Dulbecco's modified eagle medium (F12:DMEM). Harvested chondrocytes were washed and re-suspended in PBS and counted, before being seeded onto the gels.

The cells were set up in the two configurations shown in Figure 53: a) the cells were seeded on top of the gel (all gel types), as such it could be expected that the cells would move down through the gel over the course of the experiment and each cell would be easily distinguishable b) the cells were put in pellets of gel at the bottom of the wells (alginate

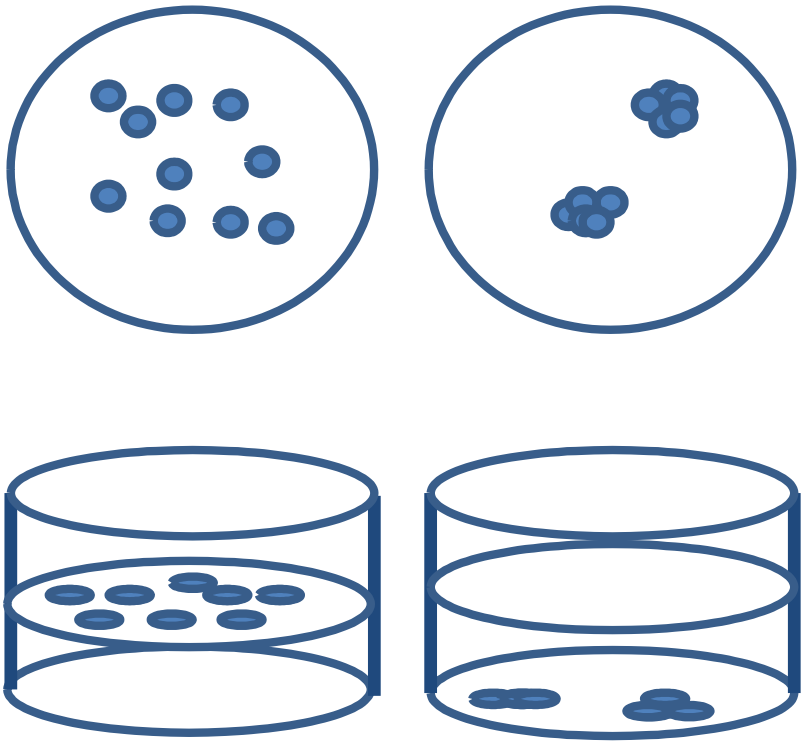

Figure 53:Experimental set up showing a) cells seeded on top of the gel and b) cells seeded in pellets under the gel

only), the cells would still move down though the gel but there would be less room for them to move and they were densely packed so that each cell is hard to distinguish form the others.

7.2.2. Imaging

The experiments were carried out on the Cell-IQ platform, a multimodal microscopy system which uses phase contrast and multichannel fluorescence microscopy, providing automated imaging in 2-D or 3-D cultures. The integrated incubator is also designed to accommodate analyses of two standard micro-plates simultaneously, allowing quantitative cellular parameters to be measured non-invasively from the long time-lapse image sequences. The equipped high precision motorized z-stage of the automated microscope allows the acquisition of 3D image stacks, with a minimum measured volume (voxel) which is characterised by an anisotropic (x,y,z) resolution at 0.18x0.18x0.4 μm3.

An important requirement of the algorithms developed to study the cell cycle is that it is necessary to track each cell throughout the experiment whilst the cell is in the field of view. In addition, the dynamic depth position of the cells in the z-plane had to be tracked. Here, images of the cells were captured using automated microscopy with a high precision z-stage, from which a series of 89 images could be collected at different focal heights. The z-position of the cells are then estimated by means of determining the most in-focus pixels in each image. This computational procedure has been used successfully in previous work with mesenchymal stems cells and hippocampal neurons, section 5.

7.2.3. Focus measures

The focus measure was found by taking advantage of the limited depth of field of the phase-based microscopy systems, where images are retrieved with discernible quality differences given the relatively narrow depth of field or in-focus limits; that is, cell object/features captured at different depths from the camera may appear out of focus if they are away from

the focus plane. Using the widely documented computer vision technique of shape-from-focus , several measures of quality of image focus (or focus depth measures) have been considered in order to best compute the in-focus image frame for a particular point in the image space (Carlton et al., 2010; Smith et al., 2012). An important step in applying the shape from focus technique in this study involves the focus depth computation of each pixel for every image frame from the z-stack of the focusing sequence; that is, to generate the so-called all-in-focus image (Tarvainen et al., 2002).

7.2.4. Tracking methods

For the cells seeded on the gels, as in Figure 53a computational tracking was possible. This was achieved by taking advantage of the textural difference between the cells and the background, since the difference in intensity is too small to measure. Having, thus, distinguished the positions of the cells in the first image, normalized cross correlation could be used to map the cells between each image. Here, the Cross Correlation, which has been used previously in various types of image tracking (Feng Zhao et al., 2006; Norman & O'Reilly, 2002; Tsai & Lin, 2003) among others, is defined as below:

Equation 9

$$\gamma(u,v) = \frac{\sum_{x,y}\left[f(x,y) - \overline{f}_{u,v}\right]\left[t(x-u,y-v) - \overline{t}\right]}{\left\{\sum_{x,y}\left[f(x,y) - \overline{f}_{u,v}\right]^2 \sum_{x,y}\left[t(x-u,y-v) - \overline{t}\right]^2\right\}^{0.5}}$$

Such that:

- f Is the image.
- $\overline{t}$ is the mean of the template
- $\overline{f}_{u,v}$ is the mean of $f(x,y)$ in the region under the template

Using Equation 9 the position of the cells in the subsequent image can be estimated by looking at their sum aggregated displacement in Fourier space. Using the fast Fourier transform reduces the computational complexity therefore makes it a more practical method to use in real time analysis. More importantly, the results obtained could also determine whether the cell has changed morphology significantly.

Computationally, Equation 9 assumes that the cells only change position, and not shape, in each time frame; in order to account for the changing of shape, the results found by Equation 9 have to be compared with the results found by the entropy studies described in section 0, in order to determine the place of the cells in the first image. This combination can produce a mask of the position of the cells, including those in high confluent religions. The results of this for cell finding are shown in Figure 54. To test this, masks produced were compared to masks created manually using the CROIEditor (Jun, 2013), which allowed the *ground truth* to be constructed manually via measurements taken from freehand drawings overlaid on the all-in-focus images.

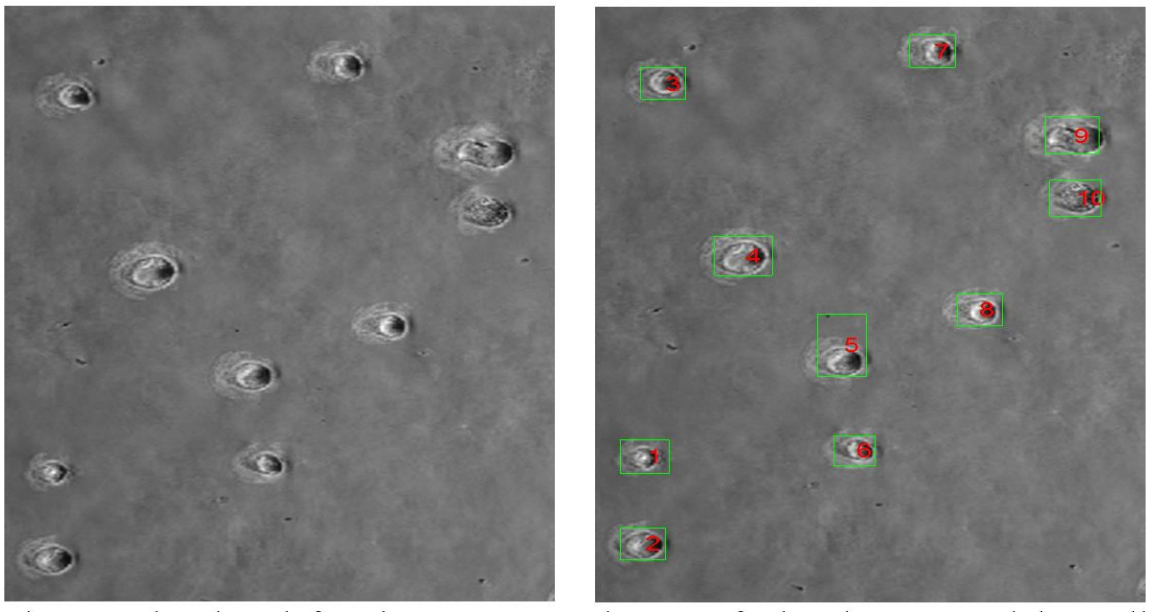

Figure 54: Showing left: phase contrast image of chondrocytes. Right: cells identified

Once a mask containing the position of the cells had been found, extracting depth and morphological data could be done for each cell on each image in the time series. By storing this data along with the cell ID, it was possible to see how this changed over time and hence deduce the cell cycle. To find the position in the z-plane and whether the cell was adhered to the surface of the plate the most in focus pixel was calculated from the Minimum Description Length (MDL) (Koenderink, 1984), since for this experiment there is a z-stack of images as used in our previous work on neurite depth tracking, this is defined as below

Equation 10

$$L(I_0|\sigma) = L(I_\sigma) + L(\varepsilon_\sigma)$$

Where L represents the MDL, I_σ is a Gaussian smoothed image at scale σ, I_0 is the original image and ε_σ is the residue. Here, σ gives a quantitate measure of local texture granularity. Using **Error! Reference source not found.** the position of the chondrocyte cells in the z-direction can be estimated for each time frame, given that a high variation in pixel intensity in a predefined neighbourhood is attributed to a sharper image focus. This in turn helps to estimate the z-position of the cells. From that it is possible to determine the depth of the cells, since adherent cells will have lower values of MDL. More importantly, from this it can be deduced whether a cell is going through apoptosis, since such cells do not adhere to the surface.

The studies presented here sought to further the earlier investigation on using the *depth from focus* technique to quantify the movement of neurites in 3-D (chapter 5) and quantifying of vesicles on spinal disk cells, in 2-D (chapter 6).

7.2.5. Algorithm

1. Find the position of the cells in 2 dimensions as detailed in section 6.
    a. The entropy of each pixel was determined by calculating the entropy of the 5x5 pixel region around a pixel from the equation 5.

b. The entropy map of the image was then plotted in a region of the size of the original input image. Here the intensity of the pixel represented the entropy rather than the image intensity of the input images.
c. From this entropy plot the cells were then found using the same edge detection methods described in chapter 3.
    i. Find the edge of the cells using the Canny edge detection. This creates a black image with the outlines in white. This was used with a Gaussian filter of size 5x5 with a σ of $\sqrt{2}$. The upper and lower threshold values were selected dynamically by the MATLAB algorithm.
    ii. Dilate the edges by 2 pixels to ensure proper connection.
    iii. Fill in the cells location by filling in regions in contact. Creating a black background with the approximate locations of the cells in white.
    iv. Erode the edges by two pixels to account for step two, the area is now considered to be a rough estimation of the location of the cell.
    v. To clean up the image, the small particles (area <= 300 pixels) and holes (area <= 256 pixels) were removed by applying a particle filter to the thresholded image of the region of interest. The area of the particles and holes to be removed was determined manually by measuring their average sizes across a range of typical images. At this stage, the output of the image was a black and white mask.

2. Track the cell movement as detailed in section 6.2.4
    a. The position of each cell was defined as the position of the centre of the cell. Thus, each cell was given x, y coordinates in relation to the top left of the image frame.
    b. The most likely candidate for cell mating was then found by taking an area of the target frame 100 pixels around the coordinates of the centre of the cell location form the previous frame. The SAD was then found for each set of possible locations within this area.
    c. The region with the smallest SAD was then examined to see if:
        i. It contained a cell.
        ii. If the mean intensity, entropy and smoothness of that cell were within 10% of the original cell.

d. If both i and ii in step c were not met then the search moves to look at the region with the second smallest SAD.

3. Determine the location of the cells of the z-plane by creating a depth map following the method of (Smith et al., 2013a).
4. By overlaying masks created in section 1 it is possible to determine the average depth of the cells by finding the average depth of the pixels covered by the cell.
5. Combine the results of the tracking and the depth to find the change in depth over time.

7.3. Results

Previous work utilizing standard 2-D imaging technologies has shown that chondrocytes growing in three dimensional structures display a different morphology to those growing on the bottom of a culture dish. However current methods in 3-D imaging are not yet sufficient for the demands to image such cells in phase contrast microscopy. This study was designed to investigate different types of gel that could be used in conjunction with the extracellular matrix to see whether the depth of the cells within those gels could be determined. In particular, this data would allow us to quantify such data via the dynamic measurement of position and depth in the different gels.

The procedure here is based off of that described in chapter 6. It is first used to locate the cells within the x-y plane, from the contrasting texture of the cells to that of the gel. Then using normalized cross-correlation the cells are tracked and identified across the culture. Finally, the position of the cells in the z-direction is found by computing the depth at which the FOV was most in focus. From this, the algorithm quantified the movement of the cells using the 3-D locations of the most in focus pixels that were estimated for each time frame, particularly along the z-direction where movement was anticipated (Smith et al., 2013a). By examining such focus/depth changes, it was also possible to see how far in a culture a cell could be tracked in different types of gel. To corroborate the results the findings of the depth

found by the normalized cross correlation algorithms were compared to that of the sum modified Laplacian (SML) operator, defined in equation 4 (Duthaler & Nelson, 2005b),

Equation 11

$$\nabla^2_{SML} I = \left|\frac{\partial^2 I}{\partial x^2}\right| + \left|\frac{\partial^2 I}{\partial y^2}\right|$$

A principle advantage of SML is that it provides an isotropic measure of the second derivative for which the strength or amount of edges present in a textured FOV can be determined (Ho & Punzel, 2003). This is particularly useful in phase contrast microscopy where there is a combination of strong and weak edges.

Figure 55 shows the changes in estimated focus in terms of assumed depth (in µm) of the z-stacks of the image sequences over the course of the collagen gel set up with the cells seeded on top of the gel as shown in Figure 53a. Every graph shows the change in depth for three cells relative to their position at time t=0. In (a) as found by the normalized variance algorithm method shown in section three, (b) the sum modified Laplacian. It is to be noted here that the deeper the cell has gone the higher the value of the normalized depth. It is to be expected that the cell will move down through the gel towards the bottom of the dish. It can be seen here that the collagen gel does show this pattern as would be expected up to a depth of ~50 µm, as confirmed by both algorithms. After this point, the cells seen to oscillate within the gel and both algorithms return very different results. This suggests that at this depth within the culture such cells cannot be tracked.

Figure 56 shows the changes in estimated focus in terms of assumed depth (in µm) of the z-stacks of the image sequences over the course of the gellum gum set up with the cells seeded on top of the gel as shown in Figure 53a. Every graph shows the change in depth for three cells relative to their position at time t=0. In (a) as found by the normalized variance

algorithm method shown in section three, (b) the sum modified Laplacian. In this case to a depth of 30 μm the cell does behave as expected but after this these cells cannot be monitored. Since the depth of the gel in this instance was ~7 mm there was still room for the cells to move in the z-direction. The difference in depth that the cells can no longer be tracked, compared with the cells seeded in collagen gel suggests that for larger cultures such gel may be less suited to this type of cell tracking since it is more opaque.

Figure 57 shows the changes in estimated focus in terms of assumed depth (in μm) of the z-stacks of the image sequences over the course of the collagen gel set up with the cells seeded in a pellet of alginate gel at the bottom of the dish as shown in Figure 53b. Every graph shows the change in depth for three cells relative to their position at time t=0. In (a) as found by the normalized variance algorithm method shown in section three, (b) the sum modified Laplacian. Due to the high confluence of the cells they have less degrees of freedom and so can be expected to move less.

By monitoring the amount of downward movement of the computed depth throughout the three experiments the rigidity of the gels can be seen, particularly in respect of its role in supporting cellular structures. Here the results show that the cells seeded onto the collagen gel show distinctively larger movement than those seeded on the other gels. The amount of such movement computed is also consistent with the visual inspection of the all-in-focus images collated.

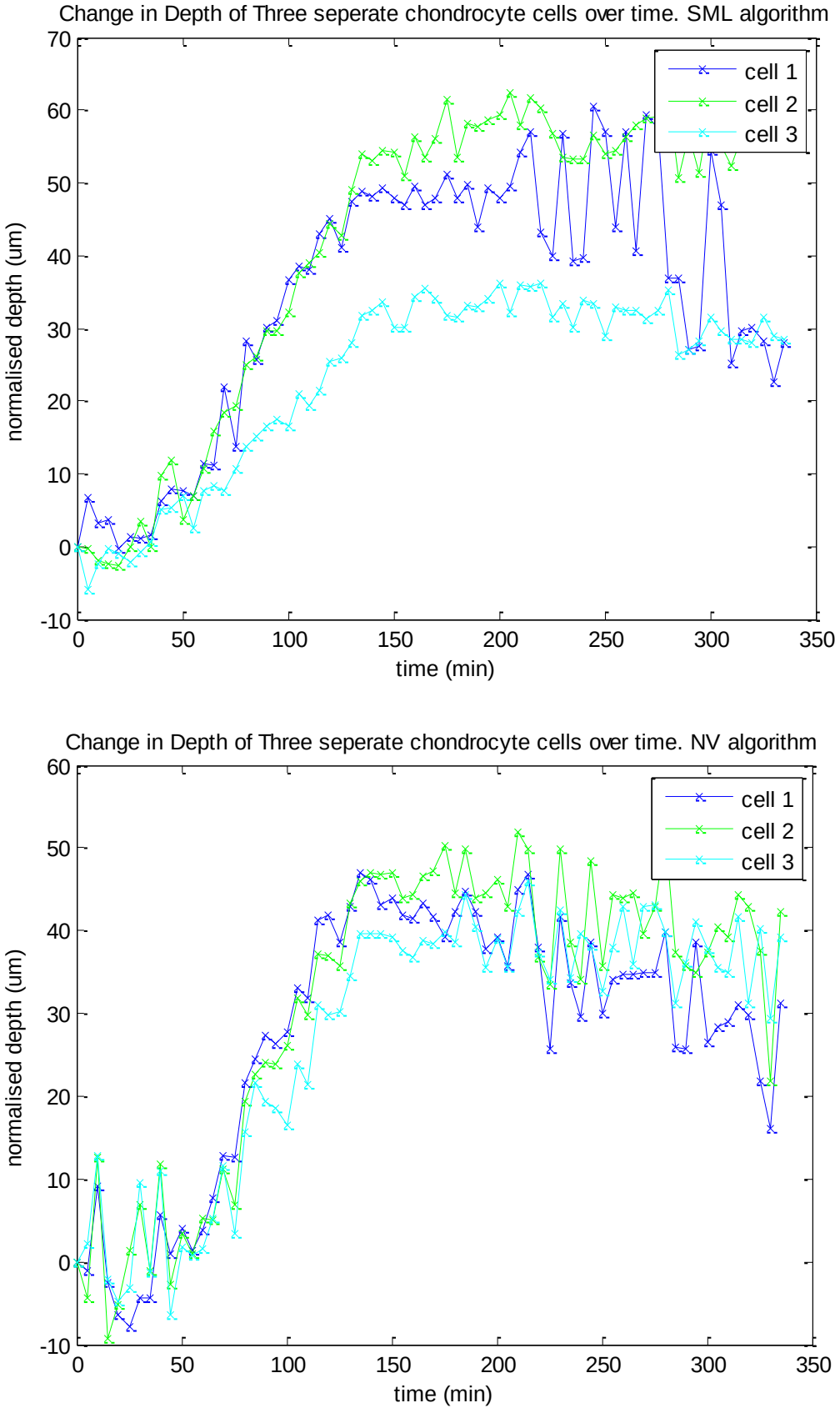

Figure 55: Mean estimates for the focus/depth of cell features during the course of the collagen experiments. Top: depth found using SML. Bottom: Depth found using MDL

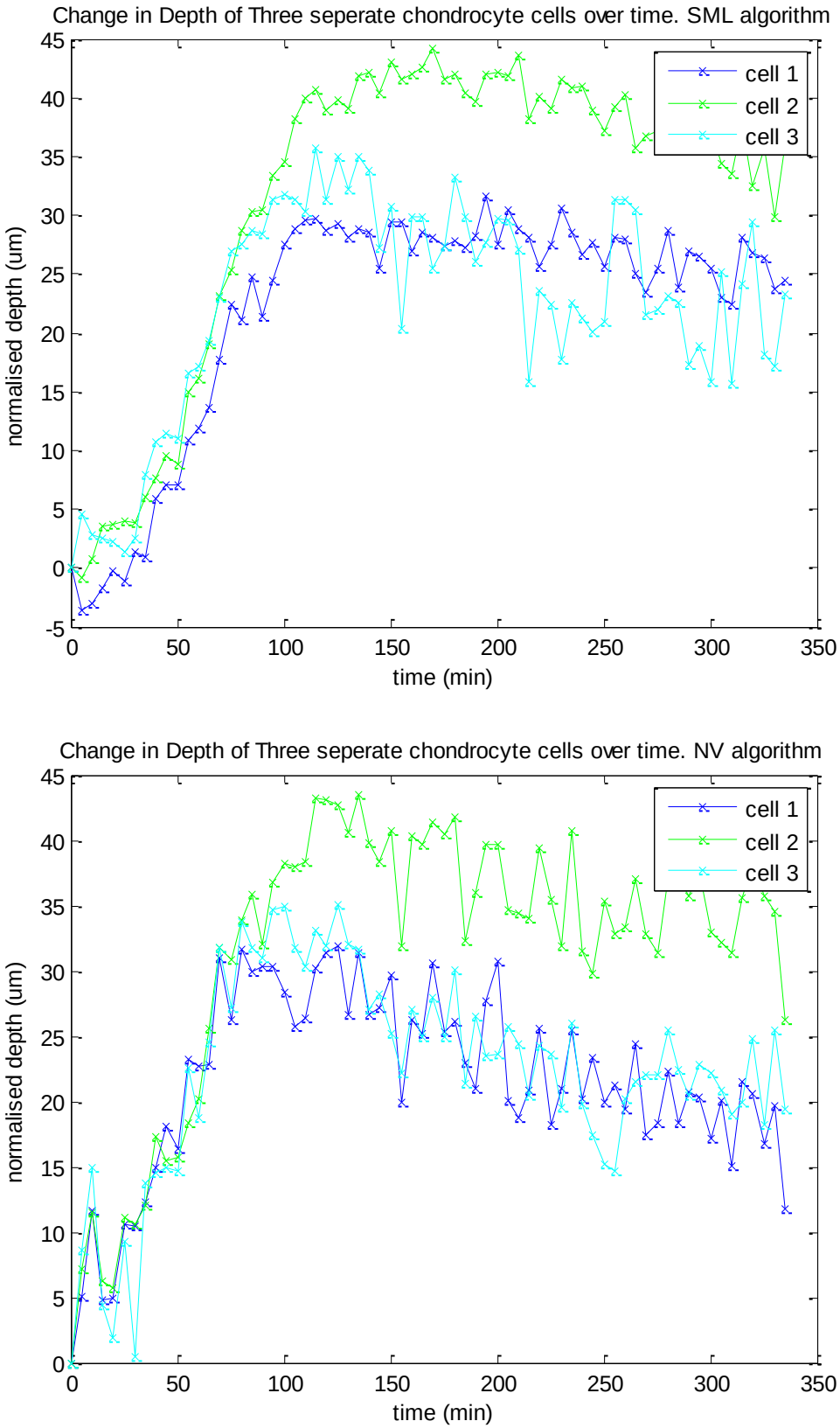

Figure 56: Mean estimates for the focus/depth of cell features during the course of the gellan gum experiments. Top: depth found using SML. Bottom: Depth found using MDL

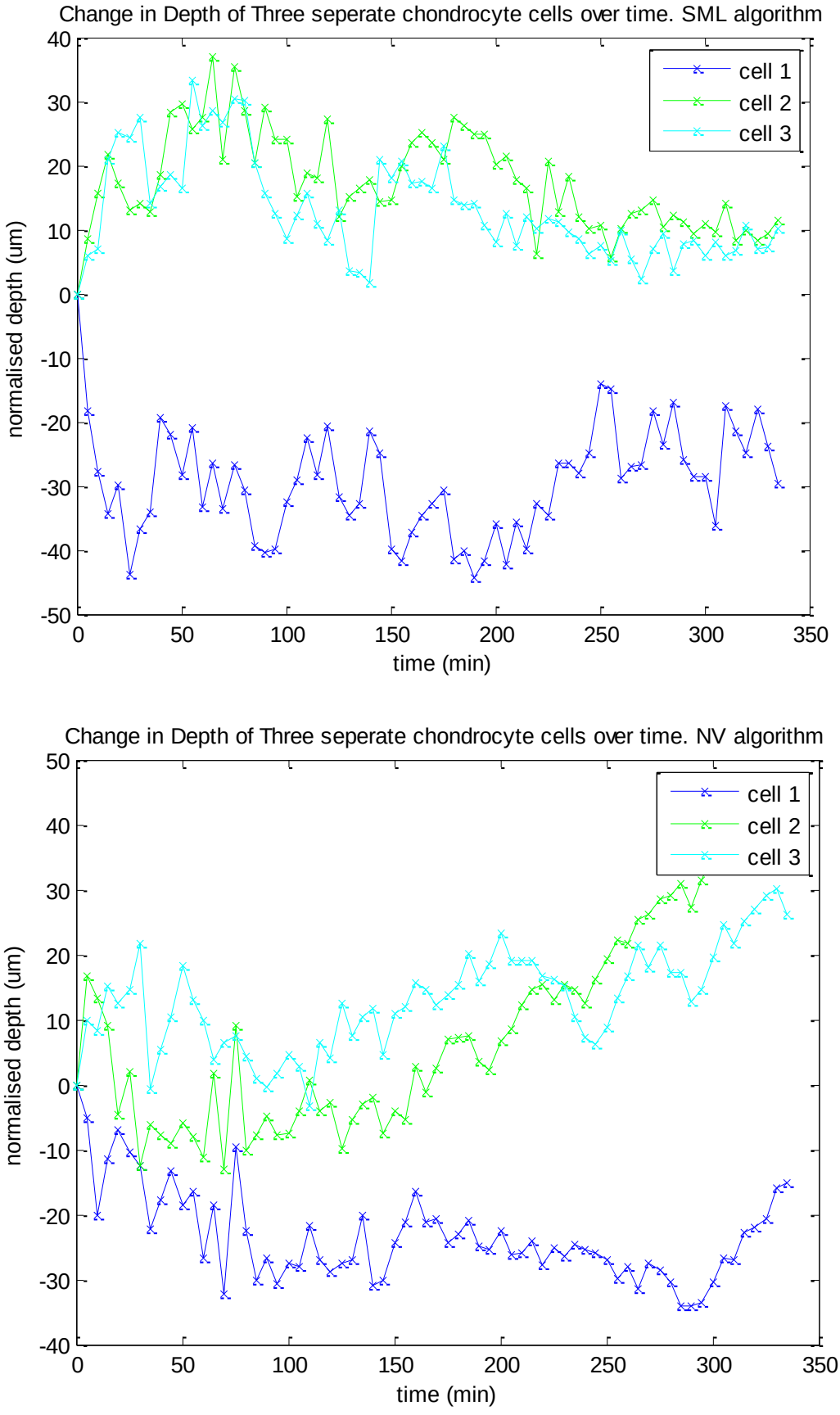

Figure 57: Mean estimates for the focus/depth of cell features during the course of the pellet experiments.

7.4. Observations and Further Work

Phase contrast microscopy is widely available and allows visitation of live cells without fundamentally altering their biology. Existing computational methods, however, are rather limited in dealing with large volumes of dynamic, image datasets generated from time-lapse phase contrast microscopy; focusing instead on the images generated by fluorescence microscopy. In this section, the work presented is a new method to fill this gap. Here a strategy has been developed using image analysis that can detect cellular events by finding changes in the z-direction. This work used methods previously developed to segment, classify, and track individual cells in a dynamic cell population accurately and reliably. The experimental results reported in Section 6 for back disk cycle studies showed that the proposed method is efficient and effective in cell tracking and phase identification. The availability of such an automated analytic solution removes a major obstacle in the bioassay development using time-lapse florescence microscopy. The main contribution here was to show that the work in chapter 6 can be extended into three dimensions. It is also noted that depth was able to be calculated on the different gel types used, whilst it had been hypothesized that only the clear gellum gum would provide differentiation needed to determine the position of the cells from the background of gel. The findings of this study are further discussed in Chapter 9.

8. Monitoring Stem Cells in Phase Contrast Imaging

This chapter makes use of the tracking aspect of the algorithm from chapter 6. Within this chapter, the cells studied are chondrocytes and MSCs (as described in section 2.1.1). Within this study these cells are co-cultured with the biological object of understanding how they interact. This chapter specifically seeks to address the objectives 1, 3 and 4 as detailed in section 1.7. The main contribution of this section is the feature extraction algorithm from chapter 6 with singular spectrum analysis to investigate whether chondrocytes and MSCs were distinguishable from each other when cultured together unlabelled.

8.1. Introduction

The automation of cell tracking *in vitro* using phase contrast time-lapse microscopy is vital for the quantitative and systematic study of cell behaviours. These behaviours are based on the phenotypic traits of interest extracted during the course of a biological experiment. The spatiotemporal characterisation of (2-D) morphology and cellular processes and events which are used to analyse the individual cells. In an atypically heterogeneous cell system this method can offer important capabilities to resolve the complex dynamics of such a system, whilst avoiding the generalisation of results associated with traditional population-based assays (Acharya et al., 2012). In this current investigation of stem cell co-cultures in the context of ACI for cartilage injuries, an automated cell tracking tool was developed incorporating:

1. The textural based work as described in section 6.
2. A fully integrated and commercial image analytics software suite available on an automated PC imaging platform (CellIQ-2®) from which all the time-lapse microscopic image sequences presented in this paper were obtained (Tarvainen et al., 2002).

It is believed that techniques and processes developed here can be applied to other soft tissue engineering (Tsuchiya, Chen, Ushida, Matsuno, & Tateishi, 2004). This chapter uses cell tracking and quantifying to determine the cell type within a mixed population and to determine whether the MSCs within such a population had differentiated. The main contribution here is the use of morphological features to determine cell type.

8.2. Methods

Over the past four decades, significant advances in tissue engineering have already been made by employing co-cultures of stem cells, particularly adult stem cell such as the MSCs, together with terminally differentiated cells or target cells, in this case chondrocytes.

Methods to control and employ stem cells have been of paramount interest (Bigdeli et al., 2009; Fisher & Mauck, 2013) in orthopaedic soft tissue engineering and regenerative medicine, for example, a direct co-culture of MSCs with chondrocytes has been demonstrated to provide increased growth of chondrocytes and chondrogenic differentiation of the MSCs (Acharya et al., 2012; Tsuchiya et al., 2004). Here, co-culture systems control the behaviour and actions of cells through the interaction of the multiple cell types commonly referred to as the target cells (chondrocytes) and assisting cells (MSCs). Generally speaking, target cells are those that will eventually compose the engineered tissue and are responsible for the tissue's function, whilst assisting cells guide the target cells to display a range of desired behaviours, including proliferation or differentiation, matrix production or organisation by direct cell to cell contact, adhesion of cells to extracellular matrices (produced by the assisting cells) and/or secretion of signalling molecules. However, the underlying interactions between assisting and target cells are often too complex to be understood.

8.2.1. CMT's Image Analyser (Version MA4.3.0.0)

The Image Analyser is an integrated software platform developed by the Chip-Man Technologies Ltd (CMT Ltd, Finland) that enables the detailed computational analysis of images of label-free live cells captured by its time-lapse microscopes for observing cell cultures. In short, the analyser allows users to examine the images taken previously from the microscope and create a video that combines successive images of adjacent regions. In addition, it has the unique capability to create sample libraries to include different cell types and/or regions of cells from which a protocol can be developed (by training) or refined in order to identify individual cell types. This is illustrated in Figure 58 below. By building a library of, say, 100-150 cells of each type, for example, it is possible to use the inbuilt tools to track the individual cell, compute its morphological features and subsequently summarise its movements over the course of the experiment.

In this study, the Image Analyser was used to track a total of 24 cells - 12 articular chondrocytes and 12 MSCs, in two identically constructed co-cultures, plus 12 in each of two monocultures designed for each cell type. The process of tracking these cells and quantifying their movements over time was achieved in three main steps;

i. Creating a sample library,
ii. Checking the viability of the sample library on a selection of images across each time frame, and confirming visually that the individual cells are correctly segmented and labelled,
iii. Enabling tracking to generate results for the tracked cells.

Broadly speaking, a sample library was specifically constructed for each culture and consisted of a collection of exemplars of the relevant cell type(s) of interest as selected by the user. Between 100 and 150 samples were provided for each cell type/class including,

where applicable, either or both of MSCs and chondrocytes to form the basis of the protocol for each cell culture. Additionally, in order to improve identification results, the exemplars also included the nucleus of each cell type where this was feasible.

Once the first iteration of step (ii) was completed, it was found that, due to the uneven lighting of the phase contrast images, parts or regions of the background had been segmented and mislabelled as valid cells. To counter this, a third class named Background was also created, with 20 samples or exemplars selected from the relevant parts of the background. Using this additional library, the cell protocol was repeated until the number of correctly labelled cells was deemed adequate. Here, the cells in the library were edited to remove cells that were too similar between the groups during this iterative process until the all the tracked cells were correctly labelled, that is whist some cells were not labelled <5% were labelled

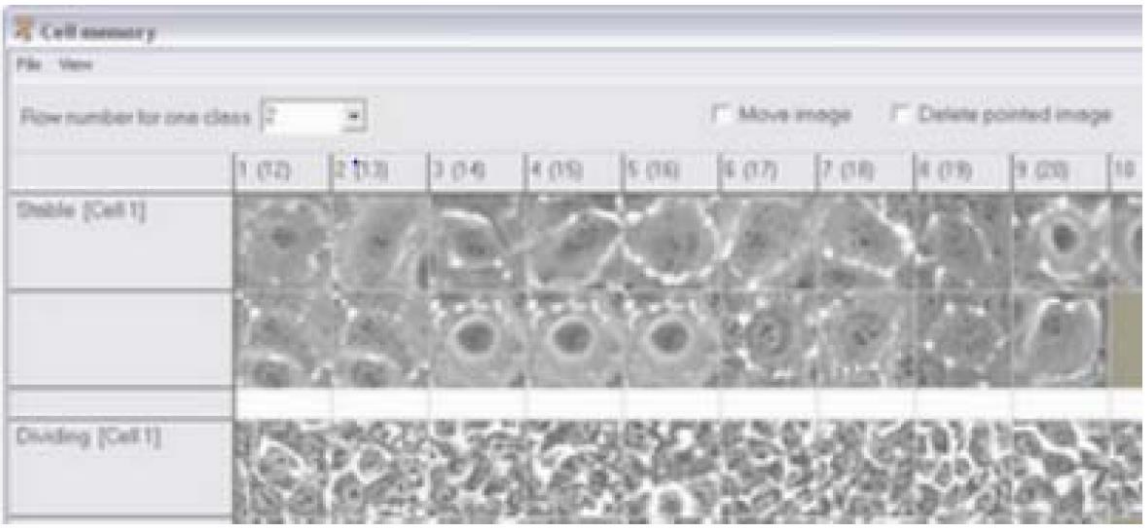

Figure 58: An example library constructed by the Analyser. Depending on the application at hand, it should be noted that a library is often constructed for each cell type and, as such, the technology is not specific to any one type of cell and can thus be used for a variety of studies.

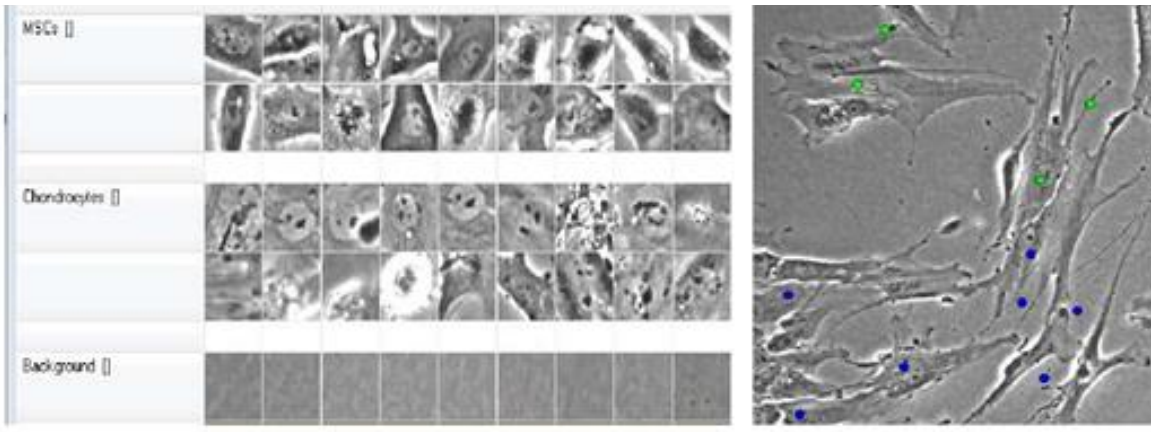

Figure 59: (Left) The first part/section of the sample library constructed for the co-culture to define, from top to bottom, MSCs, chondrocytes and background. (Right) Labelled cells based on the constructed library are displayed in each image/time frame of the specified image sequence, with blue dots representing the MSCs and green the chondrocytes respectively.

incorrectly, these were removed from the final analysis. Figure 59 shows an example for one of the libraries constructed and the corresponding results displayed to the user.

Once the cells have been correctly segmented and labelled, the analyser can perform the relatively more complex task of cell tracking. The latter enables the cells of interest to be selected from the first image of the time-lapsed sequence, with each of these cells given a label in order for it to be tracked over the specified image sequence. The tracking is then

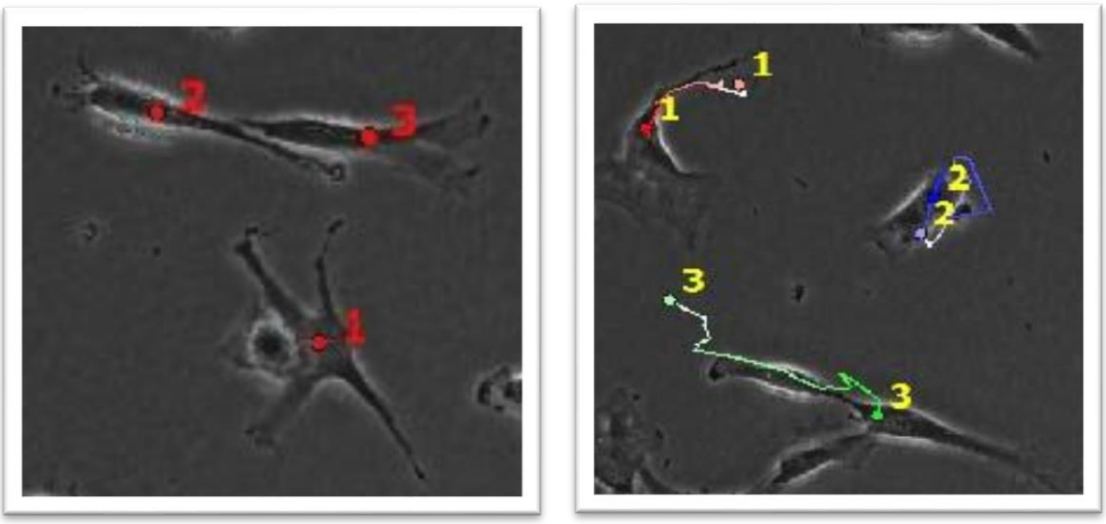

Figure 60: : (Left) An example showing the individually labelled cells at each time frame as a result of the tracking performed. (Right) Labelled cells as shown in the left figure, with the individually marked path of movements for each tracked cell covering the user specified time period of interest.

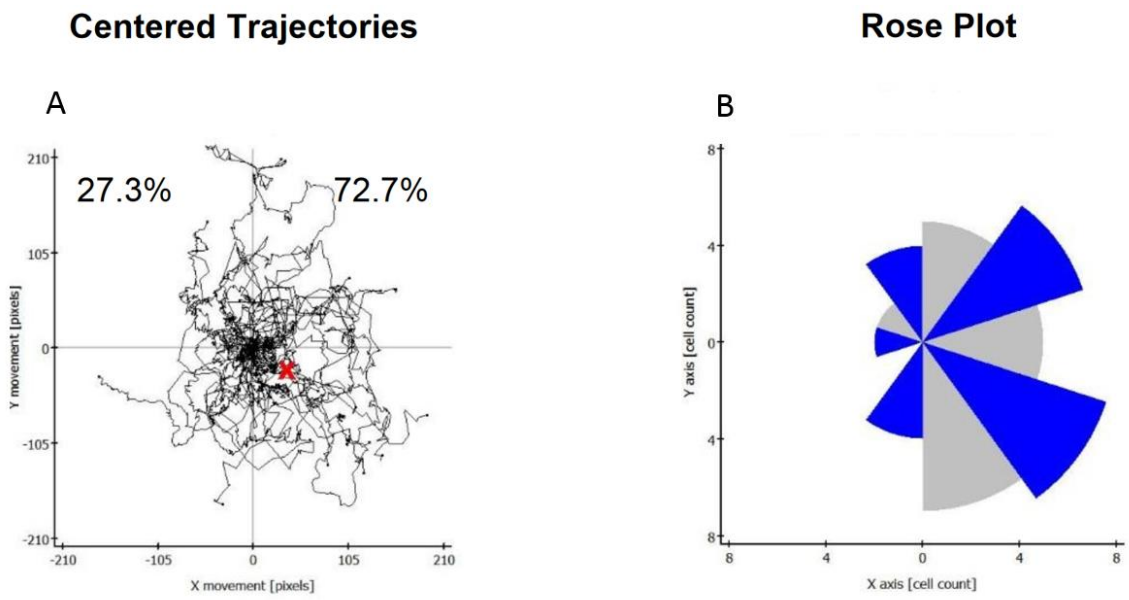

Figure 61:Showing A) a map of the trajectory of the cells and B) a rose plot of the cell trajectories.

performed automatically (using a propriety shape recognition algorithm (Tarvainen et al., 2002)) to enable movements of the individual cells to be computed and recorded for the specified length of the image sequence as determined by the application at hand. The output is finally shown to the user, as shown in Figure 60.

In addition to the capability of tracking cells as described above, the Analyser also generates an output that summarises the results of the tracking performed. This output is based on population-based analysis. This includes, for example, a Rose chart which shows the proportion (%) of the individual cell population against the angular displacement or direction of movement (0-360 degrees) from the start to the end points over the course of tracking Figure 61B and, similarly, a 2-D plot that displays the average distance of the movement (in micrometres) between the time frames Figure 61A. The Analyser also generates a spreadsheet that records at each time frame the (x,y) position, displacement and speed of each individually labelled/tracked cell over the course of tracking.

It should be noted here that, for the purposes of labelling, the full image of the individual cell is not required in general; indeed, users are often required to specify the maximum diameter of the individual cell as well the minimum distances between cells interactively during the refinement steps of (i) and (ii) as described above. Consequently, the geometric or morphological information including particularly the exact outline (or silhouette) of the individual cells is unavailable following the implicit segmentation process required for step (ii).

8.2.2. Microscopy

The microscopic image/data sequences studied here were obtained using the high-throughput time lapsed microscopy equipped with a high precision motorised z-stage that enables the automated acquisition of the so-called all-in-focus images frame-to-frame over time. Coupled with the use of PC optics, the imaging platform allows the integration of high speed and continuous focusing software to keep cells in focus before their acquisition. These images were then segmented with individually tracked cells linked as described in chapter 6 using MATLAB® analysis code developed in-house. In essence, the tracking implemented connects cells from one frame to the next in the image sequence captured over the entire course of the experiment (~ 100 hours). To facilitate analysis of the tracked cell in each culture/well, the positions of the cells are computed (and labelled) in each time frame on the basis of their dynamic (2-D) centroid coordinates; see Figure 62. While this is an essential step for data reduction, further insights into the dynamics of each cell type were obtained by computing and studying biologically meaningful quantitative measures, as biometric features from these coordinates. In this exploratory study, these measures included cell areas, equivalent diameter, movement - scalar displacement and angular direction, orientation, circularity and aspect ratio (major-minor axis ratio) as determined by the minimum enclosing box (J. Li, 2014) .

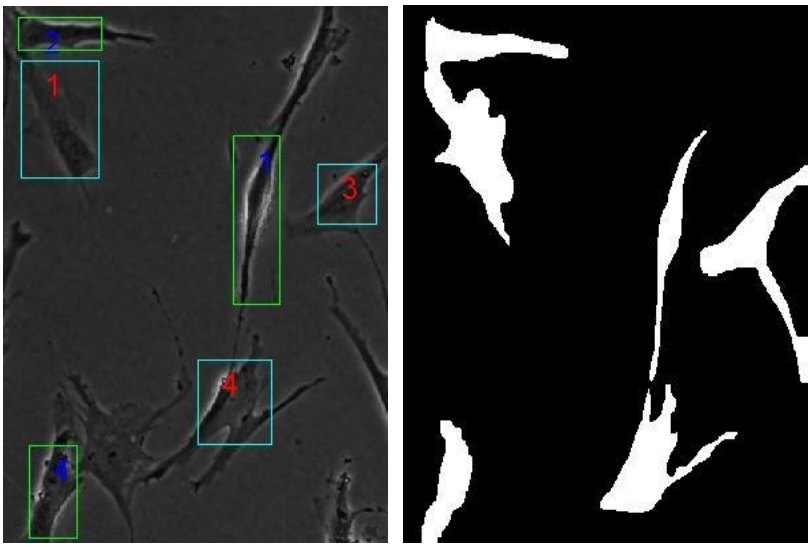

Figure 62: (Left) An example showing the individually labelled cells using the NCC based procedure for cell linking and tracking. (Right) The entropy based segmentation was used to separate background from the labelled cells as shown on the left.

As with the precursor work on the Image Analyser as described in section 0, a total of 24 cells consisting of 12 chondrocytes and 12 MSCs were tracked in the two identically constructed co-cultures constructed for this study. In addition, two further sets of six chondrocytes and six MSCs were also followed respectively in each of the two monocultures dedicated for each cell type. Finally, an individual time sequence was then collated for each of the dynamic measurements described above from the original microscopic image sequences of these cells.

Two monocultures consisting of articular chondrocytes and MSCs respectively, plus a co-culture where the two cell types are directly mixed have been constructed, to help explore the relevant biometrics of the chondrocytes and MSCs, as described above, this was achieved in two-dimensional (2D) systems with a culture environment where the respective single and mixed-population mono-layers were used to study the specific aspects of cellular interactions and behaviours of interest. The cells were grown to their seventh passage in the laboratory, with 50,000 cells seeded in each experiment. So that there were 25000 cells of each type in the co-cultures.

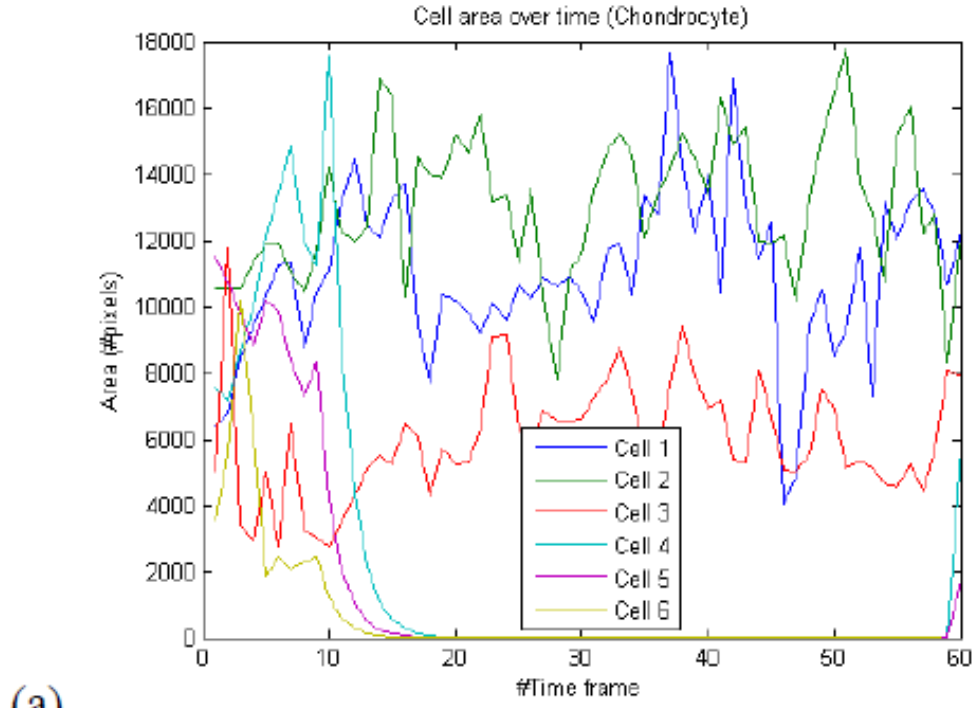

Figure 63: An example of the spatiotemporal measurements for the (two) different cell types (chondrocyte and MSC) in the co-culture studied in this work. From top to bottom: (a) Cell areas measured in number of pixels (#pixels) over time for chondrocytes. (b) As (a) for MSCs.

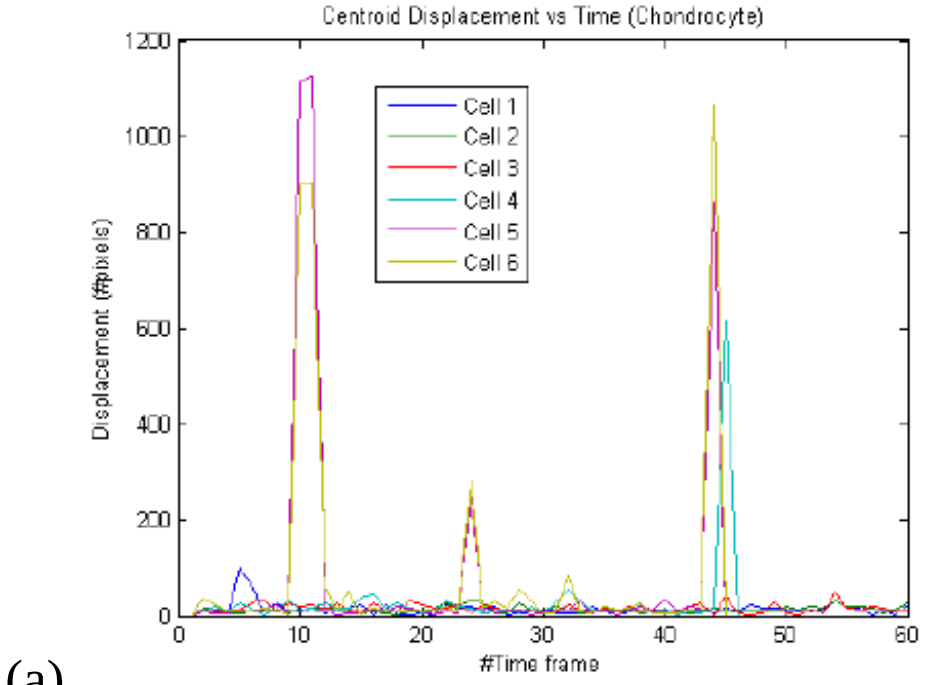

(a)

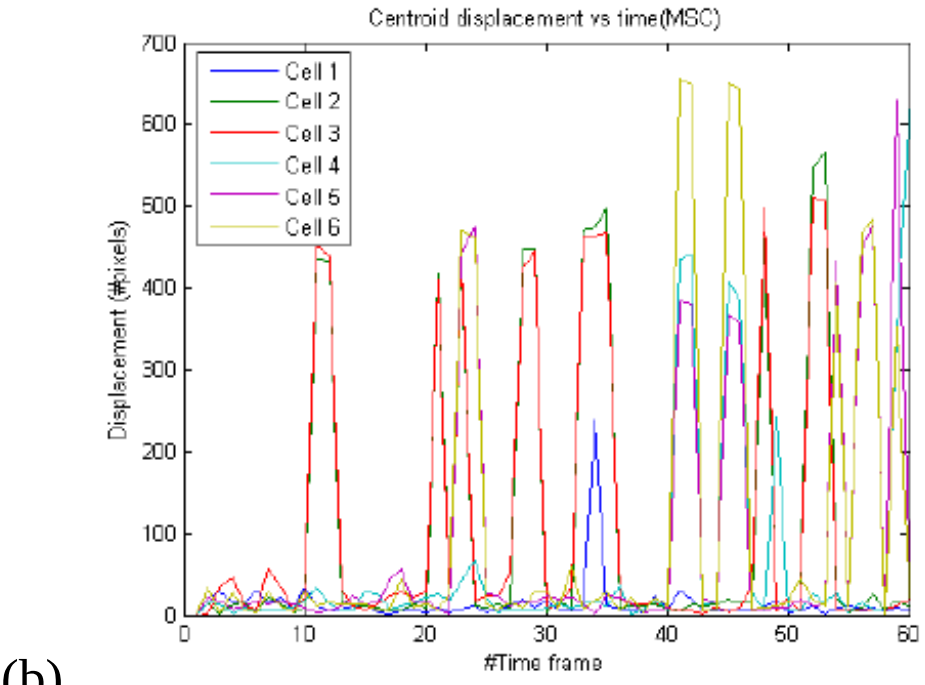

(b)

Figure 64: An example of the spatiotemporal measurements for the (two) different cell types (chondrocyte and MSC) in the co-culture studied in this work. From top to bottom: (a) Centroid displacement (# pixels) over time for chondrocytes. (b) As (a) for MSCs.

Additionally, fluorescent labelling was also used in order to establish a ground truth. In all 50,000 cells were seeded in each well; i.e., in the case of the chondrocytes/MSCs co-culture, 25,000 of each cell type were present.

8.2.3. Algorithm

1. The position of the cells in the x-y plane was determined by hand. This was done using the CROIEditor (Jun, 2013), which allowed the ground truth to be constructed manually via measurements taken from freehand drawings overlaid on the all-in-focus images
2. Features of the cells were identified by
    a. Area - total number of pixels
    b. Perimeter- number of pixels that make up the edge of the cells
    c. Orientation- angle between the major and minor axis
    d. Aspect ratio- minor divided by major axis length
    e. Circularity - per equation 2
    f. Displacement (length) change in central pixel location
    g. Displacement (angle)- change in orientation with relation to an arbitrary x axis
3. Change in feature over time was recorded for all feature types

8.3. Results

The collated time sequences for each cell as described above collectively provide the complete profile of dynamic measurements for the respective biometric features at successive (and uniformly spaced) time points/frames over the course of the experiment. As such, they have formed the basis of the exploratory analysis carried out in this study as described below.

8.3.1 Preliminary exploratory analysis

Initially, the collated sequences were examined visually using simple data plots as show in in Figures 63 and 64. Additionally, simple descriptive statistics including mean, standard

deviation, correlations, minimum, maximum, etc., were also computed with the goal to uncover consistent patterns (such as cycles/periods) and, importantly, significant trends as well as any outliers that might require further investigation. In particular, this study sort to investigate the widely debated topic of the properties of chondrogensis in MSCs in co-culture systems that could be attributed to (or even quantified by) the different behaviours exhibited in mono-cultures. This is illustrated by the comparative example shown in Figures 63 and 64, where the same set of measurements was obtained for the two cell types (chondrocytes and MSCs) in their respective monocultures. A cursory study of the displacement profiles of the two cell types in the mono and co-cultures (in Figures 65 and 66) revealed that the chondrocytes have a lower mean displacement (measured as number of pixels moved) than the MSCs' over the same time period in both culture systems. In addition, the variation in displacements over the same time period (or speeds) of the individual MSCs in the co-culture appeared to be significantly larger in the co-culture. This latter observation is attributed to the recording of consistently higher variations in their speeds in the co-culture system, which is obtained by computing the standard deviations (STDs) of the individual MSC displacement profiles.

A cursory study of the displacement profiles of the two cell types in the mono and co-cultures (in Figures 63-66) revealed that the chondrocytes have a lower mean displacement (measured as number of pixels moved) than the MSCs' over the same time period in both culture systems. In addition, the variation in displacements over the same time period (or speeds) of the individual MSCs in the co-culture appeared to be significantly larger in the co-culture. This latter observation was attributed to the recording of consistently higher variations in their speeds in the co-culture system, which is obtained by computing the standard deviations (STDs) of the individual MSC displacement profiles.

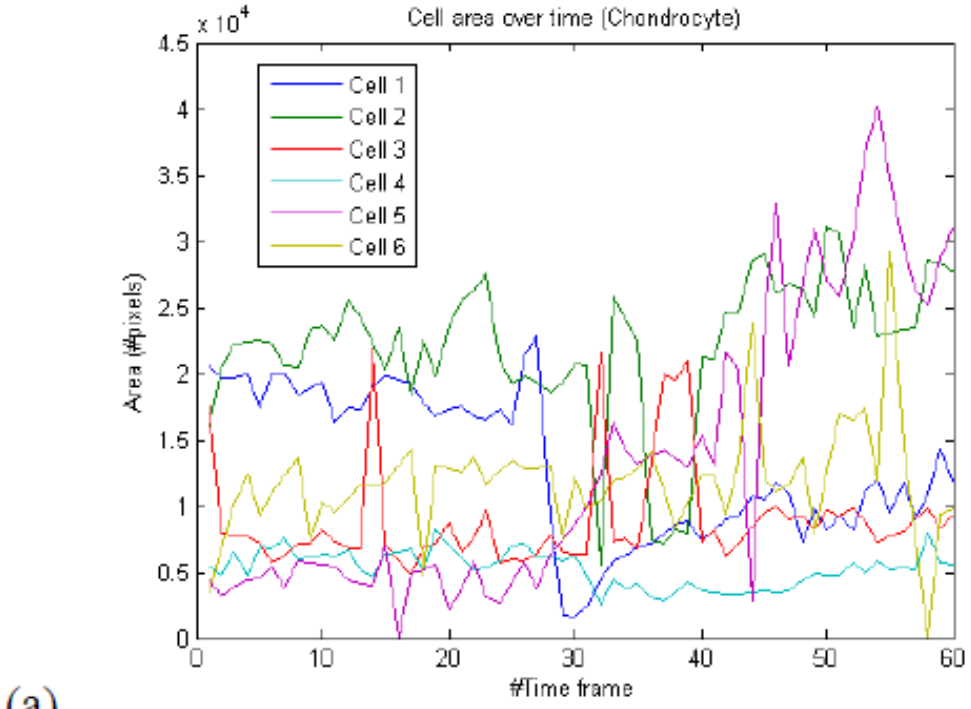

(a)

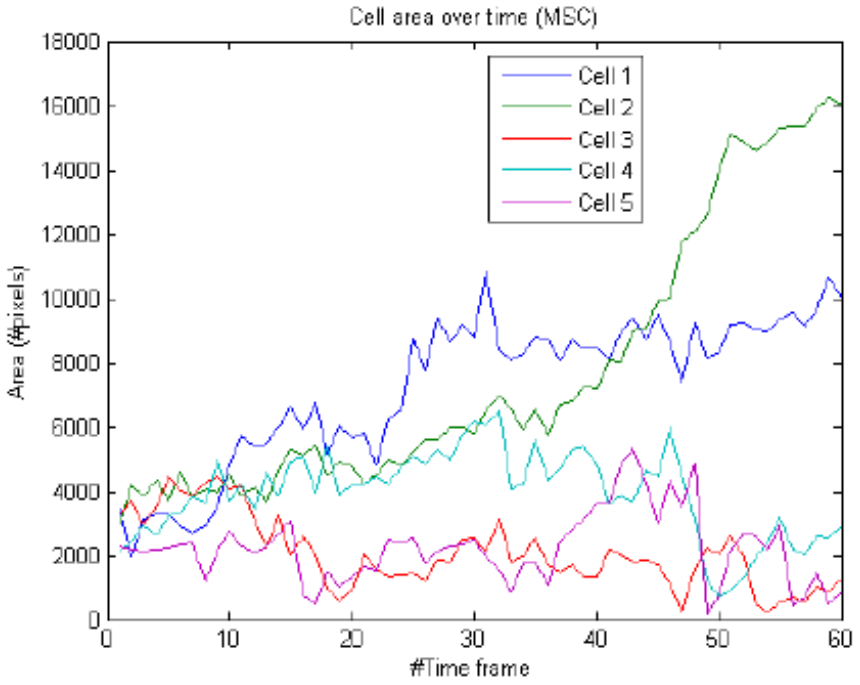

(b)

Figure 65: A comparative example for the notably different phenotypic behaviour observed in the monocultures dedicated for ACs and MSCs. From top to bottom: (a) Cell areas measured in number of pixels (#pixels) over time for chondrocytes. (b) As (a) for MSCs.

(a)

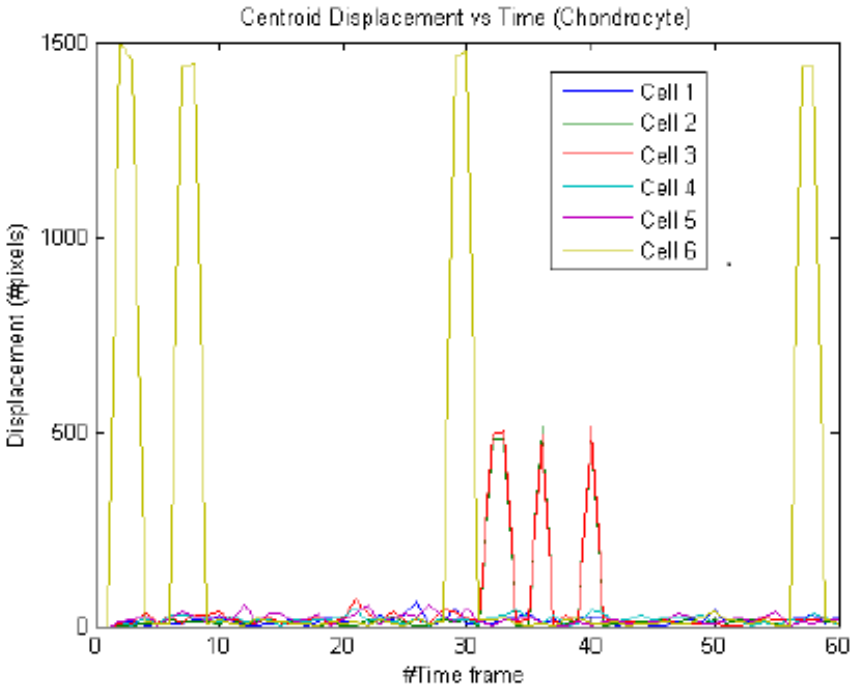

(b)

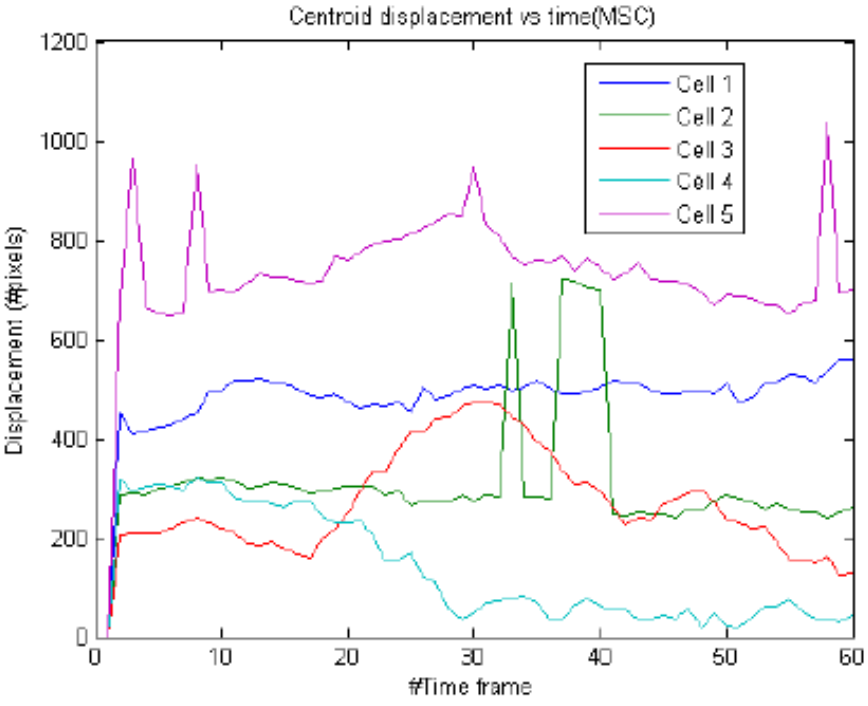

Figure 66: An comparative example for the notably different phenotypic behaviour observed in the monocultures dedicated for ACs and MSCs; From top to bottom: (a) Centroid displacement (#pixels) over time for the ACs. (b) As (a) for MSCs.

A further study of the two figures incorporating the area profiles obtained in the two culture systems appeared to show that a different pattern was displayed by the two cell types. In particular, whilst the chondrocytes are generally larger in size than the MSCs, their (size) changes were also consistently larger in the mono-culture than in the co-culture system, as is evident by the calculation of the STDs of the areas for the individual size profiles measured in the two culture systems. However, the notable trends displayed by the sizes of the MSC as evident in Figure 66b were not obvious by the descriptive statistics of the STDs. The need for sophisticated analytical procedures to reveal such trends became apparent.

8.3.2. Singular spectrum analysis

Singular spectrum analysis (SSA) is a non-parametric technique which has been widely used to handle a very broad class of time series that can contain combinations of complex periodicities and polynomial or exponential trends (Golyandina, Nekrutkin, & Zhigljavsky, 2001). It has found applications for a wide range of applications including trend or quasi-periodic component detection and extraction, de-noising, forecasting and change-point detection. The basic SSA method consists of two complementary stages: decomposition and reconstruction; each includes two further separate steps:

- Decomposition
    - Embedding: embedding can be regarded as a mapping that transfers a one-dimensional time series into a multidimensional series
    - Singular value decomposition (SVD): a factorisation of the matrix created in the embedding stage
- Reconstruction
    - Grouping: splitting the matrices created by the SVD into several groups and summing the matrices within each group

- Diagonal averaging: produces time series which, if added together, would recreate the original time series

A key concept in studying the properties of SSA is “separability”, whose absence is often observed in series with complex structure. For such series and series with special structure, such as the ones generated for this study that have no repetition, several variants of SSA have been developed (Golyandina et al., 2001; Sanei & Hassani, 2015). The approach used in this study was adapted from the work by (Alonso, Castillo, & Pintado, 2005) and consists of four key steps:

1. Embedding,
2. SVD of the so-called trajectory matrix,
3. Grouping and
4. Reconstruction.

Briefly speaking, a Hankel matrix is constructed from the time series of interest in step 1 by sliding a window (of width L) that is shorter in length than the original series. This matrix is then decomposed into a number of elementary (rank one) matrices of decreasing norm by means of SVD (step 2). The approximation of the matrix is obtained by selecting and grouping these elementary matrices necessary for the extraction of the behaviours or tendencies of interest from the original time series (i.e. step 3). The latter is reconstructed in the final step by retaining the desired number of elementary time series (r) commonly referred to as the principal components via the diagonal averaging of the associated elementary matrices. An example that applies this algorithm to the time series depicted in Figure 62 is given in Figure 67.

8.3.3. Biological results

As described in Section 8.1, a total of 36 cells with both chondrocytes and MSCs were selected for this study from two culture systems respectively consisting of two monocultures developed for each cell type and two identically constructed co-cultures where the chondrocytes and MSCs were mixed. For each cell, dynamic biometric features including seven measurements (cell area, displacement: distance, displacement, angle, circularity,

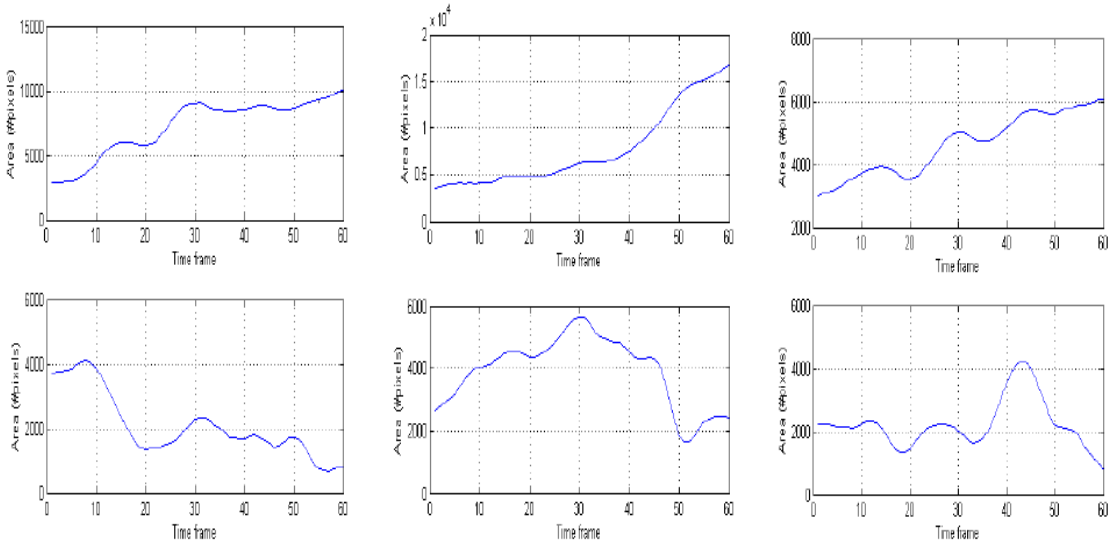

Figure 67: An example of using SSA (L= 5, r=1,2) to extract trends in the area measurements for the individual MSCs shown in Figure 6b. The cell labels are reordered to illustrate the apparently upward and downward trends which are shown in the top and bottom row of the figure respectively.

perimeter, aspect ratio, orientation) were computed over the course of this study and the respective time series were constructed for further exploratory analysis. The descriptive statistics as described in Section 8.3.1 are summarised in Table 7 below.

The following observations are made. First, the chondrocytes are much larger in size when compared to MSCs in both cultures (see Area and Perimeter measurements). Second, the averaged displacement/movement of the MSCs appeared to be significantly bigger in the monoculture than in the co-cultures, where such measurements were much smaller and, surprisingly, in line with the measurements obtained for the chondrocytes (see marked

averages in green and cyan). Third, the variations in shape and sizes of the individual MSCs as measured by the standard deviations of the respective measurements across the individual cells (under STD (cell)) in both culture systems are relatively and consistently larger than the chondrocytes, which supports the general belief that MSCs are mixtures of different cell types. Last and perhaps most interestingly, asides from the overall larger size, the shape of the chondrocytes appeared to look more like the MSCs when they are mixed in the co-cultures; see marked averages (in yellow).

A closer examination of the related shape profiles of the MSCs measured in both culture systems confirms the last note above and, importantly, offers a greater insight into the dynamic process involved. Using the SSA technique described in the preceding section, it was shown that both the circularity and aspect ratio measurements have revealed some demonstrably consistent trends in the change of the shape of the MSC in the co-culture. This is summarised in Figure 68a, where the decline in the circularity measures over time and the related (but different) measurements for the aspect ratio computed for the individual cells are apparent. Indeed, the same analysis applied to the change in orientation over successive time frames further supports this finding and, collectively, they have revealed dynamic patterns which were absent in chondrocytes in either of the two culture systems shown in Figures 63 and 64.

Table 7

	Monoculture						Co-Culture					
	Articular Chondrocyte			MSC			Articular Chondrocyte			MSC		
	Mean	STD (time)	STD (cell)	Mean	STD (time)	STD (cell)	Mean	STD (time)	STD (cell)	Mean	STD (time)	STD (cell)
Area (pixel)	12454	5272	5637	4640	2005	2703	9969	4030	3129	3280	1907	1487
Displ (pixel)	57	129	73	387	108	231	47	128	33	51	115	39
Displ (pixel)	3.094	1.73	0.169	3.076	1.808	0.136	2.862	1.893	0.34	2.92	1.83	0.456
Orientation (radian)	0.156	0.646	0.475	-0.33	0.942	0.255	0.06	0.86	0.602	0.167	0.641	0.219
Circularity	0.277	0.121	0.086	0.46	0.153	0.114	0.57	0.151	0.068	0.366	0.196	0.115
Perimeter (pixels)	797	262	280	358	121	102	475	149	85	308	160	113
Aspect ratio	0.448	0.2	0.0811	0.486	0.176	0.132	0.568	0.172	0.061	0.392	0.235	0.124

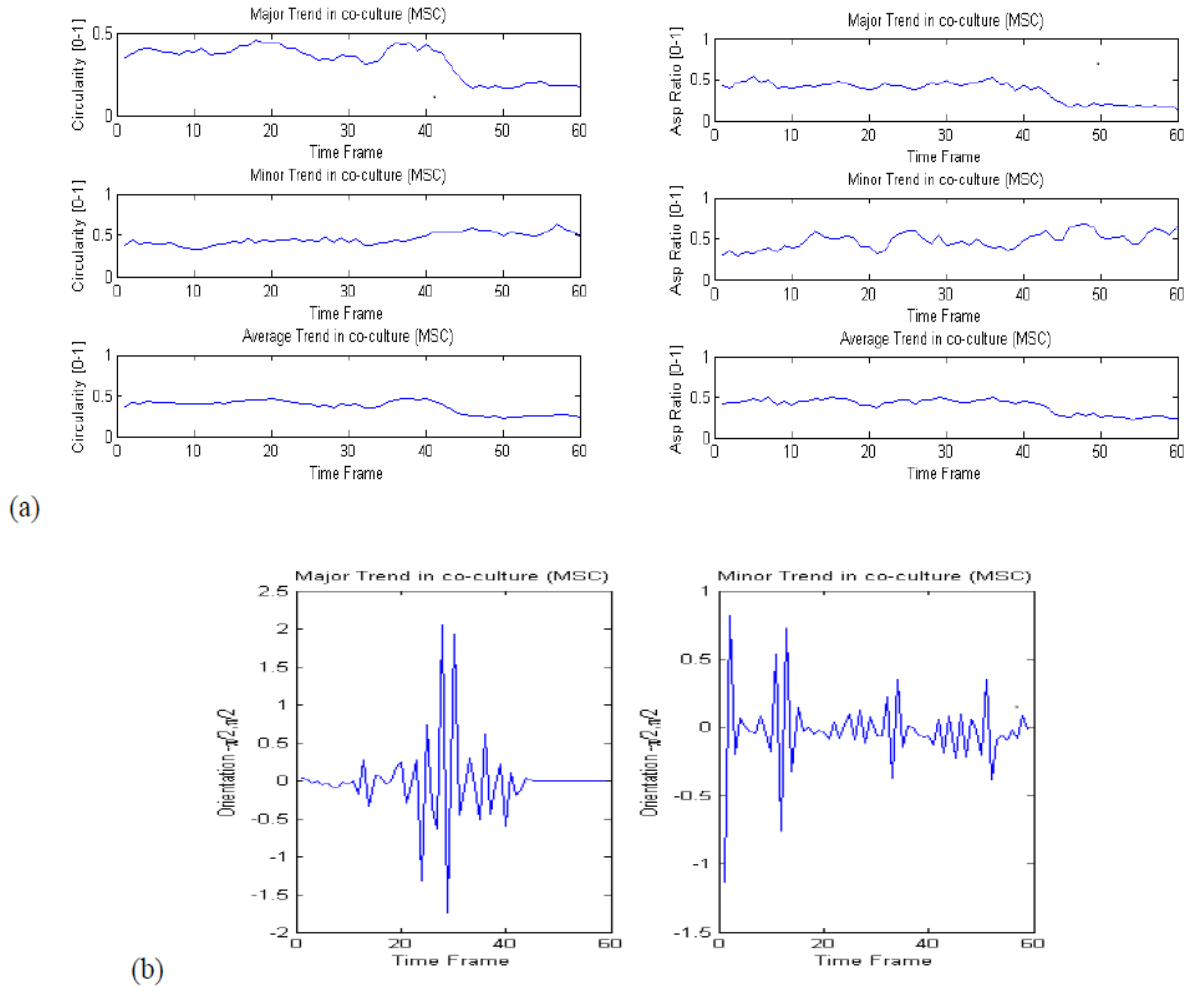

Figure 68 : a) (Left) The circularity trend extracted from 75% of the MSCs using SSA (L=5, r=1,2,5) (Right) The corresponding trend in the aspect ratio measurements for the individual groups (majority and minority). (b) The associated changes in orientation as measured over successive time frame, suggesting that the majority of the MSCs have undergone relatively significant changes in shape/orientation (~2x in amplitude) and over a relatively short time period when compared to the minority group.

8.4. Observations and further work

Quantitative measurements that describe cell motility and morphology, as biomarkers, were examined with the goal of assisting the phenotypic characterisation or profiling of chondrocytes and MSCs, particularly in the direct co-culture system where the two cell types are mixed. In addition to using standard, though relatively simple, descriptive statistics further studies based on the non-parametric SSA technique reveal significant morphological changes in the MSCs that were absent in the similarly constructed monocultures. In

agreement with recent work on co-cultured chondrocytes and MSCs (e.g. (Acharya et al., 2012; Xie et al., 2012)), the results support the increasingly held view that MSCs enhance AC proliferation, while concurrently chondrocytes promote the differentiation of MSCs. To facilitate investigation of chondrogenic markers that would enable full AC phenotype characterisation, additional work building on this study is planned. This necessitates a top-down approach to analysis of the biometric features derived from related studies or experiments on cellular interactions and behaviours of interest, with further refinements of the SSA algorithm described here to study the individually tracked cells.

9. Discussion and Summary

The purpose of this thesis was to create an algorithm capable of finding the features of a single cell in a culture and hence extracting some biologically meaningful data as a whole. Section 3 looks at a single part of the cell cycle, mitosis, and whether an algorithm could be developed here to alert a user to the presence of this event. This was achieved at a greater success rate than other algorithms but on its own does not provide much biological context. Section 4 investigates growing neurites in a co-culture with MSCs, specifically whether the presences of the MSCs help the neurite growth. The algorithm for this had focused on the neurites and was able to show that the presence of the MSCs did help the neurites grow. In general, the algorithm developed was as effective as judging by eye the effect of MSCs on SCI. That said it did succeed in quantifying the growth better than manual methods did. A novel feature introduced here was the use of fractal mathematics to investigate branching in the neurites. Section 5 takes this further to look at the growth of individual neurons. From this, tools are developed to look at the 3D growth of the neurons. These tools give a new way of looking at the nanofiber based hippocampal model and found the biologically relevant result that the neurons respond more to the topographical cues than to the presence of the chemoattractant. Section 0 looked at a different cell type entirely and found an improved way of locating the cells in a culture. In addition to this the algorithm developed here counted the vesicles on the cells and through this it was discovered that smaller cells tend to have more vesicles on the surface, an observation that would have taken significantly more time to make by manual inspection. Section 0 combines the work done in sections 5 and 0 to look at the movement of chondrocytes in a gel. The purpose of this work was to find which gel worked best for 3D image tracking since the algorithm developed here is one of the few that looks at 3D tracking in PC imaging, and as such, it was necessary to determine with which gel it worked best. Finally, section 0 looked to see whether building up a database

of morphological features of two cells would allow them to be distinguished in a mixed culture. The results of this are promising but more work would need to be done to determine the accuracy of this technique.

9.1. Tracking the movement of non-neural type cells.

Sections 0-0, and to a lesser extent section 3 deal with the tracking of non-neural cells. The objective of this was to be able to track all cells in cultures of up to 100% confluence. Throughout the time spent on this thesis the algorithm for cell tracking was constantly improved, the tracking of the MSCs described in section 3 could only identify cells in cultures of up to 40 % confluence. This was because it could not distinguish cells touching since the border between the cells looked too similar to the middle of a cell. Initial methods to overcome this looked into the time dimension, assuming that by predicting the path of the cell it would be possible to determine the location of cells within the clumps. This proved to be an unsatisfactory solution for two main reasons:

1. The algorithm created was very memory heavy and thus was not amenable to real time measurements for live cell imaging,
2. There remained a problem with cells that started in clumps and thus could not be distinguished.

The initial solution to 2 was just to remove the cells that started in clumps from the analysis by assuming that any large areas were clumps of cells rather than single cells. This was obviously unsatisfactory as cells would have to be excluded from any subsequent analysis.

An improved method of distinguishing the cells from the background is described in section 0 where, rather than just using an edge detector to determine the position of the cells, the image is first parsed to look at the entropy of the image. Cells have higher entropy than the background and the edges of the cells have higher entropy than the bodies of the cells. From

this, it is possible to create an algorithm that can distinguish the cells in the clumps. This algorithm performed better than other commercially and freely available algorithms with cultures of up to 80% confluence. The actual tracking part of the algorithm also went through stages of development. Originally, the algorithm just relied on nearest neighbour matching. This was improved with the use of NCC described in section 0. This acted to speed up the algorithm to make it more efficient and thus more amenable to real time implementation.

A problem presented by these studies is that there was no way to make the field of view large enough to take in all of the possible positions a cell could move to (i.e. the whole of the well). It was decided to work with this as this is the standard for the biological experiments that the algorithms created were supposed to support. It was decided that the algorithms were more likely to gain traction if they did not impede the normal running of the laboratory. The biggest problem that this created was the issue of the cells going out and then returning into the field of view. With this problem, there seemed to be two possible solutions:

1. Ignore and do not measure or record all cells entering the field of view
2. Treat every cell that enters the field of view as a new cell.

Solution 1 acts to reduce the potential pool of data as the cells that enter the field of view may go through an event of interest (e.g. mitosis or apoptosis) and, in the case of population studies, will reduce the number of cells studied. A more extreme version of solution 1 is to measure only those cells that never leave the field of view, this has the advantage that the same amount of information can be gathered for all of the cells but results in bias sampling towards the more sedentary cells which can be problematic especially in looking at cellular activity. Solution 2 does generate more data but there is no way to tell if a cell that previously left the field of view has been reassigned as a new cell. The result of this is that there appears to be more cells in the study than there actually are. This would be problematic in the case

of population studies where the overrepresentation cannot be accounted for as it is not known how many apparently new cells are actually new. An attempt was made to account for the cells that came into the field of view by looking to see if they matched the features of the cells that had previously left the field of view. It was found however that the cells, particularly the MSCs, changed their morphology so regularly that it was impossible to say if a cell matched one that had left the field of view with any degree of certainty. This problem was compounded by the fact that there is no reliable standard to test against. Once the algorithm had been created it was constantly tested against other algorithms and the current standard practice of manually tracking.

The final challenge presented in section 0 was to track these cells in three dimensions. This is a challenge as the image produced by the microscope is in two dimensions. As a consequence, the algorithm could not be tested against an absolute value created by hand as in the other experiments. This is because there is not a projection created along the z-plane, instead the location of the cell is built up by determining the depth where it is most in focus. As a result, the initial algorithm was tested against a metal sheet of a known thickness (Smith et al., 2012). Once this had been used to establish the accuracy of the algorithm as a whole it could then be used to track the cells. The results that were obtained from section 0 show that it is possible to track the cells in all the gels tested using this method. Nevertheless, unsurprisingly, it is beneficial to have more transparent gels with which to work. In addition, there was a problem with the fact that the microscope used could only move to a certain limit in the z-direction, constraining the amount of depth data that could be obtained. The nature of a z-stack of images means that there will always be information missing from between the planes so the resolution of the z-axis is lower than that of the xy-plane.

Overall, this thesis has achieved the objective of creating an algorithm capable of tracking the movement of non-neural type cells, with the caveat that cells can only be tracked in

cultures of up to 80% confluence and in 3D cultures with more transparent gels. Further work needs to be done to enable the tracking of the cells in cultures with higher confluence levels. Additional benefit would be obtained from a developing a better protocol to deal with cells that leave and/or enter the field of view.

9.2. Tracking of neural tips as they grow in vitro

The main results that look into the growth of neurons are displayed in sections 4 and 5. The primary objective was to track the movement of the tip of the neurons. As discussed above in section 0 the first stage of the algorithm is to determine the part of the image that contains the cell. The initial attempt used the approach described in section 3 – to find the edges of the cell and then assume that the rest of the cell is in the middle of this. This approach did not work for the neurons however as they formed a complex pattern that overlapped creating an array of shapes. To overcome this, an algorithm was developed that looked for almost parallel lines to define the edges of the cells and thus the cells could be assumed to be in the middle of these. A few tests were run based on the entropy method described in sections 5.2.3 and 0. This was again found to be a superior method as there was no ambiguity about the location of the cells, however the processing time for this was far longer and thus not amenable to real time analysis of the problem. In the study of neurons, the exact thickness of the cells was not found to be important so for most of the methods described below a skeleton of the original image was used instead. This was simpler to work with and still carried the important information about the location of the cells.

It was found, however, that in culture the axon and dendrites are indistinguishable from each other. Consequently, different methods of neuron growth had to be established. The first of these is based off of a measure that is already used in neuroscience – branching. Branching normally involves counting how many branches a dendrite is away from the original axon. It can be used as a method for quantifying growth as the more branches that an axon has the

more it can be said to have grown. There is commercially available software that can quantify branching to an extent. The Chipman Analyser (section 2.2.4.2) can quantify branching if the main axon is user defined. It will first create a stick image of the neuron from the user library of sample images (Figure 21), once the user has defined the axon. It can then calculate how many branches each individual axon is away from it. Within the context of the experiment described in chapter 5 it was not possible to determine which part of the cell was the axon so this method could not be used. In addition, the nature of the experiment was that there were, in some wells, two types of cells – MSCs and neurons – that proved difficult for the program to distinguish. As a result, a new method was created that quantified branching complexity in a different way. The box method detailed in section 4.3.1 provided information about cell growth despite not knowing the exact location of the axon. The result provided could be compared across all cultures and within the individual cultures across timeframes making it a viable result. Whilst it is not directly comparable to the original method of determining branching complexity it can be used as an alternative method. This method was also used to look at the growth of neurons in three dimensions as described in section 5, here again it proved to be useful as one of a number of methods to described growth of the neuron.

Another problem of working with neurons, as opposed to the other cells in the thesis, is that neurons do not form a monolayer culture. Cells, such as the MSC, will not overlap with each other in a standard culture at the bottom of a 16 well plate. Instead they adhere only to the plastic and cells that cannot do this die off. Indeed, there is a large body of research that looks into creating more realistic structures with scaffolds that give form to the whole culture. Whist the cell bodies of the neurons will also adhere to the plastic the axons and dendrites will grow over each other without any problem, thus looking at the cells in a standard two-dimensional planer configuration can make it hard to distinguish what is a

division and what is a crossing over of two different axons/dendrites. The obvious solution to this problem is to look at the cells in three dimensions. The microscopy techniques used throughout this thesis do not allow for a truly three-dimensional approach. Instead the z-stack of images, shown in Figure 34, can be put together to create what is known as a 2.5 D image of the cell culture. The objective here is not to recreate the image so that it can visualised, but rather to create a set of coordinates that allow computational manipulation. Since this work relies on the z-stack of images the resolution will be limited by the distance between the images in the stack. Since this is dependent on the mechanical movement of the microscope it will always be inherently limited. In the case of the microscope used throughout this thesis the theoretical limit was at $0.4\mu m^3$ at a X40 magnification. Whilst this resolution was sufficient to determine whether the cells had adhered to the plastic, as shown in section 4.2.3.2; it was not sufficient to determine which neurite belonged to which cell. As such another method was proposed that looked at the growth of the neurites over time. Since this added another dimension to the study it was hoped that the individual neurites could be tracked back to the original cell body. Ultimately this was found to be a problem due to the rate at which the neurites grew (particularly when co-cultured with MSCs) and the thickness of the neurites, meaning that one neurite could ultimately be hidden under another for several time frames. Since the experiment had several different components that needed to be imaged there was a limit on the time resolution. This limit was created by a need to obtain biologically meaningful data from the experiment. From a computational standpoint, it would be interesting to remove this limit to improve the tracking of the individual cells.

The three-dimensional nature of the neurons is investigated more in section 5. In this instance, the neurons have more space to grow in the z-direction and so it is possible to study them with a resolution that did not work with the neurons that can only grow on the plastic

of the plate. A consequence of this was that when tracking the neuron tips their relative depth could be determined (Figure 53-Figure 55). Whist this is a useful measurement; it does not help in the presence of the nanofiber scaffolds that efficiently block the image of the neurites below them. A solution to this would be to use another form of microscopy or to make fluorescent hippocampal neurons that would allow for easier detection, however such an experiment would be outside of the scope of this project.

9.3. The extraction of a suitable set of cell biometrics that can be used in the context of cell cycle to determine the points of mitosis, differentiation and apoptosis.

Morphological markers were also investigated in sections 3, 0, 0 and 0 to see whether it was possible to predict the points at which a cell would go through any one stage of the cell cycle. Section 3 looked mostly at mitosis and attempted to link that to the differentiation of the stem cell. By contrast section 0 looks at the effects of vesicles on apoptosis. The cells in this experiment were deliberately cultured in hydrogen peroxide in order to encourage an early cell death. In sections 0 and 0 the cell cycle was not the sole focus, the experiments in question were created to look at other elements of the uses of cellular morphology. Nevertheless, there was some interesting cell cycle information generated in these experiments. The neuron does not fit into the classical model of cell cycle since it does not go through cellular apoptosis, programmed cell death, nor does it divide and renew itself. As such the work on the neurons in sections 4 and 5 cannot be viewed as being part of the aim here. However, the experiment on the neural cells do provided some interesting work on how the neuron grows that has been discussed in section 0, which could be viewed as an insight into the life of a neuron.

The first step in investigating the cell cycle of MSCs is to look at when they go through mitosis, (i.e. cell division). In the case of MSCs, and other stem cells, the point of mitosis means that either a cell is going though self-renewal, i.e. creating another stem cell, or it is

differentiating, i.e. the daughter cell is a different type of cell. In a single culture, it would be expected that no differentiation would take place as it has been shown previously that cells tend to differentiate when they are cultured with other cell types. As such the point of mitosis was originally viewed as an important point to identify as this is when the cell could potentially be differentiating. Commercially available software exists that can spot the point of mitosis. The Chipman Analyser could find the point of mitosis if examples of such points had been entered into the library initially. The only contribution here was to integrate the finding of the point of mitosis into the tracking algorithm in a way that would potentially allow for linage tracking, a tool that had never been fully automated for PC microscopy.

With regards to determining whether the cells had gone through differentiation after they had divided initial work proposed looking at whether the cells changed morphology over time, as described in section 0. However, without any standard markers for the difference between an MSC and another cell (mostly articular chondrocytes in this study) it was impossible to say with any certainty when a cell had divided. One possible candidate proposal is that when a cell differentiates it will lift off of the mother cell so being able to accurately measure the position of the cells in 3D might provide an answered. This theory was met with two main problems, firstly that this theory is by no means fully established and without better methods to determine the identity of a single cell it would not be possible to say whether it was correct. Secondly the resolution in the z-dimension was not sufficient to be able to tell whether this had happened. Overall, whilst the algorithm created was capable of detecting mitosis it fell short of detecting when the mitotic event was also a differentiation event.

The second large event in the cell cycle is apoptosis (i.e. programmed cell death). This was mostly investigated with regards to the back-disk cells described in section 5. The incentive for this study came from a biological study that had previously shown that the back-disk

cells seemed to exhibit more vesicles on the cell surface before the cells went through apoptosis. Without any method to automate cell counting the researchers were forced to manually analyse each cell. As such it was known that apoptosis was an event that would be expected to happen. Apoptosis is easy to find in three dimensions as when the cells die they float up to the top of the culture. The main contribution here was determining the morphological markers that determine when apoptosis will take place – cells with more vesicles are more likely to go through apoptosis sooner. Several interesting results came from this work that were not directly linked to the aims of the thesis but those that do serve to highlight the importance of algorithms that track single cells within cultures. The first of these is that the smaller cells, in terms of area, tend to have the most vesicles visible on the surface. This would imply that the smaller cells are less viable and so should not be used in regenerative medicine.

9.4. The behaviour of cells in gels and to determine the limits of microscopy on the gels.

In nature cells are grown in three dimensional structures rather than in the two-dimensional cultures on Petri dishes. In order to give cultures a three-dimensional structure it is customary to use a gel in the place of an extracellular matrix. The gels proved support to the cells while still being soft enough to allow movement and division of the cells. Section 5 looks at the study of the cells within the gel. Section 6 focuses on which of the gels provide the best imaging support. This is a subject that does not receive much attention in biological literature, with most studies focusing on which gels are best for culturing cells.

Since the cells are in three dimensional structures now some thought has to go into how they can be imaged. The ideal would be some form of three-dimensional imaging that allowed the user to see the structures from all angles. To do this properly would require that the microscope or the objects being imaged could be rotated. There are some devices that allow for this, but they are very expensive and not normally used outside of specialist laboratories.

In addition to their cost such machines are also not practical for live cell imaging as it is not possible to know which angle contains the most interesting piece of imaging data. An alternative method to this would be to create a three-dimensional image of the cells after imaging has taken place. Whilst this would create a visual image, the purpose of this study was to determine cellular characteristics rather than to create better visualisation. To facilitate this an autofocusing algorithm was used that provided details of where the objects being imaged were in relation to a z-stack of images. From this it was possible to see if the cells had moved within the gel. This is important because the direction of the movement of the cells can give some clues as to the behaviour of the cells. In section 5 the experiment investigates whether hippocampal neurons move in the direction of a chemoattractant or in the direction of the topographical cues provided by the nanofibers. Through the use of the comparative z-stacks it was possible to determine that he cells were most affected by the topological cues rather than the chemo-attractant despite the fact that this could not be seen physically down the microscope.

In section 0 it was the gels rather than the cells themselves that were investigated. Here, it was important to look at the cells within the context of the gels. Nevertheless, some information about the gels was unknown in terms of imaging. It was found that whilst more opaque gels, such as collagen gel, are more widely used the more expensive gels make for better imaging. This is an important factor in the making of an algorithm that can track the movement of cells through the gels. This finding is significant, as more work is done in three dimensions, because it helps to determine which tools are best suited to the algorithm. In addition, the usefulness of the tools was shown as it is now possible to track the movement of the chondrocytes through the gel. It is interesting to note that he chondrocytes tracked did not move together as had been predicted.

9.5. The extraction of a suitable set of cell biometrics that can be used in the context of a co-culture to distinguish the cell types without labelling

Whilst section 0 is the most focused on the distinguishing features of cells that would allow for their identification within a co-culture, every part of the work leading up to this has also focused heavily on extracting cell morphologies in such a way as to have a distinguishable set of features in any culture. Within the context of section 8 the work looked at two morphologically similar cells, articular chondrocytes and MSCs. These are often cultured together in regenerative medicine for the purposes of re-growing cartilage for arthritic joints. In this study, the cells were first labelled with fluorescent dye, as this is the standard practice for distinguishing the cells now, and where also cultured separately. This particular experiment has an additional problem in that it is assumed that the MScs will differentiate into either cell types when they are co-cultured. As a result, this experiment only looks at the first few days when it is assumed that the labelling is correct, hoping to avoid the possibility that those labelled as MSCs had differentiated into chondrocytes.

The process followed for labelling and tracking the cells was the same as that used in the sections 3, 0 and 0 so it was possible to be confident that it had been well refined by this point. Before running the experiment, it would be hard to tell which of the morphological features would be the most important in distinguishing the cells so a wide variety of possible markers was tested. These were looked over with simple descriptive statistics to see if there were any that stood out. However, this was not expected to be the case as the cells were indistinguishable by eye. Some trends were found by this method and by making use of more advanced statistics highlighted in section 0. What was perhaps more interesting is that the cells behave differently within the co-culture than they do in the single culture so without labelling the cells there would not have been any way to distinguish them. However, labelling the cells represents its own problem as the fluorescent labelling of the cells can

fundamentally alter the behaviour of the cells themselves. Whilst this is not a problem when looking for large differences in the cell it does start to be a problem when looking at small differences within each culture as was the case here. It was initially hoped that in addition to the co-cultures, the monocultures would help to determine what they were within the co-culture however this proved not to be the case as the cells in the co-culture behaved differently again. Since there is no standard protocol that allows for the identification of a single cell type without the use of labelling the cells, the problem cannot be considered fully investigated. That said, within the constraints of having labelled the cells and not being able to determine if the cells would behave differently unlabelled it has been found that there were several potential morphological markers for the cells. This is important as it marks a first step in being able to tell to actual composition of co-cultures. This will have an impact clinically as the composition of the cells being returned to the patients for cell therapy of conditions such as osteoarthritis may have an effect on the overall effectiveness of the treatment. In addition, this may provide further evidence to the debate of whether MSCs are differentiating, or helping chondrocyte proliferation. Further analysis would have to be done on a far larger data set to be confident in these results.

The problem with looking for morphological markers in MSCs is that their morphology changes regularly and so it is not possible to find such markers by just looking at a single still image. Further steps have to be taken. In a single still image of a monoculture of MSCs a whole variety of cell shapes can be seen. As such live cell imaging, where a whole series of images is taken, provides a great advantage as not only can the additional morphological information be obtained by the inclusion of time dependent measurements such as speed and direction of movement but the change in the static measurements over time can also be considered. In addition, there is a chance to study the behaviour of the cells over a whole cell cycle, from mitosis to mitosis, to see if there are any characteristic behaviours in those

time frames. Ultimately, whilst the experiments described in section 8 did show some trends MSCs and chondrocytes have too similar a morphology to be able to accurately predict on a single cell basis.

9.6. Getting the science into practice

The algorithms here are designed to work as an extension to already existing procedures in clinical studies. This can be evidenced by the fact that for the work done in sections 3, 4, and 6 the images used came directly from work already being done at the RJAH orthopaedic hospital in Oswestry, Shropshire. Unlike procedures such as flow cytometry they do not require a new machine to be used. Indeed the phase contrast microscope is a relatively cheap machine and is already widely in use (Burch & Stock, 1942) within laboratories across the country. The work presented here has already been published so that it has the potential to be used in work already. The biggest challenge that could be faced would be ensuring that it did work for all microscopes. Whilst all of the 2D work presented here should work in theory on any type of phase contrast image as the logic behind the work applies to phase contrast, there may be some practical considerations to consider with regards to differences in resolution and field of view. In terms of take up it would be necessary to work with researchers and clinicians so that they could understand the benefit of working with this level of automation. One method of achieving this would be to create a graphical user interface that was friendlier towards people who were not specialists with computers. It would also be necessary to look into the current work flow in practice and decide where these techniques would best be fitted.

There are additional problems related to the three dimensional work given that not every microscope has the capability of creating the z-stack necessary for this sort of work, and, as shown in chapters 5 and 7 the potential for this work is far more limited and requires a change in the way the experiment is run in the first place. It has been shown by the take up of devices

such as flow cytometers that if a technique is sufficiently useful to practise then the devices necessary to run it will be purchased. Nevertheless, the implications of the results found in Chapters 5 and 7 shows that the techniques trailed here only work to a certain depth and in the right conditions. As the objective, here is to provide a tool that will enhance the work done in the laboratories such restrictions would make the techniques trailed here less than ideal. Thus, in order for them to be of more use further trials would have to be carried out to improve the tracking algorithm in three dimensions. It would also be beneficial to test out other methods of three dimensional imaging, such as confocal microscopy and see whether it would be better to adapt the techniques presented here for these rather than trying to continue with the z-stack methods. This could be achieved by maintaining the two dimensional tracking parts of the algorithm and combining them with established techniques for the different three dimensional machines.

9.7.Conclusion

In conclusion, this project aimed to create algorithms that were capable of tracking a variety of cells types within both single cultures and mixed cultures, and from this to generate data that was relevant to current clinical trials. There have been some successes in tracking some cells types, most notably articular chondrocytes and spinal disk cells. However, the tracking of cells in high confluence (>80%) remains a challenge. In terms of data generated there has been successes in a whole variety of different types of clinical trials. The algorithms used here have been able to identify the point of mitosis. They have created a better method of determining neural growth and from this have shown that neurons co-cultured with MCSs can grow in places with neural inhibitors. Through the use of algorithms that can analyse culture in three dimensional algorithms it has been shown that neurons are more affected by topographical than chemical cues in their direction of growth. It has also been shown that vesicles are more likely to appear on smaller back disk cells. In the study of gels, it has been

found that the more transparent gels are better for imaging. Finally, it has been shown that MSCs and chondrocytes behave differently when in single and co-cultures. These discoveries would not have been possible without the use of the algorithms that allowed for the study of individual cells within a larger culture.

10. References

Acharya, C., Adesida, A., Zajac, P., Mumme, M., Riesle, J., Martin, I., & Barbero, A. (2012). Enhanced chondrocyte proliferation and mesenchymal stromal cells chondrogenesis in coculture pellets mediate improved cartilage formation. *Journal of Cellular Physiology*, *227*(1), 88–97. http://doi.org/10.1002/jcp.22706

Acosta, C., McMullan, S., Djouhri, L., Gao, L., Watkins, R., Berry, C., … Lawson, S. N. (2012). HCN1 and HCN2 in Rat DRG neurons: levels in nociceptors and non-nociceptors, NT3-dependence and influence of CFA-induced skin inflammation on HCN2 and NT3 expression. *PloS One*, *7*(12), e50442. http://doi.org/10.1371/journal.pone.0050442

Adanja, I., Debeir, O., Mégalizzi, V., Kiss, R., Warzée, N., & Decaestecker, C. (2010). Automated tracking of unmarked cells migrating in three-dimensional matrices applied to anti-cancer drug screening. *Experimental Cell Research*, *316*(2), 181–93. http://doi.org/10.1016/j.yexcr.2009.10.004

Al-Kofahi, O., Radke, R., & Goderie, S. (2006). Automated cell lineage construction: A rapid method to analyze clonal development established with murine neural progenitor cells. *Cell Cycle*, (February), 327–335. Retrieved from http://www.landesbioscience.com/journals/6/article/2426/

Alonso, F. J., Castillo, J. M. Del, & Pintado, P. (2005). Application of singular spectrum analysis to the smoothing of raw kinematic signals. *Journal of Biomechanics*, *38*(5), 1085–92. http://doi.org/10.1016/j.jbiomech.2004.05.031

Bajada, S., Mazakova, I., Richardson, J. B., & Ashammakhi, N. (2008). Updates on stem cells and their applications in regenerative medicine. *Journal of Tissue Engineering and*

Regenerative Medicine, *2*(4), 169–83. http://doi.org/10.1002/term.83

Baksh, D., Song, L., & Tuan, R. S. (2004). Adult mesenchymal stem cells: characterization, differentiation, and application in cell and gene therapy. *Journal of Cellular and Molecular Medicine*, *8*(3), 301–16. Retrieved from http://www.ncbi.nlm.nih.gov/pubmed/15491506

Ballard, D. (1981). Generalizing the Hough transform to detect arbitrary shapes. *Pattern Recognition*, *11*(2). Retrieved from http://www.sciencedirect.com/science/article/pii/0031320381900091

Begg, A. C., McNally, N. J., Shrieve, D. C., & Kärcher, H. (1985). A method to measure the duration of DNA synthesis and the potential doubling time from a single sample. *Cytometry*, *6*(6), 620–6. http://doi.org/10.1002/cyto.990060618

Bertossa, R. C. (2011). Morphology and behaviour: functional links in development and evolution. *Philosophical Transactions of the Royal Society of London. Series B, Biological Sciences*, *366*(1574), 2056–68. http://doi.org/10.1098/rstb.2011.0035

Bian, L., Zhai, D. Y., Mauck, R. L., & Burdick, J. A. (2011). Coculture of human mesenchymal stem cells and articular chondrocytes reduces hypertrophy and enhances functional properties of engineered cartilage. *Tissue Engineering. Part A*, *17*(7–8), 1137–45. http://doi.org/10.1089/ten.TEA.2010.0531

Bigdeli, N., Karlsson, C., Strehl, R., Concaro, S., Hyllner, J., & Lindahl, A. (2009). Coculture of human embryonic stem cells and human articular chondrocytes results in significantly altered phenotype and improved chondrogenic differentiation. *Stem Cells (Dayton, Ohio)*, *27*(8), 1812–21. http://doi.org/10.1002/stem.114

Bradhurst, C. J., Boles, W., & Xiao, Y. (2008). Segmentation of bone marrow stromal cells in phase contrast microscopy images. *2008 23rd International Conference Image and Vision Computing New Zealand*, 1–6. http://doi.org/10.1109/IVCNZ.2008.4762144

Burch, C. R., & Stock, J. P. P. (1942). Phase-Contrast Microscopy. *Journal of Scientific Instruments*, *19*(5), 71–75. http://doi.org/10.1088/0950-7671/19/5/302

Burger, J. A., Burger, M., Kipps, T. J., Kipps, T., Han, T., Barcos, M., … Burthem, J. (1999). Chronic lymphocytic leukemia B cells express functional CXCR4 chemokine receptors that mediate spontaneous migration beneath bone marrow stromal cells. *Blood*, *94*(11), 3658–67. http://doi.org/10.1002/1097-0142(1984)54:4<702::aid-cncr2820540418>3.0.co

Canny, J. (1986). A computational approach to edge detection. *IEEE Transactions on Pattern Analysis and Machine Intelligence*, *8*(6), 679–98. Retrieved from http://www.ncbi.nlm.nih.gov/pubmed/21869365

Carlton, P. M., Boulanger, J., Kervrann, C., Sibarita, J.-B., Salamero, J., Gordon-Messer, S., … Sedat, J. W. (2010). Fast live simultaneous multiwavelength four-dimensional optical microscopy. *Proceedings of the National Academy of Sciences of the United States of America*, *107*(37), 16016–22. http://doi.org/10.1073/pnas.1004037107

Carson, F., & Hladik, C. (2009). *Histotechnology: A Self-instructional Text* (3rd ed.). Hong Kong: American Society for Clinical Pathology Press.

Chatterjee, S. (2014a). Artefacts in histopathology. *Journal of Oral and Maxillofacial Pathology : JOMFP*, *18*(Suppl 1), S111-6. http://doi.org/10.4103/0973-029X.141346

Chatterjee, S. (2014b). Artefacts in histopathology. *Journal of Oral and Maxillofacial Pathology : JOMFP*, *18*(Suppl 1), S111-6. http://doi.org/10.4103/0973-029X.141346

Chen, C., Wang, W., Ozolek, J. A., & Rohde, G. K. (2013a). A flexible and robust approach for segmenting cell nuclei from 2D microscopy images using supervised learning and template matching. *Cytometry. Part A : The Journal of the International Society for Analytical Cytology*, *83*(5), 495–507. http://doi.org/10.1002/cyto.a.22280

Chen, C., Wang, W., Ozolek, J. A., & Rohde, G. K. (2013b). A flexible and robust approach

for segmenting cell nuclei from 2D microscopy images using supervised learning and template matching. *Cytometry. Part A : The Journal of the International Society for Analytical Cytology*, *83*(5), 495–507. http://doi.org/10.1002/cyto.a.22280

Chudley, L., McCann, K., Mander, A., Tjelle, T., Campos-Perez, J., Godeseth, R., … Ottensmeier, C. (2012). DNA fusion-gene vaccination in patients with prostate cancer induces high-frequency CD8(+) T-cell responses and increases PSA doubling time. *Cancer Immunology, Immunotherapy : CII*, *61*(11), 2161–70. http://doi.org/10.1007/s00262-012-1270-0

Curran, J. M., Chen, R., & Hunt, J. A. (2006). The guidance of human mesenchymal stem cell differentiation in vitro by controlled modifications to the cell substrate. *Biomaterials*, *27*(27), 4783–93. http://doi.org/10.1016/j.biomaterials.2006.05.001

Dahlin, R. L., Ni, M., Meretoja, V. V, Kasper, F. K., & Mikos, A. G. (2014). TGF-β3-induced chondrogenesis in co-cultures of chondrocytes and mesenchymal stem cells on biodegradable scaffolds. *Biomaterials*, *35*(1), 123–32. http://doi.org/10.1016/j.biomaterials.2013.09.086

de Boer, B. A., van den Berg, G., Soufan, A. T., de Boer, P. A. J., Hagoort, J., van den Hoff, M. J. B., … Ruijter, J. M. (2012). Measurement and 3D-visualization of cell-cycle length using double labelling with two thymidine analogues applied in early heart development. *PloS One*, *7*(10), e47719. http://doi.org/10.1371/journal.pone.0047719

de Windt, T. S., Saris, D. B. F., Slaper-Cortenbach, I. C. M., van Rijen, M. H. P., Gawlitta, D., Creemers, L. B., … Vonk, L. A. (2015). Direct Cell-Cell Contact with Chondrocytes Is a Key Mechanism in Multipotent Mesenchymal Stromal Cell-Mediated Chondrogenesis. *Tissue Engineering. Part A*, *21*(19–20), 2536–47. http://doi.org/10.1089/ten.TEA.2014.0673

Debeir, O., Van Ham, P., Kiss, R., & Decaestecker, C. (2005). Tracking of migrating cells

under phase-contrast video microscopy with combined mean-shift processes. *IEEE Transactions on Medical Imaging*, *24*(6), 697–711. http://doi.org/10.1109/TMI.2005.846851

Dempsey, K., Brown, S., Richardson, J., & Lam, K. (2015). On Tracking Spinal Disc Cells. *Proc. SPIE*.

Deng, W., Aimone, J. B., & Gage, F. H. (2010). New neurons and new memories: how does adult hippocampal neurogenesis affect learning and memory? *Nature Reviews. Neuroscience*, *11*(5), 339–50. http://doi.org/10.1038/nrn2822

Dominici, M., Le Blanc, K., Mueller, I., Slaper-Cortenbach, I., Marini, F., Krause, D., … Horwitz, E. (2006). Minimal criteria for defining multipotent mesenchymal stromal cells. The International Society for Cellular Therapy position statement. *Cytotherapy*, *8*(4), 315–7. http://doi.org/10.1080/14653240600855905

Dor, Y., Brown, J., Martinez, O. I., & Melton, D. a. (2004). Adult pancreatic beta-cells are formed by self-duplication rather than stem-cell differentiation. *Nature*, *429*(6987), 41–6. http://doi.org/10.1038/nature02520

Dray, N., Bedu, S., Vuillemin, N., Alunni, A., Coolen, M., Krecsmarik, M., … Bally-Cuif, L. (2015). Large-scale live imaging of adult neural stem cells in their endogenous niche. *Development*, *142*(20).

Du, C.-J., Marcello, M., Spiller, D. G., White, M. R. H., & Bretschneider, T. (2011). CellCut: A framework for interactive tracking of protein translocations between cell nucleus and cytoplasm. In *2011 IEEE International Symposium on Biomedical Imaging: From Nano to Macro* (pp. 1909–1912). IEEE. http://doi.org/10.1109/ISBI.2011.5872782

Duthaler, S., & Nelson, B. J. (2005a). Autofocusing algorithm selection in computer microscopy. *2005 IEEE/RSJ International Conference on Intelligent Robots and Systems*, 70–76. http://doi.org/10.1109/IROS.2005.1545017

Duthaler, S., & Nelson, B. J. (2005b). Autofocusing algorithm selection in computer microscopy. In *2005 IEEE/RSJ International Conference on Intelligent Robots and Systems* (pp. 70–76). IEEE. http://doi.org/10.1109/IROS.2005.1545017

Eslaminejad, M. B., Vahabi, S., Shariati, M., & Nazarian, H. (2010). In vitro Growth and Characterization of Stem Cells from Human Dental Pulp of Deciduous Versus Permanent Teeth. *Journal of Dentistry (Tehran, Iran)*, *7*(4), 185–95. Retrieved from http://www.pubmedcentral.nih.gov/articlerender.fcgi?artid=3184765&tool=pmcentrez&rendertype=abstract

Feng Zhao, Qingming Huang, & Wen Gao. (2006). Image Matching by Normalized Cross-Correlation. In *2006 IEEE International Conference on Acoustics Speed and Signal Processing Proceedings* (Vol. 2, p. II-729-II-732). IEEE. http://doi.org/10.1109/ICASSP.2006.1660446

Fisher, M. B., & Mauck, R. L. (2013). Tissue engineering and regenerative medicine: recent innovations and the transition to translation. *Tissue Engineering. Part B, Reviews*, *19*(1), 1–13. http://doi.org/10.1089/ten.TEB.2012.0723

Giovannini, S., Diaz-Romero, J., Aigner, T., Heini, P., Mainil-Varlet, P., & Nesic, D. (2010). Micromass co-culture of human articular chondrocytes and human bone marrow mesenchymal stem cells to investigate stable neocartilage tissue formation in vitro. *Eur Cell Mater*, *20*, 245–259. http://doi.org/vol020a20 [pii]

Golyandina, N., Nekrutkin, V. V., & Zhigljavsky, A. A. (2001). *Analysis of Time Series Structure: SSA and Related Techniques*. Chapman & Hall/Crc. http://doi.org/10.1198/jasa.2002.s239

Gonzalez, R. (2002). *Digital Image Processing* (2nd ed.). Prentice-Hall.

Grimm, H. P., Verkhovsky, A. B., Mogilner, A., & Meister, J.-J. (2003). Analysis of actin dynamics at the leading edge of crawling cells: implications for the shape of keratocyte

lamellipodia. *European Biophysics Journal*, *32*(6), 563–577. http://doi.org/10.1007/s00249-003-0300-4

György, B., Szabó, T. G., Pásztói, M., Pál, Z., Misják, P., Aradi, B., … Buzás, E. I. (2011). Membrane vesicles, current state-of-the-art: emerging role of extracellular vesicles. *Cellular and Molecular Life Sciences : CMLS*, *68*(16), 2667–88. http://doi.org/10.1007/s00018-011-0689-3

Hand, A. J., Sun, T., Barber, D. C., Hose, D. R., & MacNeil, S. (2009a). Automated tracking of migrating cells in phase-contrast video microscopy sequences using image registration. *Journal of Microscopy*, *234*(1), 62–79.

Hand, A. J., Sun, T., Barber, D. C., Hose, D. R., & MacNeil, S. (2009b). Automated tracking of migrating cells in phase-contrast video microscopy sequences using image registration. *Journal of Microscopy*, *234*(1), 62–79. http://doi.org/10.1111/j.1365-2818.2009.03144.x

Hanifi, A., Richardson, J. B., Kuiper, J. H., Roberts, S., & Pleshko, N. (2012). Clinical outcome of autologous chondrocyte implantation is correlated with infrared spectroscopic imaging-derived parameters. *Osteoarthritis and Cartilage / OARS, Osteoarthritis Research Society*, *20*(9), 988–96. http://doi.org/10.1016/j.joca.2012.05.007

Hesse, M., Raulf, A., Pilz, G.-A., Haberlandt, C., Klein, A. M., Jabs, R., … Fleischmann, B. K. (2012). Direct visualization of cell division using high-resolution imaging of M-phase of the cell cycle. *Nature Communications*, *3*, 1076. http://doi.org/10.1038/ncomms2089

Ho, A. D., & Punzel, M. (2003). Hematopoietic stem cells : can old cells learn new tricks ? *Journal of Leukocyte Biology*, *73*(5), 547–555. http://doi.org/10.1189/jlb.0902458.Journal

Hong, J.-H., Hwang, E. S., McManus, M. T., Amsterdam, A., Tian, Y., Kalmukova, R., … Yaffe, M. B. (2005a). TAZ, a transcriptional modulator of mesenchymal stem cell differentiation. *Science*, *309*(5737), 1074–8. http://doi.org/10.1126/science.1110955

Hong, J.-H., Hwang, E. S., McManus, M. T., Amsterdam, A., Tian, Y., Kalmukova, R., … Yaffe, M. B. (2005b). TAZ, a transcriptional modulator of mesenchymal stem cell differentiation. *Science*, *309*(5737), 1074–8. http://doi.org/10.1126/science.1110955

Huh, S., Ker, D. F. E., Bise, R., Chen, M., & Kanade, T. (2011). Automated mitosis detection of stem cell populations in phase-contrast microscopy images. *IEEE Transactions on Medical Imaging*, *30*(3), 586–96. http://doi.org/10.1109/TMI.2010.2089384

Jaccard, N., Griffin, L. D., Keser, A., Macown, R. J., Super, A., Veraitch, F. S., & Szita, N. (2013). Automated method for the rapid and precise estimation of adherent cell culture characteristics from phase contrast microscopy images. *Biotechnology and Bioengineering*. http://doi.org/10.1002/bit.25115

James, S., Fox, J., Afsari, F., Lee, J., Clough, S., Knight, C., … Genever, P. (2015). Multiparameter Analysis of Human Bone Marrow Stromal Cells Identifies Distinct Immunomodulatory and Differentiation-Competent Subtypes. *Stem Cell Reports*, *4*(6), 1004–15. http://doi.org/10.1016/j.stemcr.2015.05.005

Jun, L. (2013). Dicom Operator - EsmeProcess: CROIEditor - File Exchange - MATLAB Central. Retrieved September 30, 2013, from http://www.mathworks.com/matlabcentral/fileexchange/43397-dicom-operator-esmeprocess/content/lib/@CROIEditor/CROIEditor.m

Kapur, J. N., Sahoo, P. K., & Wong, A. K. C. (1985). A new method for gray-level picture thresholding using the entropy of the histogram. *Computer Vision, Graphics, and Image Processing*, *29*(3), 273–285. http://doi.org/10.1016/0734-189X(85)90125-2

Koenderink, J. J. (1984). The structure of images. *Biological Cybernetics*, *50*(5), 363–370.

Lam, K. P., Dempsey, K. P., Collins, D. J., & Richardson, J. B. (2016). Monitoring stem cells in phase contrast imaging. In D. L. Farkas, D. V. Nicolau, & R. C. Leif (Eds.) (p. 97110E). International Society for Optics and Photonics. http://doi.org/10.1117/12.2211017

Lam, K. P., Dempsy, K. P., Smith, W. A., Wright, K. T., Masri, W. E., & Richardson, J. B. (2013). A Computational Approach to Quantifying Axon Regeneration in the Presence of Mesenchymal Stem Cells (MSCs)*. *IEEE Neural Engineering Conference*.

Lam, K., & Richardson, J. B. (2012). FACE - Fractal Analysis in Cell Engineering. *CISSE*.

Landecker, H. (2006). Microcinematography and the History of Science and Film. Retrieved from http://philpapers.org/rec/LANMAT-8

Lazarus, H. M., Haynesworth, S. E., Gerson, S. L., Rosenthal, N. S., & Caplan, A. I. (1995). Ex vivo expansion and subsequent infusion of human bone marrow-derived stromal progenitor cells (mesenchymal progenitor cells): implications for therapeutic use. *Bone Marrow Transplantation*, *16*(4), 557–64. Retrieved from http://europepmc.org/abstract/med/8528172

Lee, S. U., Yoon Chung, S., & Park, R. H. (1990). A comparative performance study of several global thresholding techniques for segmentation. *Computer Vision, Graphics, and Image Processing*, *52*(2), 171–190. http://doi.org/10.1016/0734-189X(90)90053-X

Levorson, E. J., Santoro, M., Kasper, F. K., & Mikos, A. G. (2014). Direct and indirect co-culture of chondrocytes and mesenchymal stem cells for the generation of polymer/extracellular matrix hybrid constructs. *Acta Biomaterialia*, *10*(5), 1824–35. http://doi.org/10.1016/j.actbio.2013.12.026

Li, F., Zhou, X., Zhao, H., & Wong, S. T. C. (2009). Cell segmentation using front vector flow guided active contours. *Medical Image Computing and Computer-Assisted*

Intervention : MICCAI ... International Conference on Medical Image Computing and Computer-Assisted Intervention, *12*(Pt 2), 609–16. Retrieved from http://www.ncbi.nlm.nih.gov/pubmed/20426162

Li, J. (2014). Dicom Operator - EsmeProcess - File Exchange - MATLAB Central. Retrieved from http://uk.mathworks.com/matlabcentral/fileexchange/43397-dicom-operator-esmeprocess

Li, K., Miller, E. D., Chen, M., Kanade, T., Weiss, L. E., & Campbell, P. G. (2008a). Cell population tracking and lineage construction with spatiotemporal context. *Medical Image Analysis*, *12*(5), 546–566. http://doi.org/10.1016/j.media.2008.06.001

Li, K., Miller, E. D., Chen, M., Kanade, T., Weiss, L. E., & Campbell, P. G. (2008b). Cell population tracking and lineage construction with spatiotemporal context. *Medical Image Analysis*, *12*(5), 546–566. http://doi.org/10.1016/j.media.2008.06.001

Li, W., Jiang, K., & Ding, S. (2012). Concise review: A chemical approach to control cell fate and function. *Stem Cells (Dayton, Ohio)*, *30*(1), 61–8. http://doi.org/10.1002/stem.768

Lou, X., & Hamprecht, F. A. (2011). Structured Learning for Cell Tracking. In *Advances in Neural Information Processing Systems* (pp. 1296–1304). Retrieved from http://papers.nips.cc/paper/4484-structured-learning-for-cell-tracking

MATLAB and Statistics Toolbox. (2012). Natick: The MathWorks, Inc.

Meijering, E., Dzyubachyk, O., & Smal, I. (2012). METHODS FOR CELL AND PARTICLE TRACKING. *Imaging and Spectroscopic Analysis of Living Cells: Optical and Spectroscopic Techniques*, *504*, 183–200. http://doi.org/10.1016/13978-0-12-3918574.00009-4

Meretoja, V. V, Dahlin, R. L., Kasper, F. K., & Mikos, A. G. (2012). Enhanced chondrogenesis in co-cultures with articular chondrocytes and mesenchymal stem cells.

Biomaterials, *33*(27), 6362–9. http://doi.org/10.1016/j.biomaterials.2012.05.042

Meretoja, V. V, Dahlin, R. L., Wright, S., Kasper, F. K., & Mikos, A. G. (2014). Articular chondrocyte redifferentiation in 3D co-cultures with mesenchymal stem cells. *Tissue Engineering. Part C, Methods*, *20*(6), 514–23. http://doi.org/10.1089/ten.tec.2013.0532

Nayar, S. K., & Nakagawa, Y. (1990). Shape from focus: an effective approach for rough surfaces. In *Proceedings., IEEE International Conference on Robotics and Automation* (pp. 218–225). IEEE Comput. Soc. Press. http://doi.org/10.1109/ROBOT.1990.125976

Naylor, A. J., Azzam, E., Smith, S., Croft, A., Poyser, C., Duffield, J. S., … Buckley, C. D. (2012). The mesenchymal stem cell marker CD248 (endosialin) is a negative regulator of bone formation in mice. *Arthritis and Rheumatism*, *64*(10), 3334–43. http://doi.org/10.1002/art.34556

Norman, K., & O'Reilly, R. (2002). Modeling hippocampal and neocortical contributions to recognition memory: a complementary-learning-systems approach. *Psycholgical Review*, 3–44. Retrieved from http://www.princeton.edu/~compmem/psyrev_inpress.pdf

Nöth, U., Steinert, A. F., & Tuan, R. S. (2008). Technology insight: adult mesenchymal stem cells for osteoarthritis therapy. *Nature Clinical Practice. Rheumatology*, *4*(7), 371–80. http://doi.org/10.1038/ncprheum0816

Olivos-Pérez, L., Iturbe-Castillo, M., Sánchez-de-la-Llave, M., Ramos-García, R., & Treviño-Palacios, C. (2006). Nonlinear phase contrast microscope. *Proc. SPIE 6332*.

Patel, S. V., McLaren, J. W., Hodge, D. O., & Bourne, W. M. (2001). Normal Human Keratocyte Density and Corneal Thickness Measurement by Using Confocal Microscopy In Vivo. *Invest. Ophthalmol. Vis. Sci.*, *42*(2), 333–339. Retrieved from http://www.iovs.org/content/42/2/333.short

Pelvig, D. P., Pakkenberg, H., Stark, A. K., & Pakkenberg, B. (2008). Neocortical glial cell

numbers in human brains. *Neurobiology of Aging*, *29*(11), 1754–1762. http://doi.org/10.1016/j.neurobiolaging.2007.04.013

Pertuz, S., Puig, D., & Garcia, M. A. (2013). Analysis of focus measure operators for shape-from-focus. *Pattern Recognition*, *46*(5), 1415–1432. http://doi.org/10.1016/j.patcog.2012.11.011

Richardson, I. E. (2003). *H.264 and MPEG-4 Video Compression: Video Coding for Next-generation Multimedia*. John Wiley & Sons. Retrieved from http://books.google.co.uk/books/about/H_264_and_MPEG_4_Video_Compression.html?id=ECVV_G_qsxUC&pgis=1

Romanov, Y., Svintsitskaya, V., & Smirnov, V. (2003a). Searching for alternative sources of postnatal human mesenchymal stem cells: candidate MSC-like cells from umbilical cord. *Stem Cells*, 105–110.

Romanov, Y., Svintsitskaya, V., & Smirnov, V. (2003b). Searching for alternative sources of postnatal human mesenchymal stem cells: candidate MSC-like cells from umbilical cord. *Stem Cells*, 105–110. Retrieved from http://onlinelibrary.wiley.com/doi/10.1634/stemcells.21-1-105/full

Ross, D. T., Scherf, U., Eisen, M. B., Perou, C. M., Rees, C., Spellman, P., … Brown, P. O. (2000). Systematic variation in gene expression patterns in human cancer cell lines. *Nature Genetics*, *24*(3), 227–35. http://doi.org/10.1038/73432

Ryter, A. (1988). Contribution of new cryomethods to a better knowledge of bacterial anatomy. *Annales de l'Institut Pasteur. Microbiologie*, *139*(1), 33–44. http://doi.org/10.1016/0769-2609(88)90095-6

Sacan, A., Ferhatosmanoglu, H., & Coskun, H. (2008). CellTrack: An Open-Source Software for Cell Tracking and Motility Analysis *. *BIOINFORMATICS*, *0*(0), 1–3. Retrieved from http://db.cse.ohio-state.edu/CellTrack

Sachs, P. C., Francis, M. P., Zhao, M., Brumelle, J., Rao, R. R., Elmore, L. W., & Holt, S. E. (2012). Defining essential stem cell characteristics in adipose-derived stromal cells extracted from distinct anatomical sites. *Cell and Tissue Research*, *349*(2), 505–15. http://doi.org/10.1007/s00441-012-1423-7

Sanei, S., & Hassani, H. (2015). *Singular Spectrum Analysis of Biomedical Signals*. CRC Press. Retrieved from https://books.google.com/books?id=fwVCCwAAQBAJ&pgis=1

Schneider, C. A., Rasband, W. S., & Eliceiri, K. W. (2012a). NIH Image to ImageJ: 25 years of image analysis. *Nature Methods*, *9*(7), 671–675. http://doi.org/10.1038/nmeth.2089

Schneider, C. A., Rasband, W. S., & Eliceiri, K. W. (2012b). NIH Image to ImageJ: 25 years of image analysis. *Nature Methods*, *9*(7), 671–675. http://doi.org/10.1038/nmeth.2089

Smith, W. A., Lam, K., Collins, D., & Richardson, J. (2013a). On 2.5D Surface Reconstruction of cell Cultures. *Accepted for Publication in Procs IPAS 2013, IEEE Signal Processing Society*.

Smith, W. A., Lam, K. P., Collins, D. J., & Richardson, J. B. (2013b). On 2.5D surface reconstruction of cell cultures. In *2013 8th International Symposium on Image and Signal Processing and Analysis (ISPA)* (pp. 218–223). IEEE. http://doi.org/10.1109/ISPA.2013.6703742

Smith, W. A., Lam, K. P., Collins, D. J., & Tarvainen, J. (2012). Estimation of Depth Map using Image Focus : A Scale-Space Approach for Shape Recovery. *CISSE*, *2*(1), 10–12.

Stuurman, N. (2003). MTrack2. Retrieved January 9, 2017, from https://valelab4.ucsf.edu/~nstuurman/ijplugins/MTrack2.html

Tarvainen, J., Saarinen, M., Laitinen, J., Korpinen, J., & Viitanen, J. (2002). Creating Images with High Data Contents for Microworld Applications. *Industrial Systems Rewiew*, 17–23.

Tsai, D.-M., & Lin, C.-T. (2003). Fast normalized cross correlation for defect detection. *Pattern Recognition Letters*, *24*(15), 2625–2631. http://doi.org/10.1016/S0167-8655(03)00106-5

Tsuchiya, K., Chen, G., Ushida, T., Matsuno, T., & Tateishi, T. (2004). The effect of coculture of chondrocytes with mesenchymal stem cells on their cartilaginous phenotype in vitro. *Materials Science and Engineering: C*, *24*(3), 391–396. http://doi.org/10.1016/j.msec.2003.12.014

Walsby, A. E. (1994). Gas vesicles. *Microbiological Reviews*, *58*(1), 94–144. Retrieved from http://www.pubmedcentral.nih.gov/articlerender.fcgi?artid=372955&tool=pmcentrez&rendertype=abstract

Wells, J. C. K., DeSilva, J. M., & Stock, J. T. (2012). The obstetric dilemma: An ancient game of Russian roulette, or a variable dilemma sensitive to ecology? *American Journal of Physical Anthropology*, *149*(S55), 40–71. http://doi.org/10.1002/ajpa.22160

Whitehurst, D. G. T., Bryan, S., Hay, E. M., Thomas, E., Young, J., & Foster, N. E. (2011). Cost-effectiveness of acupuncture care as an adjunct to exercise-based physical therapy for osteoarthritis of the knee. *Physical Therapy*, *91*(5), 630–41. http://doi.org/10.2522/ptj.20100239

Wong, S., Vassiliadis, S., Cotofana, S., Ce, S., & Tudelft, E. T. (2002). A Sum of Absolute Differences Implementation in FPGA Hardware. *Proceedings/ IEEE Euromicro Conference*, 183–188.

Wright, K. (2013). Spinal motor neurite outgrowth over glial scar inhibitors is enhanced by co-culture with bone marrow stromal cells. *Spine Journal (Under Review)*.

Wright, K. T., El Masri, W., Osman, A., Roberts, S., Chamberlain, G., Ashton, B. a, & Johnson, W. E. B. (2007). Bone marrow stromal cells stimulate neurite outgrowth over neural proteoglycans (CSPG), myelin associated glycoprotein and Nogo-A.

Biochemical and Biophysical Research Communications, *354*(2), 559–66. http://doi.org/10.1016/j.bbrc.2007.01.013

Wu, L., Leijten, J., Blitterswijk, C. A. van, & Karperien, M. (2013). Fibroblast Growth Factor-1 Is a Mesenchymal Stromal Cell-Secreted Factor Stimulating Proliferation of Osteoarthritic Chondrocytes in Co-Culture. Retrieved from http://online.liebertpub.com/doi/abs/10.1089/scd.2013.0118

Xie, X., Yu, G., Liu, N., Bao, Z., Criddle, C. S., Cui, Y., … Fredrickson, J. K. (2012). Graphene–sponges as high-performance low-cost anodes for microbial fuel cells. *Energy & Environmental Science*, *5*(5), 6862. http://doi.org/10.1039/c2ee03583a

Yang, F., Mackey, M. A., Ianzini, F., Gallardo, G., & Sonka, M. (2005). Cell segmentation, tracking, and mitosis detection using temporal context. *Medical Image Computing and Computer-Assisted Intervention : MICCAI ... International Conference on Medical Image Computing and Computer-Assisted Intervention*, *8*(Pt 1), 302–9. Retrieved from http://www.ncbi.nlm.nih.gov/pubmed/16685859

Yang, Y., Wimpenny, I., & Ahearne, M. (2011). *Portable nanofiber meshes dictate cell orientation throughout three-dimensional hydrogels*. *Nanomedicine: Nanotechnology, Biology and Medicine* (Vol. 7). Retrieved from http://www.sciencedirect.com/science/article/pii/S1549963411000104

Yin, Z., Li, K., Kanade, T., & Chen, M. (2010). Understanding the optics to aid microscopy image segmentation. *Medical Image Computing and Computer-Assisted Intervention : MICCAI ... International Conference on Medical Image Computing and Computer-Assisted Intervention*, *13*(Pt 1), 209–17. Retrieved from http://www.ncbi.nlm.nih.gov/pubmed/20879233

Yong, Y.-C., Dong, X.-C., Chan-Park, M. B., Song, H., & Chen, P. (2012). Macroporous and Monolithic Anode Based on Polyaniline Hybridized Three-Dimensional Graphene

for High-Performance Microbial Fuel Cells. *ACS Nano*, *6*(3), 2394–2400. http://doi.org/10.1021/nn204656d

Zheng, Y., Lv, H., Wang, Y., Lu, H., Qing, L., & Xi, T. (2009). Performance of novel bioactive hybrid hydrogels in vitro and in vivo used for artificial cartilage. *Biomedical Materials (Bristol, England)*, *4*(1), 15015. http://doi.org/10.1088/1748-6041/4/1/015015